INVESTIGATION INTO FREE FLIGHT IMPACT ON AIR TRAFFIC CONTROL

by

Alexander B. Suchkov

Thesis submitted to the faculty of the
Virginia Polytechnic Institute and State University
in partial fulfillment of the requirements for the degree of

MASTER OF SCIENCE
IN
CIVIL ENGINEERING

APPROVED:

Antonio A. Trani, Ph.D., Chairman

Donald R. Drew, Ph.D. Antoine Hobeika, Ph.D.

April, 1998
Blacksburg, Virginia

Keywords: Free Flight, Air Traffic Control, Aircraft

INVESTIGATION INTO FREE FLIGHT IMPACT ON AIR TRAFFIC CONTROL

by

Alexander B. Suchkov

Dr. A. A. Trani, Chairman

Civil Engineering

(ABSTRACT)

This thesis deals with an innovative concept of air traffic operations called Free Flight. First, a baseline is established to determine how controllers operate under the current operation guidelines. Then flight trajectories are developed for different alternatives to the Free Flight operational concept. A comparison of these Free Flight alternatives with current operational concept is conducted to investigate the impact of Free Flight on Air Traffic Control.

With the powerful features of optimization, graphics, and hierarchical modeling, the MATLAB® toolboxes proved to be effective in the modeling process involved in this research.

Acknowledgments

I sincerely wish to express my gratitude to my advisor Dr. Antonio Trani for his full support, expert guidance, understanding and encouragement throughout the course of my study and research at Virginia Tech. Also, I am greatly indebted to him for his critical review of the manuscript of my thesis.

I would like to thank my committee members, Dr. Donald Drew and Dr. Antoine Hobeika, for serving on my committee, and providing me with excellent course instruction during my graduate years at Virginia Tech.

Special thanks are going to all my colleagues at CSSI, Inc. for their continuos support and providing me with all necessary data and valuable comments that helped in the completion of this thesis.

It is my greatest pleasure to dedicate this thesis to my parents, my dream was accomplished by their help.

0Table of Contents

1 List of Figures

List of Tables

Chapter 1 Introduction

1.1 Background

For nearly 50 years, commercial aircraft traffic flying in American airspace has conformed to the rules of the National Airspace Plan of the Federal Aviation Administration (FAA). It is more commonly known as “positive control”, and requires that every airliner be under the direct supervision of ground-based Air Traffic Control (ATC) as long as it is in the air. Industry analysts estimate this policy to cost the airlines as much as 3 billion dollars each year [1]. United Airlines, alone, estimates excess costs of $670 million annually due to an outdated ATC system. UAL also estimates an additional $1.3 billion in lost productivity for a total $2 billion annual loss directly attributable to ATC. American Airlines has publicly stated that its internal estimates are similar.

Positive control lines airliners up on invisible jetways in the sky, routing them point-to-point along paths of radio navigation aids that were developed largely in the 1950s. It creates much longer routes than would be flown using Great Circle navigation techniques. It requires airliners to depart within specific time frames, or “gates”, so they can be lined up as soon as they begin their take-off roll. It ignores the winds aloft, and requires an aircraft to fly in winds that may be less than optimal. It slows the parade of jets down to the speed of the slowest plane in the sky. It results in delays, which means missed connections, rebooking passengers, and frustration. On average, every flight wastes 18 minutes of the average traveler’s life due to delays. And, most importantly, it funnels ever-greater numbers of aircraft into a very small airspace.

Over the last few years Wall Street has been looking for the reason airlines are not profitable. Research, over the last 15 years, has led to the conclusion that the problem is the stagnation of the airline production process. Airline aircraft speed has actually dropped by over 8% or 30 miles per hour over the last 15 years. As an example, Continental has a jet flight into Newark that has a scheduled effective speed of 133 mph, even though the aircraft is capable of speeds of 500 mph. FAA’s own analysis shows that delay per operation increased 38% between 1976 and 1986. As outlined above the leading cause of this productivity stagnation and decrease in production line speed is the outdated ATC system.

In June, 1995 the number of passengers transported in the United States by carriers offering scheduled air service passed the 10 billion mark. Based on latest forecasts for scheduled passenger traffic, sometime in the year 2007 U.S. air carriers will transport their 20 billionth passenger.

Free Flight is an innovative concept that will improve the efficiency of the National Airspace System (NAS). Using supporting procedures and technologies, pilots operating under instrumental flight rules (IFR) will be able to select the aircraft's course, speed, and altitude in real time. From pre-flight planning to destination parking, Free Flight provides the aviation community with maximum flexibility and safety. This concept is being developed jointly by the FAA and the aviation community.

Currently, a pilot establishes a flight plan with ATC. This plan requires the aircraft to fly along a specific route. Any deviation from the designated route must be pre-approved by an air traffic controller. For example, if a thunderstorm is encountered along the flight path, the pilot must notify the ATC of a need to change course. The controller would then designate a course for the plane to avoid the storm. Under the Free Flight concept, the pilot will be able to choose the route, speed an altitude to achieve the desired results, notifying the air traffic controller of the new route. The pilot's flexibility will be restricted only:

- to ensure separation;
- when traffic density at busy airports or in congested airspace precludes Free Flight:
- to prevent unauthorized entry into special use airspace; and
- to ensure safety of flight.

Generally speaking, an activity that removes restrictions represents a move toward Free Flight. Full implementation of Free Flight requires varying degrees of modifications to procedures, along with the use of current and new technologies and new ground and air-based communications, navigation, and surveillance equipment and avionics.

The United States operates the safest airspace system in the world. Free Flight continues clear-cut lines of authority and responsibility between the pilot and controller.

1.2 Thesis Organization

This thesis is the logical compilation of different related studies, performed by the author at Virginia Tech and CSSI, Inc. Chapter 2 describes analysis of conflict resolution techniques, used by the air traffic controllers under current concept of operations. Chapter 3 deals with the development of free flight alternatives and provides an insight in both theoretical and practical approaches to it. Chapters 4 and 5 provide some qualitative and quantitative comparisons of the future free flight and current concepts of operation. Each of these four chapters has a related literature overview and presents the results of the corresponding studies. Finally, Chapter 6 provides final conclusions and recommendations.

Chapter 2 Controller Conflict Resolution Baseline Analysis

The purpose of this analysis [2] is to investigate typical controller conflict resolution actions to determine the types of resolutions typically made under today's Air Traffic Control (ATC) concept of operations, and the resultant deviation from intended path in order to establish a conflict resolution baseline. A conflict resolution baseline is critical to determining the overall benefits of future implementations of air traffic control decision support tools. As part of this analysis, the FAA developed SATORI (Situation Assessment through the Re-creation of Incidents), a tool (see Appendix B and Reference [3]) used to explore the situational dynamics that occur in the ATC environment wherein conflict resolution strategies are selected and implemented based upon individual controllers' training and previous experiences. The SATORI tool provides an accurate replay of the situation as it occurs in an en route sector including the capability for replaying digitized voice.

Since the SATORI tool is primarily suited for replaying the scenarios as they occurred in the real environment, additional analysis tools were developed to aid in the data reduction, exploration, and analysis phases of this project. These tools were developed to complement the existing functionality resident in SATORI. They require as input processed SATORI scenario data with the exception of digitized voice. This chapter describes the methodology that was employed, the results of the analysis, conclusions, and possible future analysis.

2.1 Study Approach

The study approach that was utilized in developing a controller conflict resolution baseline involved performing a literature search to identify relevant research pertaining to conflict resolution. The goal of this activity was to gain an understanding of the situational dynamics that affect the selected maneuver and the associated constraints. With this information it was then possible to replay scenarios that contain conflict resolution maneuvers in SATORI. The sample size consisted of 25 scenarios varying in length from 12 to 30 minutes. Each scenario contained traffic for the entire Atlanta Air Route Traffic Control Center (ARTCC) and an associated voice file for one sector within the ARTCC. The scenarios were originally generated to investigate operational errors and as such contain a single instance where loss of separation occurred within the sector for which digitized voice existed. Of the 25 scenarios with digitized voice, several were either missing files or the quality of the voice file was inadequate to enable their inclusion for the analysis using SATORI. Therefore, a methodology was developed that would allow use of virtually all of the data contained in the scenarios from analysis. The methodology involved developing a data filter that screened the raw SATORI data to identify aircraft that were potentially maneuvered as part of a conflict resolution strategy. The data filter allowed the sample size of potential conflict resolution maneuvers to expand from dozens to hundreds of cases. For each of the resolution maneuvers identified, a wide range of data was collected and analyzed. The final step in the analysis was to compare the resolution maneuvers with the intended path to determine how far from the intended path the resolution maneuver moved the aircraft.

2.2 Literature Review

As previously discussed, the purpose of the literature search was to gain a better understanding of conflict resolution by controllers and current research pertaining to the topic [4], [5], [6], [7]. Achieving this objective required understanding the functional responsibilities of an en route controller, gaining an understanding of the routine cognitive demands placed upon them, understanding the typical and atypical operating constraints that they are working under, and gaining an understanding of other external factors that often affect conflict detection and resolution. These external factors can potentially further constrain the set of possible resolution maneuvers, and the magnitude of the desired maneuver.

2.2.1 Controller Training

En route controllers mainly deal with traffic that is navigating across the country, as opposed to entering a terminal area. Currently, most en route traffic navigates via established airways between VORs. En route traffic must be separated by 5 miles laterally, or either 1,000 feet vertically below FL290 or 2,000 feet at and above FL290. The controller's responsibility is to move traffic safely and efficiently through the sector while maintaining at least the prescribed separation. The controller also attempts to accommodate the needs of individual aircraft by allowing them to climb or descend to more favorable altitudes, granting direct routes to selected fixes, and granting speed changes where possible. Safety is always the paramount goal for the controller and he/she will forego efficiency for safety when required.

Initial training for students with no prior experience is conducted at various FAA certified locations. One such location is the Minnesota Air Traffic Control Training Center which offers a six month class to give students the fundamentals necessary for FAA training. The FAA Academy located in Oklahoma City is responsible for training all air traffic controllers. The initial training is focused on learning the basics of the equipment that controllers use while performing their duties. The majority of the training is conducted through laboratory exercises as opposed to reviewing scenarios in a workbook. Controllers are presented with various types of simulated conflicts and are instructed on the proper procedures for resolving conflicts. This form of instruction allows the student to learn control techniques in the environment in which they will be applied.

2.2.2 Standard Operating Procedures And Letters Of Agreement

The Standard Operating Procedures (SOPs) and Letters Of Agreement (LOAs) for Atlanta Center were reviewed to gain an understanding of the standard traffic patterns and operational constraints for each sector that was analyzed in this study. These documents describe the physical boundaries, major fixes, and jet routes that aircraft typically use while navigating through the sectors. Additionally, the documents show the bounding flight levels for each sector and the adjacent sectors.

For this analysis, conflict resolution maneuvers that occur in over-flight sectors only were examined. This was done in an effort to isolate controller actions initiated to resolve conflicts from those actions initiated to transition arriving or departing aircraft or sequence arrivals. Table 2.1 summarizes the sectors and their corresponding flight levels for each of the sectors examined in this analysis.

Table 2.1 Selected Sectors

Sector	Name	Flight Levels
2	Gunter Ultra High	FL350 and above
8	Martin Lake Ultra High	FL350 and above
11	Monroeville High	FL240 - FL330
12	Birmingham	Surface - FL230
13	Montgomery	Surface - FL230
28	High Rock Ultra High	FL350 and above
32	Spartanburg High	FL240 - FL290
33	Charlotte High	FL240 - FL330
34	Georgia High	FL310 - FL330
36	Allatoona	FL350 and above
40	Blue Ridge Ultra High	FL350 and above

2.3 Methodology

The methodology applied to this analysis involved reviewing the SATORI scenarios for which adequate voice files existed and were of sufficient quality to gain an understanding of the types of maneuvers performed in the Atlanta Center. Since voice data exists for only one sector per scenario, the SATORI-based analysis was somewhat limited. However, since all of the information available to the controller was available in each scenario, this phase of the analysis yielded significant insight into the types of maneuvers that occur within the ARTCC. A set of data filters was subsequently developed to pre-process the large scenario track files to generate a list of aircraft that appear to have been maneuvered for traffic. The Conflict Analysis Resolution Display System (CARDS) was specifically developed to aid in the conflict maneuver detection and analysis phases of this study (see Appendix A). The SATORI data for these aircraft were loaded into CARDS for a complete analysis. After identifying aircraft that were maneuvered for traffic, a more detailed investigation of the maneuver was performed. Parameters associated with individual conflicts were measured including maximum deviation from the intended path.

2.3.1 Review of SATORI Scenarios

Table 2.2 summarizes the controller-issued traffic instructions for the seven scenarios containing voice files (single-sector scenarios). For each traffic instruction the scenario, aircraft ID, time of instruction, and an abbreviated transcription of the message are shown. Based upon the message text and a review of the scenario using SATORI, a determination of whether the traffic instruction was issued for conflict resolution or for other reasons was made and is shown in the last column.

Table 2.2 Voice Scenario Traffic Instructions

Scenario / Sector	Aircraft ID	Time (approx.)	Instruction	Maneuver Type
ztl_92e011/40	N370RR	151930	Direct Knoxville via radial	
	NWA1110	152540	Pilot requests FL330	
	NWA1110	152600	Direct ATL, FL330	
	Shake82	152624	20° left for traffic	vector
	NWA1110	152640	Maintain FL370	
	NWA1110	152817	FL330, hand-off	

Scenario / Sector	Aircraft ID	Time (approx.)	Instruction	Maneuver Type
ztl_92e012/33	AAL1062	205449	Climb FL310	
	AAL711	205630	FL310	
	AAL711	205725	Descend FL280 (because USA1498 requests FL290)	altitude change
	USA40	205756	Descend FL330	
	USA1042	205815	Descend FL330	
	USA392	205956	Descend FL330	
	DAL1149	210000	Climb FL240	
	DAL711	210100	Climb FL310	
	AAL494	210239	Climb FL240	
	DAL1149	210245	Climb FL260 (final)	
	DAL1149	210300	Expedite climb to FL260	altitude change
	AAL494	210340	FL310	
	AAL494	210450	345°	
	DAL1194	210452	Direct Foothills	
	AAL494	210610	Direct Charleston, RoRU	
ztl_92e102/33	N603GY	210050	Climb FL370, direct Flat Rock (from previous resolution)	
	UAL8050	210142	Mach .76 or less	speed change
	N769KL	210143	Mach .76 or greater	speed change
	DAL1509	210235	Climb FL310	
	EJA288	210850	Left to 200°, fly 059° radial to Spartanburg, descend to FL240	
ztl_93e027/33	ACA907	143918	Climb and maintain FL330	
	USA845	144045	Climb and maintain FL330	
	USA845	144149	Climb and maintain FL350	
	N120MH	144139	Climb and maintain FL290	
	AAL535	144249	Climb and maintain FL280	
	N120MH	144500	Maintain FL290	
	USA5	144612	Climb and maintain FL310	
	N120MH	144718	Turn left to 270°	
	UAL675	144824	Climb and maintain FL280	
	USA5	145138	Climb and maintain FL390	
ztl_94e028/28	DAL878	152740	Climb to FL370 in 3 mins or less	
	DAL878	152750	10° left for traffic	vector
	ACA982	153045	10° left for traffic	vector
	ACA982	153155	Cleared direct to Ormond Beach (rest of route unchanged)	
	DAL878	153200	Cleared direct Liberty (rest of route unchanged)	
	N29CL	153340	Descend to FL350 in 2 mins or less	

Scenario / Sector	Aircraft ID	Time (approx.)	Instruction	Maneuver Type
ztl_95e003/34	DAL1455	233450	Hold at alt. Traffic is at FL310	altitude change
	N24KL	233520	Traffic pointout (no vector)	
	N351N	233750	Climb FL310	
	DAL1455	233752	Climb FL330	
	DAL222	233845	Climb FL330	
	DAL32	234010	Climb FL330, mach .78 for spacing	
	DAL222	234050	Climb FL370	
	DAL32	234100	Maintain FL300	
	DAL32	234110	Maintain FL290	
	USA2150	234150	FL330	
	DAL32	234252	Climb FL330	
ztl_95e025/12	N920C	222330	Cross 30 NE of BHM at 11000	
	SWA359	222835	Descend and maintain 15000, then cross Vulcan at 110	
	SWA359	222922	Turn left to 190° vectors to parallel	
	N303P	223210	Turn left to 245°	
	SWA359	223215	Turn right to 240°	
	SWA359	223317	Proceed direct Vulcan	

The data reveals the types of commonly used instructions and relative frequencies of individual instructions. While this data set is not nearly large enough to provide a statistically significant basis to conduct the additional analysis, it does provide insight into the maneuvers themselves. The table shows that vectors range from 10 to 20 degrees, altitude changes are at least 1000 feet, and speed changes may involve more than one aircraft and are typically given as a maximum or minimum speed not to exceed. For this data set, all forms of conflict resolution maneuvers occur in sector 33 whereas only vectors occur in sector 40.

2.3.2 Data Reduction And Conversion

The SATORI track data contains radar-correlated positions sampled every six seconds for every aircraft in the ARTCC. Included in this data are the latitude, longitude, heading, assigned altitude, reported altitude, and ground speed at each radar-hit. Also included in the SATORI scenario files are the associated high and low intensity weather and a CRD file which contains a log of messages that are sent and received from the D (departure) position, and also a listing of the fixes for the entire ARTCC. These scenario files form the raw data set. It was then filtered and converted for analysis in CARDS.

Figure 2.1 depicts the various filter and conversion programs that were developed and used for this analysis. The WxConvert and wxToMATLAB programs filter and convert the scenario weather files into a specially formatted file that can then be directly loaded into CARDS. The ODFilter program combined with the ETP and convertToMATLAB programs search through the scenario files and select aircraft that have potentially been maneuvered via a vector or altitude change and create specially formatted files that are loaded into CARDS. A corresponding data filter for detecting speed changes was not developed because an examination of the data revealed that both relative and absolute changes in speed were not good indicators of speed-control as a conflict resolution maneuver. The aircraft speeds in scenarios varied by as much as 40 knots during normal flight. An aircraft speed change could easily be attributable to changes in wind speed and direction which were not available for this study. The *ODFilter* program attempts to extract origin, destination, and aircraft type information for aircraft contained in the scenario. The *allToMATLAB* program converts lists of candidate aircraft for use with the tool and the *fixToMATLAB* program converts fixes into a CARDS usable file.

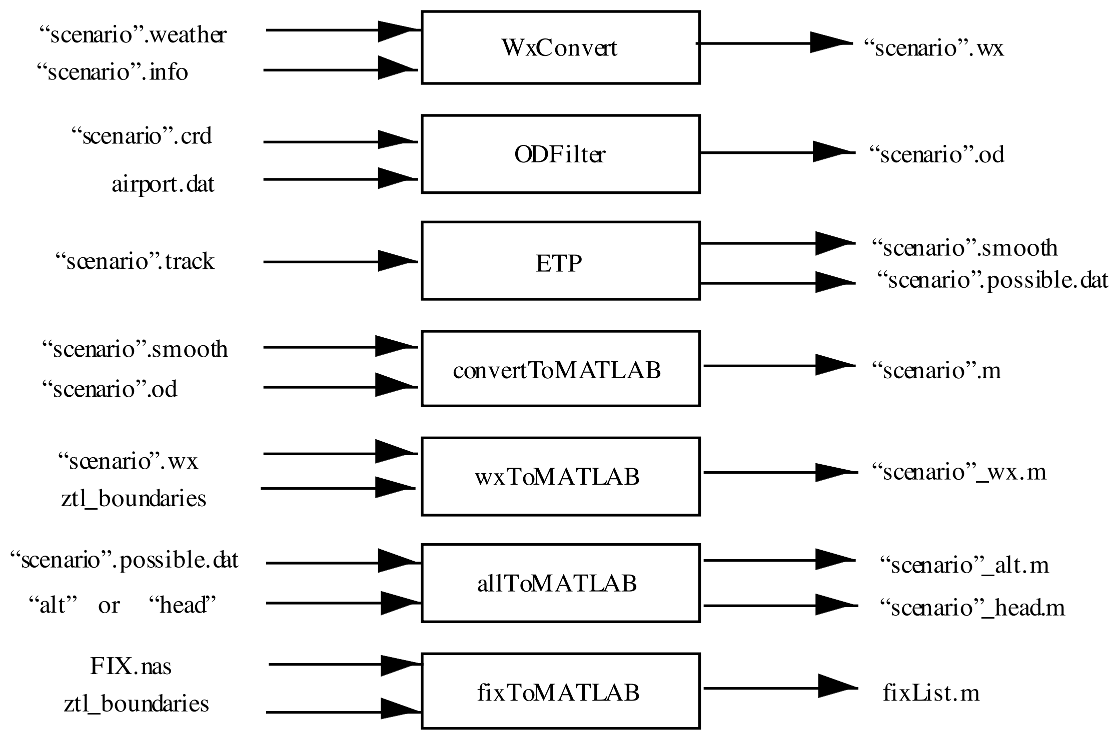

Figure 2.1 Scenario Conversion Programs

The ETP program uses a relative change in heading as an indicator that the aircraft has been vectored for traffic. The SATORI-based analysis indicated that when aircraft change heading, a nominal turn rate of 3 degrees per second is typically used which is consistent with a "standard rate" turn as defined in the Airman's Information Manual [5]. With a 3 degrees per second heading change and a 6 second sample rate, an aircraft undergoing a heading change because of a controller-issued instruction could exhibit up to an 18 degree heading change between successive radar hits. Only aircraft that fly at or above 10,000 feet were included in our analysis to eliminate possible transitioning aircraft from our sample set. The program requires as input a relative heading change threshold. For this analysis, the threshold was varied from 3 to 10 degrees and the number of candidate maneuvered aircraft were counted and subsequently examined to estimate the number of falsely identified maneuvered aircraft. A 3 degree threshold resulted in 328 candidates, a 5 degree threshold yielded 212 candidates, and a 10 degree threshold yielded only 82 candidates. A 5 degree threshold was used for this study because it effectively reduced the number of candidates while maintaining an acceptable false alarm rate. In addition to searching for vectored aircraft, the ETP program examines the assigned altitude in an attempt to select aircraft that have undergone altitude changes.

2.3.3 Conflict Resolution Maneuver Detection And Analysis

The CARDS tool was used in making the final determination that an aircraft was maneuvered as part of a conflict resolution strategy. The first step in this process was to examine the aircraft's heading vs. time, altitude vs. time, latitude vs. longitude, and ground speed vs. time plots. By examining these plots in CARDS, a subset of highly probable candidates for conflict resolution maneuvers were identified. Finally, the horizontal tracks and altitude profiles of aircraft under consideration were displayed along with neighboring traffic and altitude vs. time profiles. At the same time, airspace and operational constraints such as proximity to sector boundary and weather were assessed. Only scenarios where weather was not a constraint on maneuvers were considered in order to minimize the potential impact of this time varying constraint. CARDS provides the capability of displaying the high intensity weather for each scenario.

Conflict Resolution Maneuver Analysis Involving Altitude Assignments

The following example illustrates the process of aircraft maneuver detection and identification using CARDS for maneuvers involving temporary altitude assignments. Figure 2.2 depicts four plots; heading vs time, altitude vs. time, ground speed vs. time, and latitude vs. longitude for flight id VV2F180 which is contained in scenario ztl_93e005, sector 11. The heading vs. time plot shows that the aircraft was initially headed approximately due north (0 degrees as shown in plot). The aircraft was then vectored to a heading of approximately due west (270 degrees, -90 degrees as shown in plot) during the first two minutes of the scenario. At the same time the aircraft was vectoring it was climbing to FL260. The aircraft then initiated a climb to FL280 where it stayed for approximately 2 minutes and then climbed to FL330. The assigned altitude for this aircraft was FL350 and is also shown on this subplot. The ground speed vs. time plot shows the aircraft ground speed decreasing during the vector and climb from approximately 260 knots down to 210 knots, and then increasing to approximately 340 knots. The lower left plot shows the latitude and longitude of the aircraft originating from the middle right at the beginning of the scenario and ending at the left hand side at the end of the scenario.

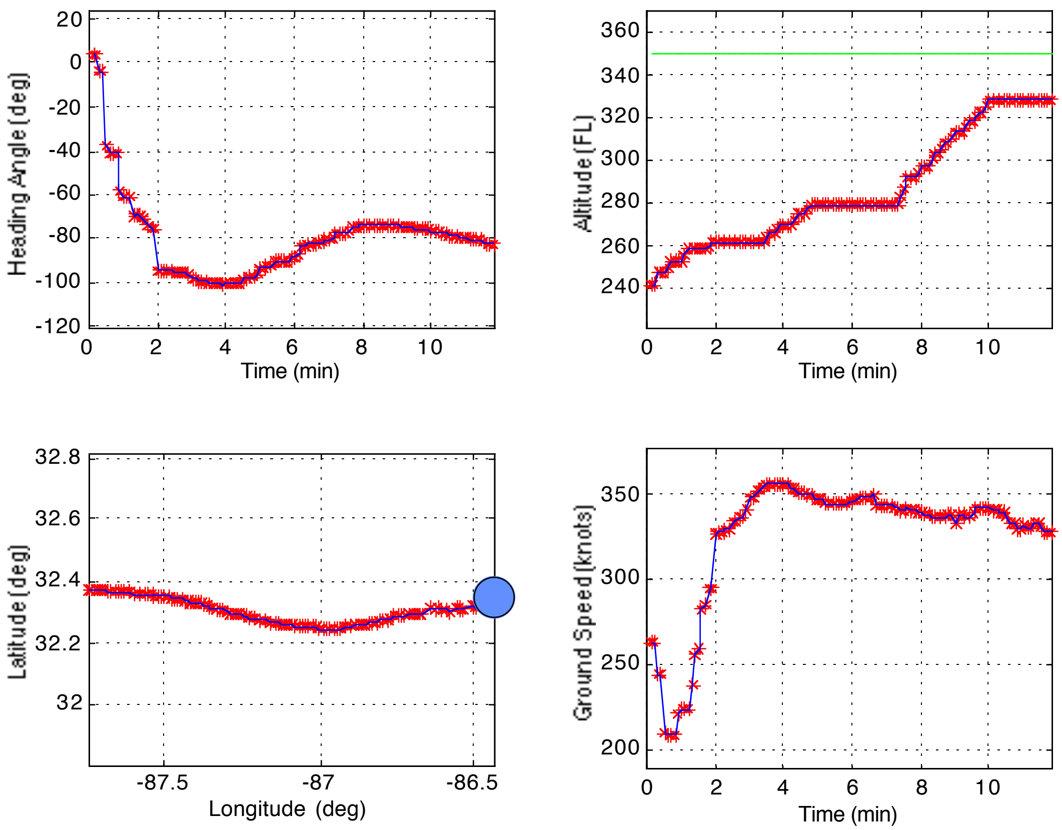

Figure 2.2 Time History Profiles For Flight ID VV2F180

Since this aircraft appears to have been maneuvered as part of a conflict resolution strategy as reinforced by the altitude vs. time plot, further investigation is required. In situations such as this, the tracks of neighboring traffic that this aircraft may have been in conflict with, or in any way constrained this aircraft's flight, would be investigated. In addition to knowing the location of neighboring aircraft, it is essential to know the intended path for the original aircraft in order to distinguish between conflict resolution maneuvers and normal route changes. The SATORI data does not provide flight plan information (such as origin, destination, aircraft type), for all aircraft. However, it is frequently possible to infer the intended path by displaying the fixes within the sector vicinity and comparing the aircraft's ground track with fixes. CARDS provides the capability for displaying fixes to aid in this analysis. The tool also provides the capability for displaying aircraft that are proximate to the aircraft in question at any time during their flights. Essentially, the tool computes the closest point of approach (CPA) for aircraft that occupy the sector. A vertical and horizontal filter are specified by the user and CARDS identifies aircraft that fall within these bounds.

Figure 2.3 depicts the neighboring traffic for flight id VV2F180. The figure shows two additional aircraft, USA270 and N12ST that are, at some time, proximate to VV2F180. For all three aircraft, the figure depicts the latitude and longitude at every radar-hit contained in the reformatted SATORI data. Additionally, the figure shows the scenario time (e.g. 0, 1, 2, ...) and the reported altitude (e.g. 290) adjacent to the tracks on a one minute interval to depict the spatial orientation of these aircraft. From these plots it is evident that both USA270 and N12ST cross the trajectory of VV2F180 and further investigation is required before a final determination can be made as to whether this scenario involves a controller issued conflict resolution maneuver.

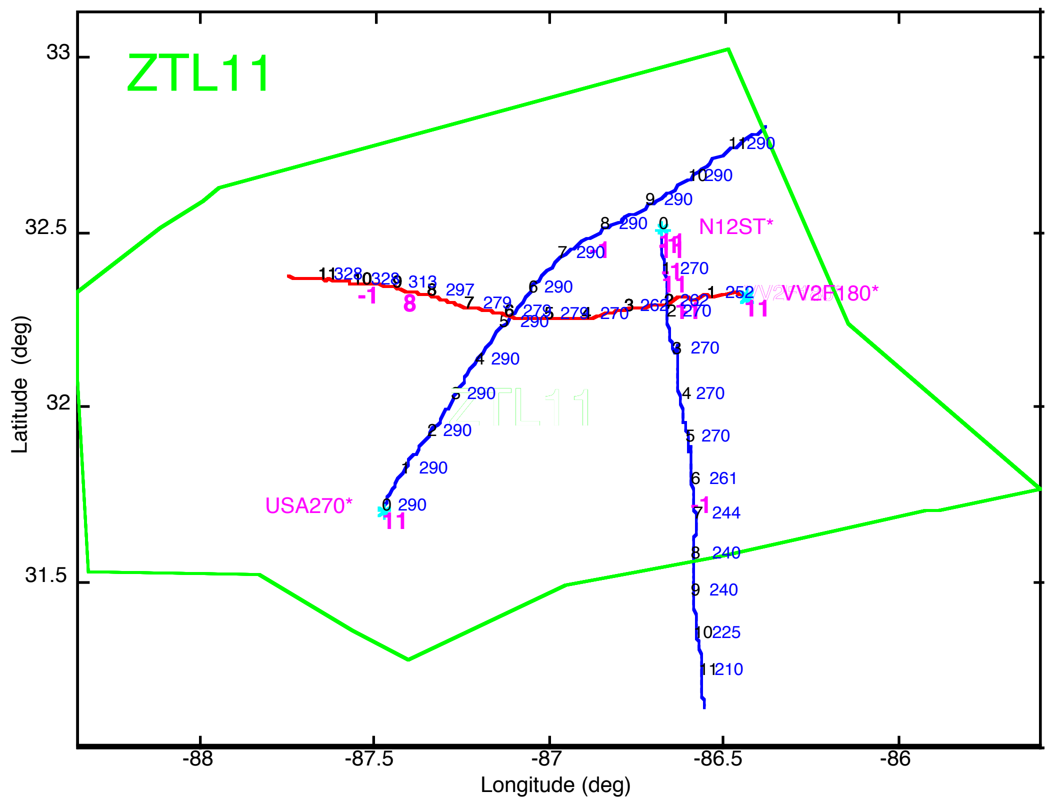

Figure 2.3 Neighboring Traffic Display For Flight ID VV2F180

Figure 2.4 depicts an altitude vs. time profile for the three aircraft that were previously identified as proximate. The plot shows the altitude bands for this sector being FL240 to FL350 (shaded gray lines) and the three aircraft. USA270 is maintaining level flight at its assigned altitude of FL290 for the entire scenario and is headed in the northeast direction (see Figure 3). VV2F180 is attempting to climb to its' assigned flight level, FL350 (dashed line), and at the same time, N12ST is descending to its' assigned flight level (FL240). By examining Figures 2.3 and 2.4, the final determination was made that VV2F180 was held by the controller at FL260 and FL280 as part of two conflict resolution maneuvers.

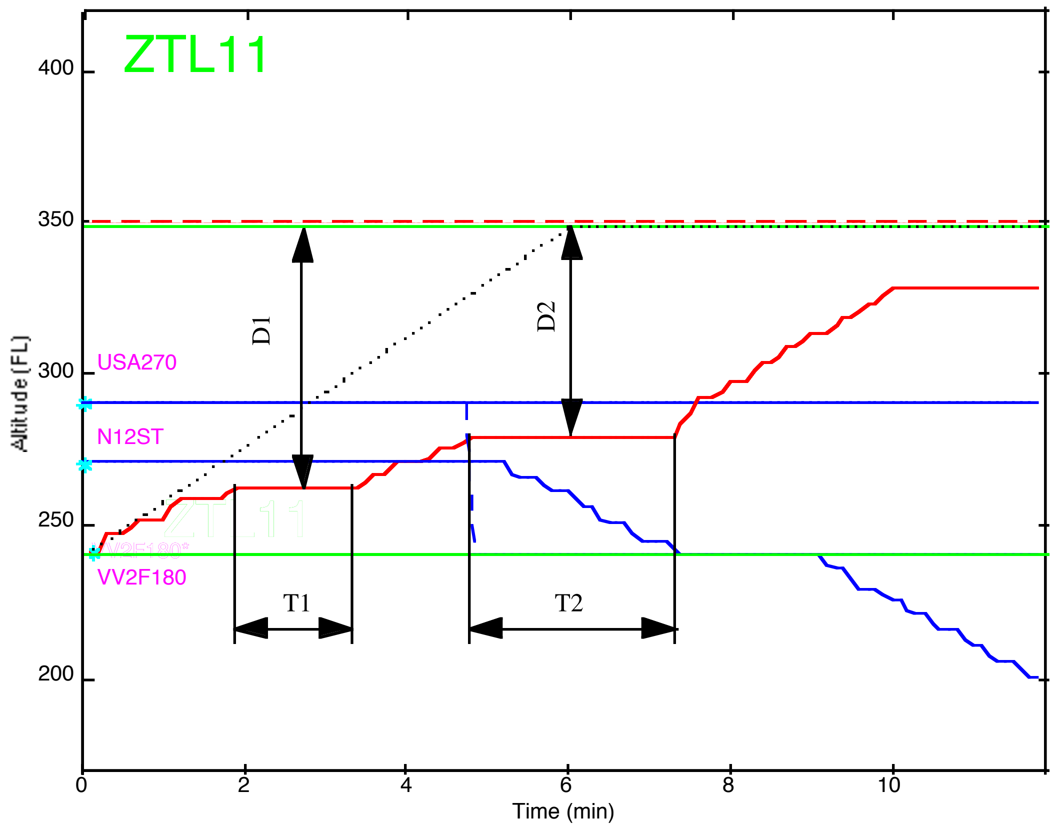

Figure 2.4 Altitude Profile For Flight ID VV2F180 & Proximate Aircraft

After identifying the type of maneuver utilized, an analysis of the associated parameters of the maneuver was performed including measuring the maximum deviation from intended path. For this type of maneuver, the maximum deviation from intended path can be described as the length of time the aircraft was held at the intermediate flight level (times T1 and T2 shown in Figure 2.4). The difference between assigned and intermediate or temporary flight levels are also used and are shown as D1 and D2. Since CARDS stores the time, latitude, longitude, and altitude information for every flight in the scenario, extracting this data is easily accomplished.

Conflict Resolution Maneuver Analysis Involving Heading Changes

The previous section discussed the process of identifying a conflict resolution maneuver involving altitude changes or temporary altitude assignments. This was performed by first examining the time history profiles for the flight that was investigated and then examining both the neighboring traffic display and the altitude profiles for proximate aircraft. In contrast, when identifying aircraft that were maneuvered using a heading change or vector, the neighboring traffic display is usually sufficient to make the final determination. Figure 2.5 depicts a scenario occurring in sector 33 where both aircraft are in level flight (FL350). The first aircraft, N78AM, is headed in the northeast direction and the second aircraft, USA269, is headed in the southwest direction. The CARDS tool provides a track extrapolation feature which allows the user to generate a pseudo-track based upon a user-input starting point and user-input track extrapolation time. After converting the user-input starting point to the track index, CARDS computes a pseudo-track based upon an average of the previous six heading and speed values. Averaging multiple heading and speed data points was necessary to reduce the noise inherent within the data. By visually comparing the original and user-generated pseudo-track, a determination as to whether the aircraft was vectored can usually be made. CARDS also provides the capability for computing the distance between any two points on the display. This allows the user to estimate whether a loss of horizontal separation could have occurred if the aircraft had not been vectored.

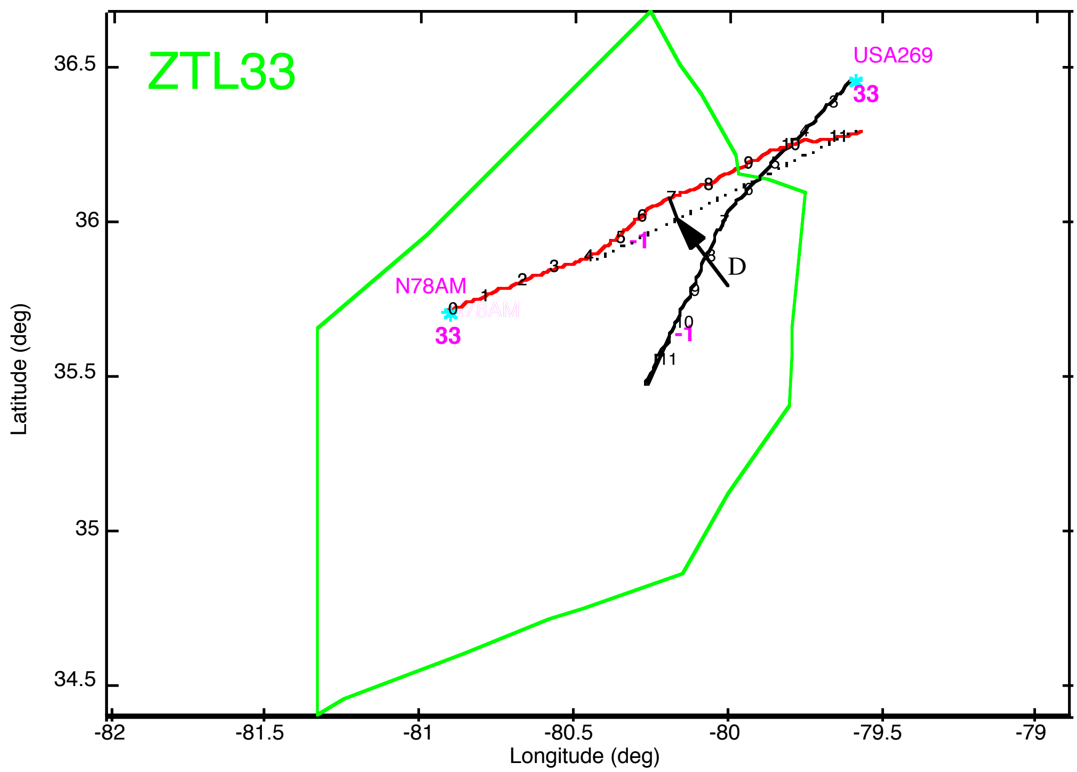

Figure 2.5 Neighboring Traffic Display For Flight ID N78AM

After making the determination that the aircraft was vectored, the appropriate parameters for this maneuver type are measured. These parameters include the conflict geometry and the maximum deviation from intended path. In this case, the maximum deviation is expressed as the angle of the vector, the maximum horizontal offset, and additional distance flown. The total duration of the maneuver is also measured. CARDS provides the capability for directly measuring all of these parameters.

0Conflict Resolution Maneuver Analysis Involving Speed Controls

The previous two sections discussed the techniques for identifying and analyzing altitude changes and heading changes as conflict resolution maneuvers. These techniques work very well on the existing data sets because data filters could be developed to accurately detect these types of maneuvers. As previously discussed, we were unsuccessful in developing a filter that could accurately detect aircraft ground speed changes in the SATORI data that were indicators of speed-control as a conflict resolution strategy. However, after analyzing the data using the two previous techniques, we identified cases where aircraft were not apparently involved in a conflict resolution maneuver that used either an altitude change or heading change but still exhibited very low closest points of approach. In addition, there were cases where aircraft were clearly traveling on the same route, maintaining the same speed, and remaining at a constant distance apart. In these cases, speed-control is most likely being applied to ensure separation.

Figure 2.6 depicts a scenario in sector 33 where two aircraft are traveling in the northeast direction at approximately the same speed and are at the same altitude (FL330). The trajectory of the first aircraft, UAL8050, crosses the trajectory of the second aircraft, N769K, at approximately 6.5 minutes into the scenario. The closest point of approach for these aircraft is 8.5 nmi. In this situation there is still some uncertainty that a speed-control was issued to either aircraft.

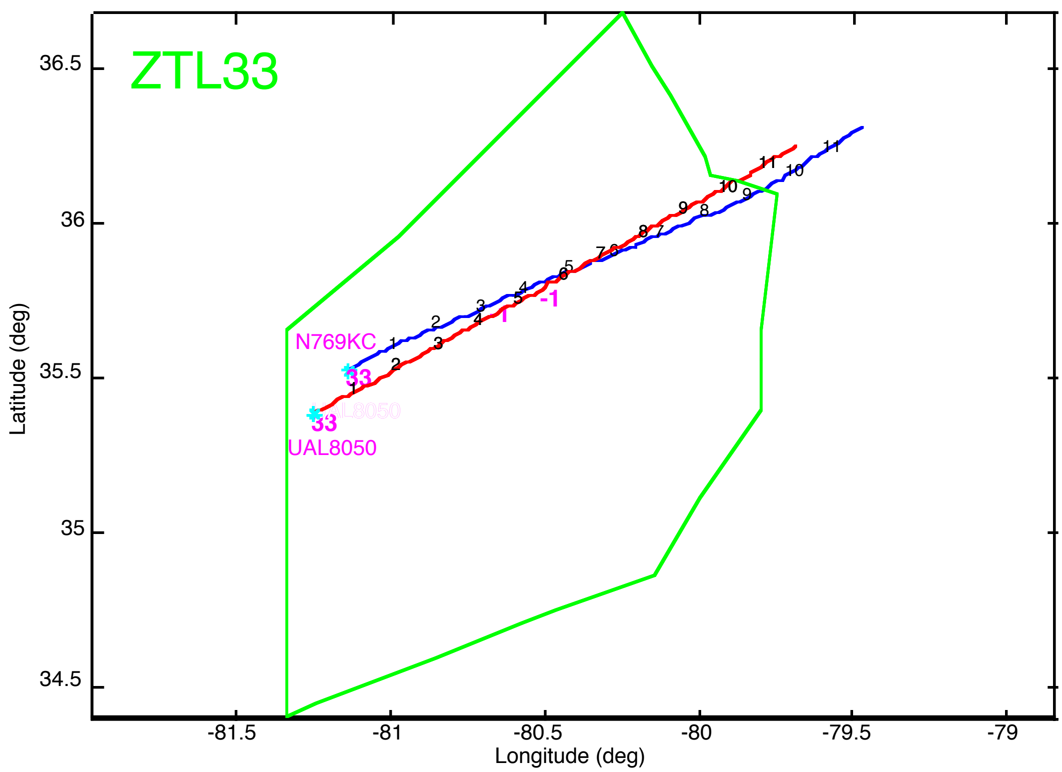

Figure 2.6 Neighboring Traffic Display For Flight ID UAL8050

Figure 2.7 displays the speed vs. time for the previously identified aircraft UAL8050 and N769K. This plot shows that for approximately the first minute of the scenario, UAL8050 is traveling about 15 knots faster than N769K, 475 knots vs. 460 knots. For the next 9 minutes, these aircraft are traveling at nearly the same speed, 470 knots. And for the last two minutes, UAL8050 maintains a speed of 470 knots, whereas N769KC decreases its speed to 455 knots From this plot a determination that a speed-control was issued to both aircraft can be inferred. After drawing this conclusion, the parameters associated with the conflict geometry and maximum deviation from intended path are extracted from the scenario. The maximum deviation from intended path is expressed as the time that the aircraft were directed to maintain the speed, and a percentage speed change which is computed by dividing the speed change by the original speed.

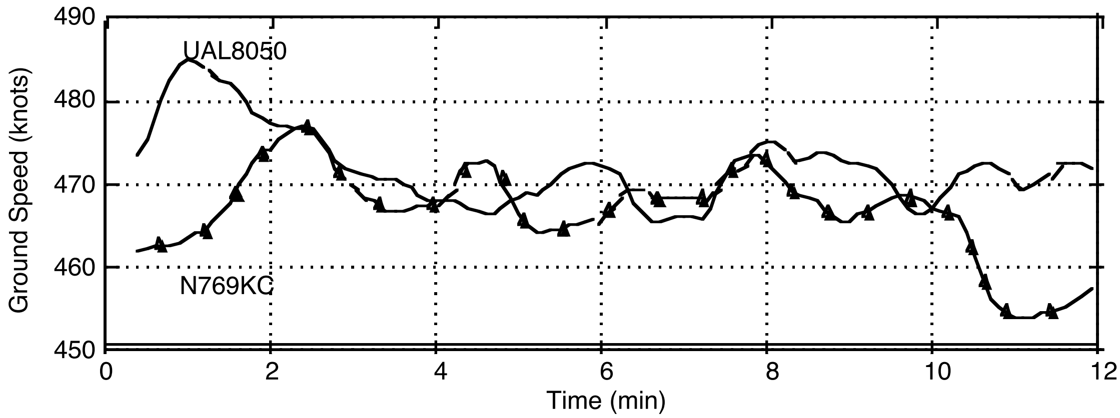

Figure 2.7 Ground Speed For Flight ID's UAL8050 & N769KC

2.4 Results

The analysis methodology as previously explained was applied to the SATORI data sets to produce the results described in the following sections. The first section provides a summary and discussion of the observed conflict maneuvers including an analysis of the relative frequencies of types of maneuvers and the associated significance. The next section discusses an analysis performed on the data to investigate the closest point of approach before and after the conflict resolution maneuver was removed, and a comparison between sectors and sector types. Finally, a discussion of the deviation from intended path and a comparison of conflict rates between sectors is provided.

2.4.1 Conflict Resolution Maneuver Summary

Table 2.3 provides a summary of the conflict resolution maneuvers identified in the SATORI data sets. The table contains 57 unique conflict scenarios involving 2 or more aircraft that were detected and analyzed using the CARDS tool. For each conflict scenario the associated parameters were extracted and analyzed. As shown in the table, the data is arranged by conflict information, geometry, and resolution parameters. Conflict information includes sector number, sector type, conflict pair, aircraft type when available, and phase of flight. The IDs of aircraft that were maneuvered are always shown first and in bold style. The conflict geometry includes the relative speed V (knots), crossing angle ψ (deg), closest point of approach with the conflict resolution maneuver removed (nmi), time before closest point of approach, CPA with conflict resolution maneuver, and the location of the conflict (e.g. latitude λ (deg), longitude μ (deg), altitude h (FL), and time offset start (min)).

Conflict resolution parameters include resolution method (e.g. parallel offset, altitude change, vector, or speed change) and deviation from intended path. For a conflict resolution maneuver classified as a parallel offset, the associated parameters are D, L, A, and T where D is defined as the maximum offset from the intended path, L is the difference between the distances flown along the intended and actual paths, A is the maximum heading change for the maneuver, and T is duration of the maneuver. The parameters associated with a speed-control conflict resolution maneuver are the speed that the aircraft are directed to maintain, the percentage difference in the speed Δ, and the time the directed speeds were maintained, T. The speed shown is either a ground speed or a mach number. In cases where the initial speed is unknown, the difference in speed cannot be computed and is not shown. Similarly, there are several cases where the time cannot be computed because the scenario ended before the conflict resolution maneuver was completed. For conflict resolution maneuvers classified as vectors, the only parameter is the maximum heading change, A.

The associated parameters for a conflict resolution maneuver containing a temporary or new altitude are the actual flight level either temporary or new, the assigned flight level which is shown in parenthesis, and the time spent at the intermediate flight level, T. In some cases, multiple assigned flight levels are shown indicating an updated flight plan. In other cases, the time or actual altitude have not been included because the scenario ended before the conflict resolution maneuver was completed or the aircraft was already in climb or descent. The final type of conflict resolution maneuver included in this table is a combination of altitude and vector wherein both sets of associated parameters have been included. In cases where the parameters associated with the conflict cannot be obtained because of missing data, the appropriate fields in the table have been left blank or have been assigned a value of “N/A”.

Table 2.3 Conflict Summary

Information					Geometry			Resolution Parameters	
#	Sector (Type)	Conflict Pair	Aircraft Type	Attitude	Relative Speed, Crossing Angle	CPA w/o Res, Time before it, CPA w. Res	Proximity Event Location	Resolution Method	Deviation from Intended Path
1	11 (H)	**USA844** UAL1214	**-** -	**Descent** Cruise	V=40 knots Ψ=10 deg	9 nmi 3 min 10 nmi	λ=32.0 deg μ=-86.75 deg h=330 FL t=5 min	Parallel Offset	D=7 nmi L=4 nmi A=20 deg T=8 min
2	11 (H)	**DAL1582** UAL521	**-** B757 (Large)	**Descent** Climb	V=920 knots Ψ=175 deg	17 nmi 0.5 min 31 nmi	λ=32.1 deg μ=-88.15 deg h=327 FL t=8 min	Altitude	Hold descent FL310 (330/290)
3	11 (H)	**UAL521** DAL1582	**B757** **(Large)** -	**Climb** Descent	V=920 knots Ψ=175 deg	17 nmi 0.5 min 31 nmi	λ=32.1 deg μ=-88.15 deg h=327 FL t=8 min	Altitude	Hold climb (310/350)
4	28 (UH)	**PACER91** LN22BM	**C21** **(Large)** -	**Climb** Cruise	V=440 knots Ψ=87 deg	9.5 nmi 3 min N/A	λ=35.0 deg μ=-81.85 deg h=410 FL t=11 min	Altitude	FL390 (410)
5	40 (UH)	**SHAKE82** NWA1110	**-** -	**Cruise** Descent	V=40 knots Ψ=5 deg	1.5 nmi 0.5 min N/A	λ=36.15 deg μ=-84.05 deg h=368 FL t=11 min	Vector	A=20 deg
6	40 (UH)	**NWA1110** SHAKE82	**-** -	**Descent** Cruise	V=40 knots Ψ=5 deg	1.5 nmi 0.5 min N/A	λ=36.15 deg μ=-84.05 deg h=368 FL t=11 min	Altitude	Maintain FL370 (370/330)

Information					Geometry			Resolution Parameters	
#	Sector (Type)	Conflict Pair	Aircraft Type	Attitude	Relative Speed, Crossing Angle	CPA w/o Res, Time before it, CPA w. Res	Proximity Event Location	Resolution Method	Deviation from Intended Path
7	33 (H)	**COA1043** VVLP492	**B727 (Large)** -	**Descent** Cruise	V=75 knots Ψ=0 deg	1.25 nmi 0 min 9.5 nmi	λ=36.3 deg μ=-79.55 deg h=310 FL t=0 min	Altitude	Hold descent FL350 (310)
8	33 (H)	**DAL1149** N5SY	**-** -	**Climb** Cruise	V=600 knots Ψ=140 deg	3 nmi 2 min 7nmi	λ=36.0 deg μ=-81.25 deg h=250 FL t=10 min	Altitude	Expedite climb (260)
9	28 (UH)	**USA1042** USA40	**-** -	**Cruise** Cruise	- Ψ=0 deg	22 nmi - 22 nmi	- - h=370 FL -	Speed	V=460 knots (FL370), 480 knots (FL330)
10	28 (UH)	**USA40** USA1042	**-** -	**Cruise** Cruise	- Ψ=0 deg	22 nmi - 22 nmi	- - h=370 FL -	Speed	V=460 knots (FL370), 480 knots (FL330)
11	28 (UH)	**USA1101** USA859	**-** -	**Cruise** Cruise	V=10 knots Ψ=10 deg	13 nmi 1 min 13 nmi	λ=36.05 deg μ=-80.0 deg h=350 FL t=8 min	Speed	V=430 knots Δ=-3.5%
12	28 (UH)	**USA859** USA1101	**-** -	**Cruise** Cruise	V=10 knots Ψ=10 deg	13 nmi 1 min 13 nmi	λ=36.05 deg μ=-80.0 deg h=350 FL t=8 min	Speed	V=430 knots Δ=-4.7%
13	28 (UH)	**N754G** N753G	**HS25 (Large)** -	**Cruise** Cruise	- Ψ=0 deg	12 nmi - 12 nmi	- - h=390 FL -	Speed	V=315 knots
14	28 (UH)	**N753G** N754G	**-** HS25 (Large)	**Cruise** Cruise	- Ψ=0 deg	12 nmi - 21 nmi	- - h=390 FL -	Speed	V=315 knots
15	28 (UH)	**USA665** USA518	**-** -	**Cruise** Cruise	- Ψ=0 deg	14 nmi - 14 nmi	- - h=390 FL -	Speed	V=470 knots

Information					Geometry			Resolution Parameters	
#	Sector (Type)	Conflict Pair	Aircraft Type	Attitude	Relative Speed, Crossing Angle	CPA w/o Res, Time before it, CPA w. Res	Proximity Event Location	Resolution Method	Deviation from Intended Path
16	28 (UH)	**USA518** USA665	**-** -	**Cruise** Cruise	- Ψ=0 deg	14 nmi - 14 nmi	- - h=390 FL -	Speed	V=470 knots
17	33 (H)	**EJA288** N804CT	**-** -	**Descent** Cruise	V=460 knots Ψ=110 deg	5 nmi - 5 nmi	λ=36.45 deg μ=-80.2 deg h=270 FL t=10 min	Altitude	Hold descent FL280 (280/240)
18	33 (H)	**N603GY** N400KV	**-** -	**Climb** Climb	V=590 knots Ψ=120 deg	8.5 nmi 3 min N/A	λ=36.15 deg μ=-80.75 deg h=330 FL t=5 min	Altitude	Climb to a new FL (290/360) T=4 min
19	33 (H)	**UAL8050** N769KC	**B73S** **(Large)** N265 (Large)	**Cruise** Cruise	V=5 knots Ψ=5 deg	8.5 nmi 4 min 8.5 nmi	λ=35.9 deg μ=-80.4 deg h=350 FL t=6 min	Speed	V=475 knots Δ=-2.5% T=8 min
20	33 (H)	**N769KC** UAL8050	**N265** **(Large)** B73S (Large)	**Cruise** Cruise	V=5 knots Ψ=5 deg	8.5 nmi 4 min 8.5 nmi	λ=35.9 deg μ=-80.4 deg h=350 FL t=6 min	Speed	V=475 knots Δ=+2.5% T= 8 min
21	2 (UH)	**DCBMW** MANGO1	**-** -	**Cruise** Cruise	V=160 knots Ψ=25 deg	13 nmi 8 min 13.5 nmi	λ=33.3 deg μ=-86.25 deg h=350 FL t=14 min	Vector	A=40 deg
22	11 (H)	**VV2F180** N12ST	**-** -	**Climb** Cruise	V=330 knots Ψ=90 deg	2 nmi 1 min 14 nmi	λ=32.25 deg μ=-86.65 deg h=270 FL t=2 min	Altitude	FL260 (350) T=1.75 min
23	11 (H)	**VV2F180** USA270	**-** -	**Climb** Cruise	V=100 knots Ψ=55 deg	5.5 nmi 0.5 min 22 nmi	λ=32.2 deg μ=-87.1 deg h=290 FL t=5 min	Altitude	FL280 (350) T=2.5 min
24	11 (H)	**COA516** DAL1088	**B73S** **(Large)** -	**Cruise** Cruise	- Ψ=0 deg	17 nmi - 17 nmi	- - h=330 FL -	Speed	V=500 knots
25	11 (H)	**DAL1088** COA516	**-** B73S (Large)	**Cruise** Cruise	- Ψ=0 deg	17 nmi - 17 nmi	- - h=330 FL -	Speed	V=500 knots

Information					Geometry			Resolution Parameters	
#	Sector (Type)	Conflict Pair	Aircraft Type	Attitude	Relative Speed, Crossing Angle	CPA w/o Res, Time before it, CPA w. Res	Proximity Event Location	Resolution Method	Deviation from Intended Path
26	33 (H)	**USA256** TWA714	**-** -	**Cruise** Cruise	V=180 knots Ψ=50 deg	7.5 nmi 8 min 16.5 nmi	λ=35.6 deg μ=-80.8 deg h=330 FL t=10 min	Vector	A=20 deg
27	28 (UH)	**N496SW** DAL215	**-** -	**Descent** Cruise	V=720 knots Ψ=160 deg	13 nmi - 13 nmi	λ=36.25 deg μ=-79.5 deg h=370 FL t=8 min	Altitude	FL370(310)
28	32 (H)	**DAL1549** EWW105	**-** DC8S (Heavy)	**Climb** Cruise	V=10 knots Ψ=0 deg	11 nmi 1 min N/A	λ=34.5 deg μ=-82.75 deg h=310 FL t=7 min	Altitude	FL280(330)
29	32 (H)	**DAL1298** DAL1549	**-** -	**Climb** Cruise	V=15 knots Ψ=0 deg	18 nmi - 18 nmi	λ=34.6 deg μ=-82.75 deg h=290 FL t=10 min	Speed	V=475 knots
30	2 (UH)	**NWA575** COA1193	**-** -	**Cruise** Cruise	V=480 knots Ψ=100 deg	9 nmi 7 min 18 nmi	λ=34.4 deg μ=-86.7 deg h=350 FL t=11 min	Vector	A=35 deg
31	32 (H)	**N105BG** TWA714	**-** -	**Climb** Cruise	V=440 knots Ψ=90 deg	2.7 nmi 1 min N/A	λ=34.45 deg μ=-82.7 deg h=270 FL t=12 min	Altitude	FL260(280)
32	2 (UH)	**AAL1972** N341AP	**-** -	**Climb** Cruise	V=95 knots Ψ=30 deg	6 nmi - 11 nmi	λ=33.7 deg μ=-86.8 deg h=370 FL t=0 min	Altitude	FL350(370)
33	36 (UH)	**DAL816** SWIFT52	**B727 (Large)** -	**Cruise** Cruise	V=460 knots Ψ=90 deg	7 nmi 4 min 18 nmi	λ=34.65 deg μ=-84.65 deg h=350 FL t=4 min	Parallel Offset	D=5.5 nmi L=4 nmi A=20 deg T=8 min
34	32 (H)	**COA1610** MACE01	**B73S (Large)** F16 (Large)	**Descent** Cruise	V=405 knots Ψ=90 deg	7 nmi 0.5 min N/A	λ=34.7 deg μ=-81.6 deg h=250 FL t=10.5 min	Altitude	FL260(250)
35	40 (UH)	**KIA42** COA1775	**-** -	**Cruise** Cruise	V=450 knots Ψ=90 deg	6.5 nmi 7 min 10 nmi	λ=34.9 deg μ=-84.8 deg h=350 FL t=7 min	Vector	A=15 deg

Information					Geometry			Resolution Parameters	
#	Sector (Type)	Conflict Pair	Aircraft Type	Attitude	Relative Speed, Crossing Angle	CPA w/o Res, Time before it, CPA w. Res	Proximity Event Location	Resolution Method	Deviation from Intended Path
36	40 (UH)	**AMT426** COA1775	**-** -	**Cruise** Cruise	V=450 knots Ψ=90 deg	7 nmi 5 min 16.5 nmi	λ=34.75 deg μ=-85.0 deg h=350 FL t=10 min	Vector	A=25 deg
37	32 (H)	**DAL1209** NWA890	**-** -	**Climb** Cruise	V=700 knots Ψ=120 deg	3 nmi 2.5 min 25 nmi	λ=34.4 deg μ=-83.0 deg h=290 FL t=6 min	Altitude	FL280(290) T=5 min
38	33 (H)	**USA5** DAL952	**-** -	**Climb** Cruise	V=750 knots Ψ=120 deg	16 nmi 2 min N/A	λ=34.8 deg μ=-81.0 deg h=350 FL t=12 min	Altitude	FL310(390) T=4.5 min
39	33 (H)	**USA845** ACA907	**-** -	**Climb** Climb	V=880 knots Ψ=170 deg	5 nmi 2 min 40 nmi	λ=35.7 deg μ=-80.8 deg h=350 FL t=2 min	Altitude	FL280(350)
40	33 (H)	**ACA907** USA142	**-** -	**Climb** Climb	V=200 knots Ψ=60 deg	- - 27 nmi	- - h=350 FL -	Altitude	FL310(330)
41	33 (H)	**N120MH** N162W	**-** -	**Climb** Cruise	V=360 knots Ψ=90 deg	8 nmi 5 min 16 nmi	λ=35.6 deg μ=-81.3 deg h=310 FL t=12 min	Altitude+ Vector	FL290(310) T=7 min A=35 deg
42	36 (UH)	**USA1507** AAL1365	**-** -	**Cruise** Cruise	V=410 knots Ψ=90 deg	4.5 nmi 4 min 19 nmi	λ=35.2 deg μ=-84.6 deg h=350 FL t=12 min	Parallel Offset	D=6 nmi L=3 nmi A=10 deg T=7 min
43	36 (UH)	**AAL1365** USA1507	**-** -	**Cruise** Cruise	V=410 knots Ψ=90 deg	4.5 nmi 9 min 19 nmi	λ=35.2 deg μ=-84.6 deg h=350 FL t=12 min	Vector	A=20 deg
44	2 (UH)	**TWA324** DAL837	**-** -	**Climb** Cruise	V=30 knots Ψ=5 deg	17 nmi 2 min 20 nmi	λ=35.6 deg μ=-86.25 deg h=370 FL t=6 min	Altitude+ Vector	FL365(370) T=2 min A=10 deg
45	36 (UH)	**COA129** AAL695	**-** MD80 (Large)	**Cruise** Cruise	V=595 knots Ψ=115 deg	7 nmi 6 min 21 nmi	λ=34.85 deg μ=-84.2 deg h=350 FL t=10 min	Vector	A=25 deg

Information					Geometry			Resolution Parameters	
#	Sector (Type)	Conflict Pair	Aircraft Type	Attitude	Relative Speed, Crossing Angle	CPA w/o Res, Time before it, CPA w. Res	Proximity Event Location	Resolution Method	Deviation from Intended Path
46	11 (H)	**LN415LJ** AAL1280	**-** -	**Climb** Cruise	V=700 knots Ψ=150 deg	8 nmi 1 min 24 nmi	λ=31.4 deg μ=-87.4 deg h=330 FL t=9 min	Altitude	FL310(390) T=2 min
47	11 (H)	**N293PC** COA464	- MD80 (Large)	**Climb** Cruise	V=110 knots Ψ=0 deg	8 nmi 3 min N/A	λ=32.6 deg μ=-85.7 deg h=330 FL t=14 min	Altitude	FL270 (330/270)
48	32 (H)	**DAL1969** USA1085	**-** -	**Descent** Climb	V=865 knots Ψ=180 deg	5 nmi 2 min 20 nmi	λ=34.85 deg μ=-82.15 deg h=265 FL t=4 min	Altitude	FL270(290) T=2 min
49	32 (H)	**USA1085** DAL1969	**-** -	**Climb** Descent	V=865 knots Ψ=180 deg	5 nmi 1 min 20 nmi	λ=34.85 deg μ=-82.15 deg h=265 FL t=4 min	Altitude	FL260(290) T=1.5 min
50	28 (UH)	**AMX405** USA1111	**DC10 (Heavy)** -	**Cruise** Cruise	V=460 knots Ψ=90 deg	7.5 nmi 9 min 21 nmi	λ=35.4 deg μ=-81.7 deg h=350 FL t=11 min	Parallel Offset	D=18 nmi L=12 nmi A=30 deg T=16 min
51	34 (H)	**N375SC** USA1731	**-** -	**Climb** Cruise	V=800 knots Ψ=160 deg	2.5 nmi 3 min 30 nmi	λ=35.7 deg μ=-81.9 deg h=330 FL t=5 min	Parallel Offset	D=13 nmi L=7 nmi A=35 deg T=11 min
52	33 (H)	**N78AM** USA269	**C560 (Large)** B73F (Large)	**Climb** Cruise	V=740 knots Ψ=150 deg	4.7 nmi 3 min 9.7 nmi	λ=36.0 deg μ=-80.05 deg h=330 FL t=7 min	Parallel Offset	D=4 nmi L=3 nmi A=20 deg T=7 min
53	28 (UH)	**ACA982** DAL878	**-** -	**Cruise** Climb	V=870 knots Ψ=130 deg	6 nmi 0.5 min 12.7 nmi	λ=35.3 deg μ=-80.7 deg h=390 FL t=6.5 min	Parallel Offset	D=1.5 nmi L=1 nmi A=10 deg T=5 min
54	28 (UH)	**DAL878** ACA982	**-** -	**Cruise** Climb	V=870 knots Ψ=130 deg	6 nmi 3 min 12.7 nmi	λ=35.3 deg μ=-80.7 deg h=390 FL t=6.5 min	Parallel Offset	D=4.5 nmi L=3 nmi A=10 deg T=8 min
55	28 (UH)	**N29CL** N78AM	**WW24 (Large)** C560 (Large)	**Descent** Cruise	V=780 knots Ψ=155 deg	1.5 nmi 1 min 1.5 nmi	λ=36.2 deg μ=-79.8 deg h=330 FL t=10 min	Altitude	Expedite climb to FL350(350)

Information					Geometry			Resolution Parameters	
#	Sector (Type)	Conflict Pair	Aircraft Type	Attitude	Relative Speed, Crossing Angle	CPA w/o Res, Time before it, CPA w. Res	Proximity Event Location	Resolution Method	Deviation from Intended Path
56	34 (H)	**DAL1455** N24KL	**-** -	**Climb** Cruise	V=880 knots Ψ=145 deg	5 nmi 1 min 40 nmi	λ=34.25 deg μ=-82.4 deg h=300 FL t=4 min	Altitude	FL287(350) T=3 min
57	34 (H)	**DAL32** DAL124	**-** L101 (Heavy)	**Climb** Climb	- Ψ=0 deg	10 nmi - 10 nmi	- - - -	Speed	V=560 knots (M=0.78) T=4 min

Of the 57 identified conflict resolution maneuvers, 14 involve speed changes, 25 involve altitude changes, 8 involve parallel offsets, 8 involve vectors, and only 2 involve a combination of altitude and vector. A comparison of the total number of maneuvers for each sector is shown in Table 2.4. The table shows that sectors 8, 12, 13 contain no detectable conflict resolution maneuvers. Sectors 12 and 13 are both low sectors that contain significant transitioning aircraft that have been excluded from this study by the altitude cutoff filter which was set at 10,000 feet. Sector 8 is an ultra-high sector that contained a small number of aircraft occupying a large sector. The remaining sectors contain a mix of resolution maneuver types ranging from vectors only, as occurs in sector 36, to all maneuver types, which occur in sector 33. Sector 28 contained the highest number of total maneuvers, 14, of which 8 were speed-controls. With the limited number of conflict resolution maneuvers for each sector, it is not possible to draw any statistically significant conclusions regarding the use of a specific maneuver type for a given sector; however, a relative comparison can be performed. For example, sector 28 does appear to have a greater total number of conflict resolution maneuvers as compared to sector 34 (14 vs. 3).

Table 2.4 Statistical Summary Of Conflict Maneuvers

Sector Number	Speed	Altitude	Vector	Parallel Offset	Altitude & Vector	Total
2	0	1	2	0	1	4
8	0	0	0	0	0	0
11	2	6	0	1	0	9
12	0	0	0	0	0	0
13	0	0	0	0	0	0
28	8	3	0	3	0	14
32	1	6	0	0	0	7
33	2	7	1	1	1	12
34	1	1	0	1	0	3

36	0	0	2	2	0	4
40	0	1	3	0	0	4
Total	**14**	**25**	**8**	**8**	**2**	**57**
Mean	**1.3**	**2.3**	**0.7**	**0.7**	**0.2**	**5.2**
Std Dev	**2.4**	**2.8**	**1.1**	**1.0**	**0.4**	**4.8**

2.4.2 Closest Point Of Approach Analysis

A Closest Point of Approach (CPA) analysis was performed by comparing the CPA before and after the conflict resolution maneuver was removed for each of the sector types (e.g. low, high, ultra-high). The CPA analysis used the altitude separation guidelines previously discussed as a rejection criteria for individual aircraft pairs. For example, if both aircraft are below FL290 and are separated by at least 700 feet vertically, they are not considered to be a conflict pair and their computed horizontal separation is not included. Similarly, if both aircraft are above FL290 and are separated by at least 1700 feet vertically, they are not considered to be a conflict pair and are not included either.

Figure 2.8 depicts a CPA histogram for aircraft pairs contained in the low sectors (e.g. 12 and 13) that are not altitude separated. The histogram shows the CPA ranging from 0 to 25 nautical miles in one mile bins. The figure shows a total of 3 aircraft pairs, two in the 18 nmi bin and one in 20 nmi bin. The figure also shows the same number of conflict pairs in each of the bins (i.e. 18 and 20) before and after the conflict resolution maneuver was removed. Since the data set is very small, no additional analysis was performed.

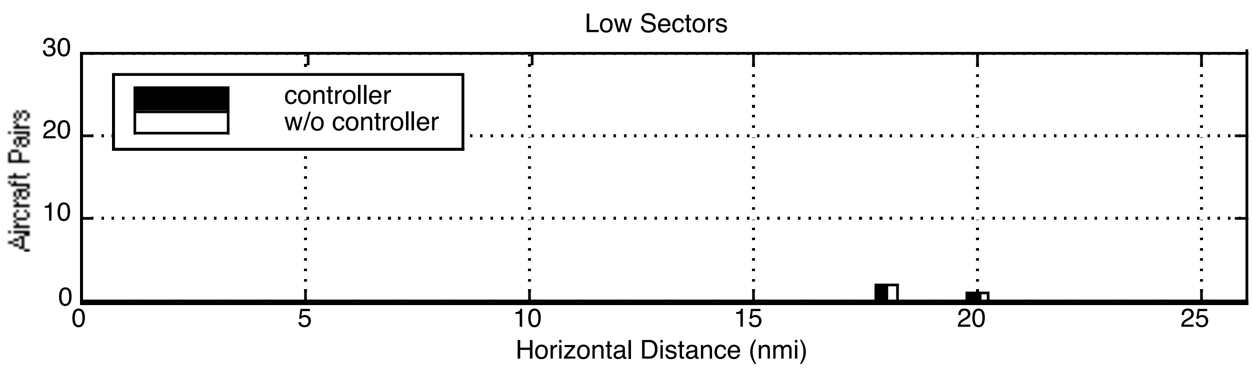

Figure 2.8 CPA Histogram For Low Sectors

Figures 2.9 and 2.10 depict CPA histograms for aircraft pairs that are not altitude separated and are contained in the high and ultra high sectors, respectively. Since the data used to create these histograms contains instances where loss of separation occurred, there are conflict pairs in the first five bins (e.g. 0-1, 1-2, 2-3, 3-4, and 4-5) representing the operational errors. These cases were later confirmed to exist in the SATORI data as the ‘known’ operational errors and subsequent analysis did not include these cases. Figure

9 shows the majority of aircraft pairs to be separated by greater than 10 nautical miles. The CPA for aircraft pairs greater than 25 nmi were not computed since the controller would most likely not consider them in any tactical conflict resolution maneuver.

Figure 2.9 shows the number of conflict pairs to be approximately 3 at the 10 nmi bin and increasing to approximately 15 at the 17 nmi bin. The number of conflict pairs then decreases to approximately 4 at the 21 nmi bin and then increases to 9 at the 24 nmi bin. While the CPA of individual conflict pairs do change after the conflict resolution maneuver is removed as shown in Table 3, the relative distribution of CPA's for conflict pairs as computed over the range 0 to 25 nmi does not change significantly as shown in Figure 2.9. The CPA with the conflict resolution maneuver is less than the CPA without the conflict resolution maneuver for vectors and parallel offsets. Table 3 typically shows the same CPA before and after the conflict resolution maneuver was removed for conflict resolution maneuvers involving speed-controls because the original speed was not available. For conflict resolution maneuvers involving altitude changes, the CPA with the conflict resolution maneuver is shown as either a real number indicating that at some time during the respective aircraft's flights they were not altitude separated or N/A indicating that the aircraft were altitude separated during the entire scenario.

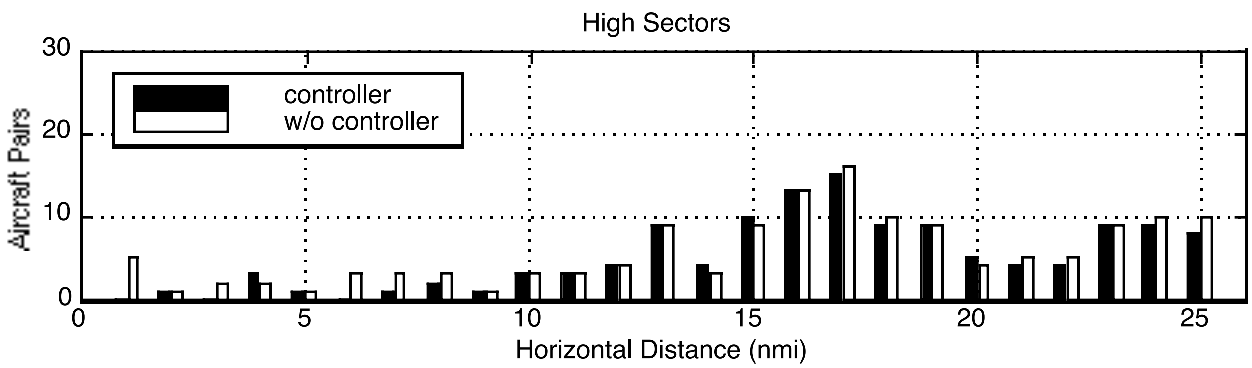

Figure 2.9 CPA Histogram For High Sectors

Figure 2.10 exhibits a somewhat different distribution of conflict pairs as compared to Figure 2.9. As in the case for the high sectors there are very few conflict pairs in the first 8 bins with a significant increase thereafter. In this histogram, there is a peak at the 9 nmi bin with a decrease occurring for the next 6 bins (e.g. 10-15). The number of conflict pairs then appears to vary randomly between 7 and 15 for the remaining bins. As was the case with the high sectors, the CPA of individual conflict pairs do change after the conflict resolution maneuver is removed; however, the relative distribution of CPA's does not change significantly.

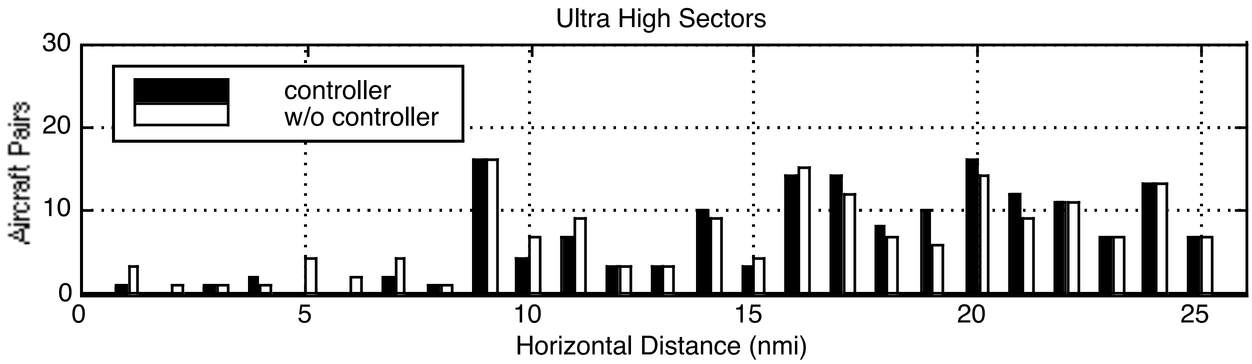

Figure 2.10 CPA Histogram For Ultra High Sectors

Figure 2.11 depicts a CPA histogram for aircraft pairs contained in the low, high, and ultra high sectors. The histogram is computed by summing the data for each of the 25 bins contained in Figures 8 through 10. As expected, the histogram exhibits some of the characteristics contained in the previous histograms namely, the peak in the 9 nmi bin and the peaks in the 16 and 17 nmi bins. The figure shows few aircraft pairs in the 1 to 8 nmi bins and a gradual increase thereafter. Based on the data contained in Figures 2.9 and 2.10, the average minimum horizontal separation was computed before and after the conflict resolution maneuver was removed. The minimum horizontal separation (i.e. CPA) was 7 nmi with controller actions (with operational errors removed) and 1 nmi without controller actions.

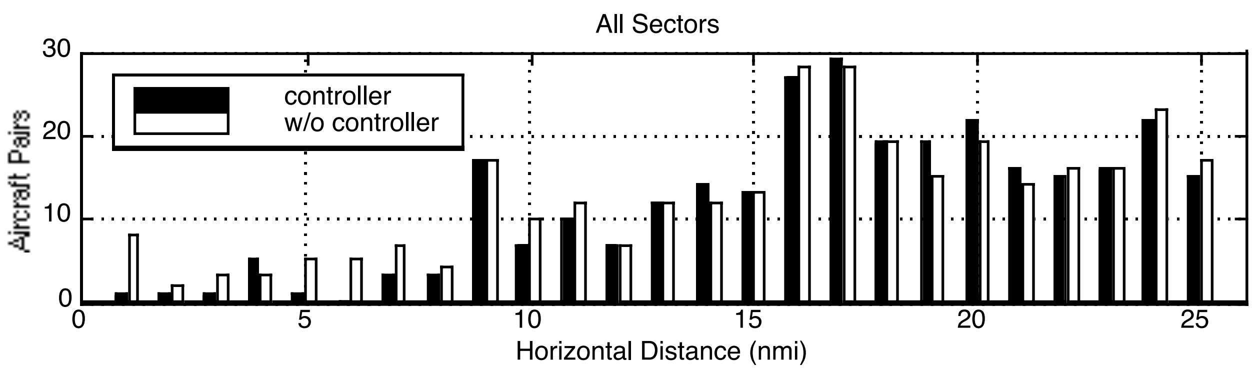

Figure 2.11 CPA Histogram For All Sectors

To examine the average CPA, a parametric approach was used because the average CPA is dependent upon a user-defined cutoff point. For example, if the average CPA is computed for aircraft pairs that are separated between 0 and 25 nmi the resulting number will be much higher than the number computed for aircraft pairs that are separated between 0 and 15 nmi. Figure 2.12 depicts the average CPA as a function of the horizontal cutoff distance for conflict pairs before and after the conflict resolution maneuver was removed. The upper curve represents the average CPA and includes the conflict resolution maneuvers. The average CPA for the upper curve ranges from 7 nmi at the 7 nmi horizontal cutoff to 17.6 nmi at the 25 nmi horizontal cutoff.

The lower curve represents the average CPA for conflict pairs with the conflict resolution maneuver removed. The average CPA for the lower curve ranges from 1 nmi at the 1 nmi horizontal cutoff to 16.4 nmi at the 25 nmi horizontal cutoff. As expected, the minimums for both curves are consistent with the minimums that were previously computed (e.g. 7 nmi and 1 nmi). This figure reveals that at all horizontal cutoffs, the average CPA is lower for conflict pairs when the conflict resolution maneuver is removed. As the horizontal cutoff is increased, the difference between the curves slowly decreases.

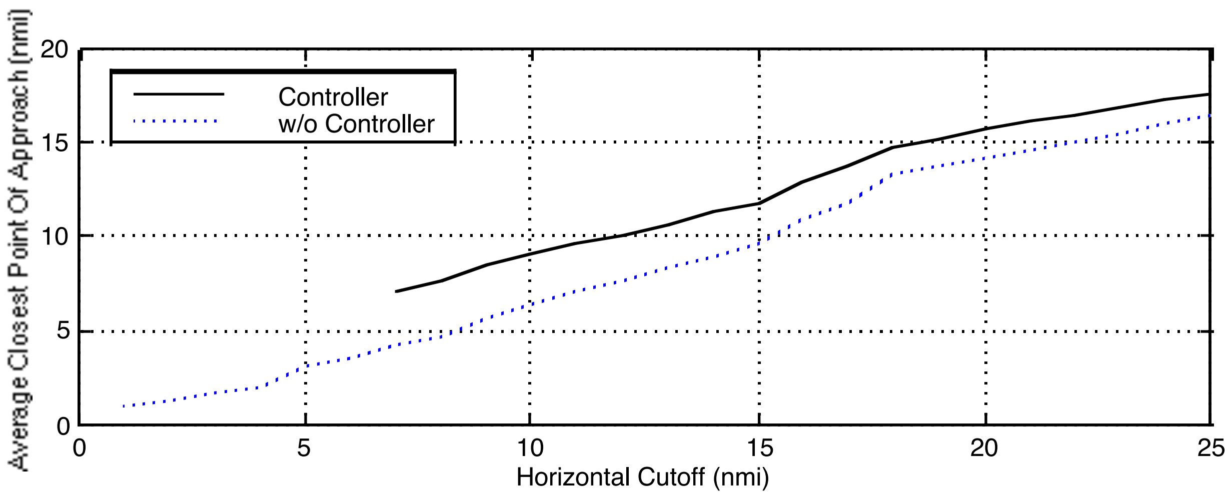

Figure 2.12 Average CPA As A Function Of Horizontal Cutoff Distance

2.4.3 Analysis Of Deviation From Intended Path

The following 6 figures summarize the results presented in Table 2.3. Figure 2.13 shows a histogram of CPA’s with the 57 conflict resolution maneuvers removed. The CPA varies from 1 nmi to 22 nmi with an average of approximately 9 nmi. The figure also shows that without controller interventions their would have been approximately 18 cases (e.g. 32%) where loss of separation occurs. Furthermore, if controllers chose to separate aircraft by a minimum of 7 nmi, then approximately 50% of these cases would have resulted in a loss of separation. This implies that controllers are quite efficient in predicting when loss of separation would occur and thereby issuing a conflict resolution maneuver. Additionally, controllers do not issue an excessive number conflict resolutions when the predicted loss of separation would not occur.

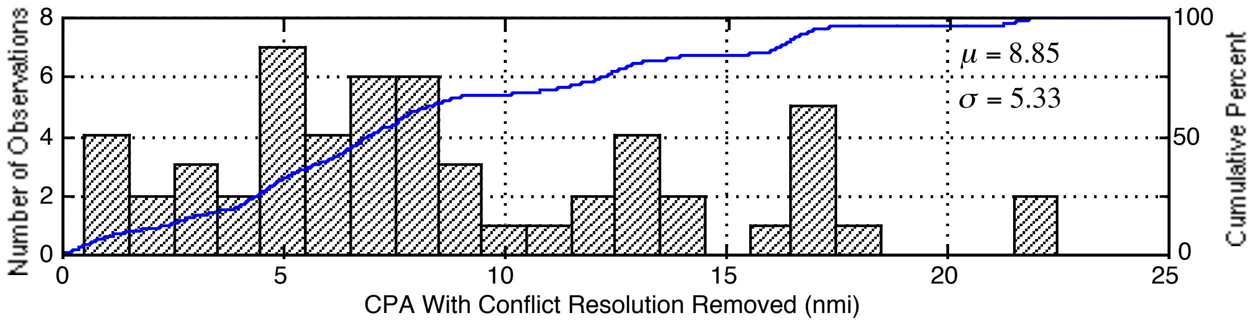

Figure 2.13 CPA Histogram With Conflict Resolution Maneuvers Removed

Figure 2.14 depicts a time to CPA histogram with the 57 conflict resolution maneuvers removed. For this study, the time to CPA is defined as the difference between the time at CPA and the time at which the conflict resolution maneuver is initiated. Since this portion of the study did not include voice, we do not know the latency between issuance of the conflict resolution maneuver and its initiation. The time to CPA ranges from 1 to 9 minutes with an average of approximately 3 minutes. This figure shows that for approximately 50% of the conflict resolution maneuvers, the time to CPA is less than or equal to 2 minutes. Furthermore, in more than 75% of all instances the time to CPA occurs within 4 minutes. While this result is not statistically significant, a majority of the time to CPA's are less than approximately 3 minutes. The distribution of time to CPA's appears to be shaped like a negative exponential. If we assume that controllers issue conflict resolution directives shortly after predicting a conflict (i.e. less than one minute), then for these scenarios controllers are, in general, resolving conflicts with a relatively short look ahead time. By using an average closing speed of 432 knots as computed from Table 2.3, and a mean time to CPA of 3 minutes, an average horizontal cutoff distance of 21.6 nmi is computed. The computed horizontal cutoff range compares favorably with the maximum horizontal cutoff used in Figures 2.8-2.12 and represents a distance filter for considering potential conflicts.

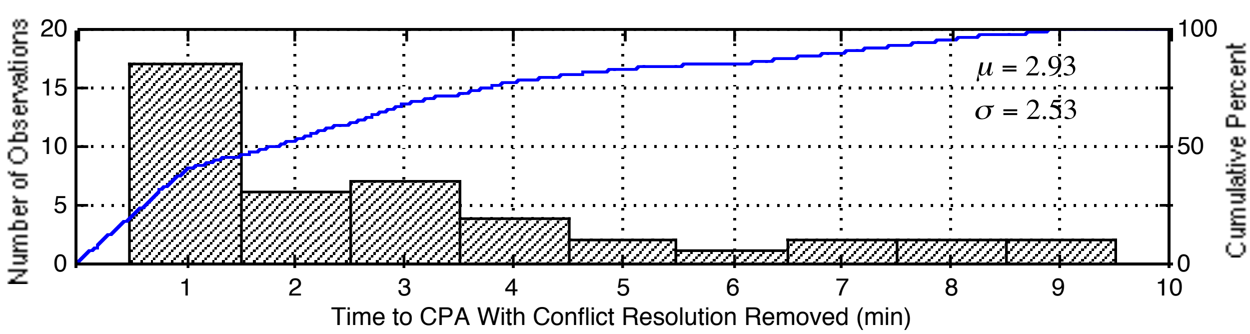

Figure 2.14 Time To CPA Histogram With Conflict Resolution Removed

Figures 2.15 and 2.16 depict histograms for the maximum horizontal offset D, and the additional distance flown L, for parallel offset maneuvers. These figures indicate that, in general, controllers attempt to separate aircraft by moderate deviations from their intended paths. The mean value of maximum offset and additional distance flown are 7.4 nmi and 4.6 nmi respectively. With an additional distance flown of 4.6 nmi, an aircraft traveling at 450 knots would incur a 37 second delay because of the conflict resolution maneuver.

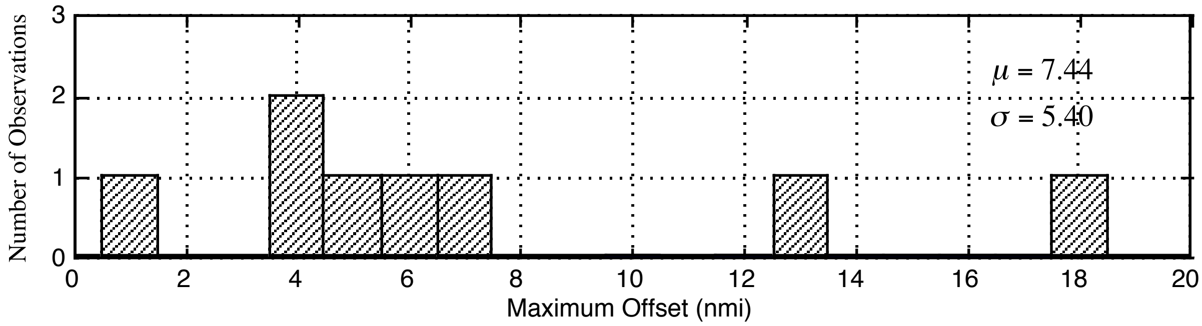

Figure 2.15 Maximum Offset Histogram For Parallel Offset Maneuvers

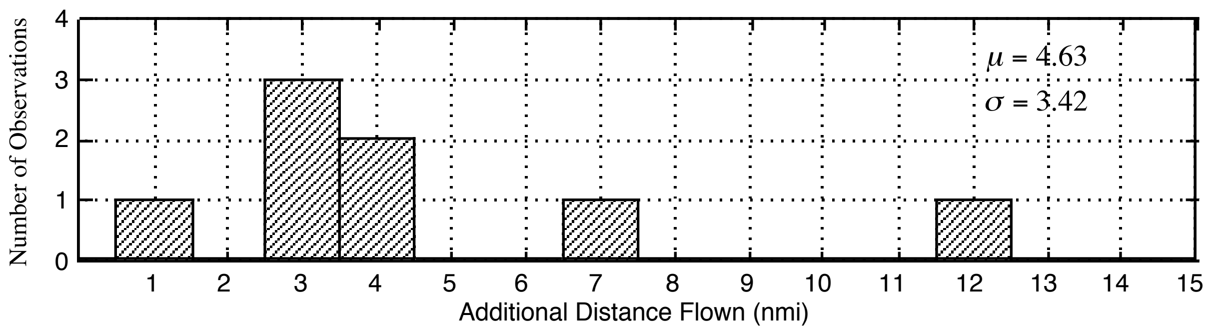

Figure 2.16 Additional Distance Flown Histogram For Parallel Offset Maneuvers

Figure 2.17 shows the distribution of vectors' magnitudes for the maneuvers classified as parallel offsets and vectors. These magnitudes vary from 10 to 40 degrees with a mean of 22 degrees. These results are consistent with the SATORI scenarios containing good quality voice where the magnitude of the observed vectors ranged from 10 to 20 degrees.

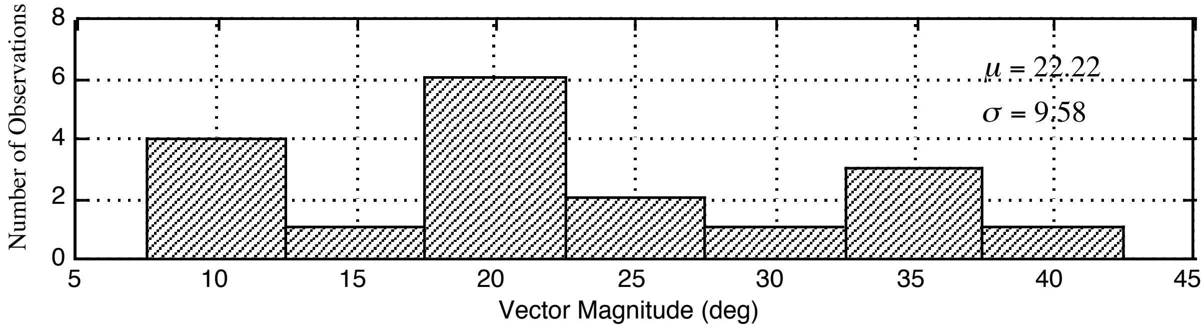

Figure 2.17 Vector Magnitude Histogram For Parallel Offset And Vector Maneuvers

Figure 2.18 illustrates conflict resolution maneuver duration times for the 57 conflict cases summarized in Table 3. The durations vary from 1 to 16 minutes with a mean duration of approximately 6 minutes. The maneuver duration time varies significantly with the maneuver type. The average maneuver duration time for parallel offsets is 8.8 minutes, 3.8 minutes for altitude manevuers, and 6.7 minutes for speed maneuvers. Since the vector maneuvers identified in Table 3 are incomplete, the associated maneuver duration times are not available.

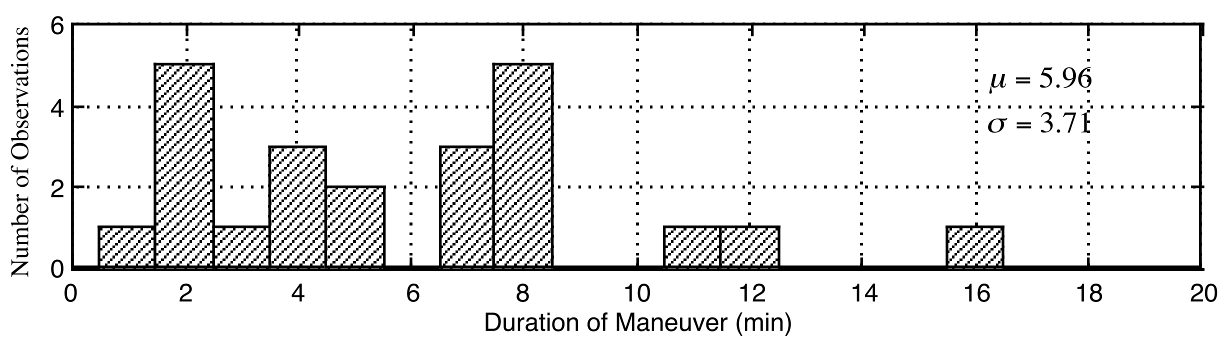

Figure 2.18 Maneuver Duration Time Histogram

2.4.4 Conflict Resolution Maneuver Rates

Figure 2.19 summarizes the total number of unique aircraft contained in the SATORI data for the 11 sectors examined. The bar chart shows the number of aircraft ranging from approximately 95 in sector 8, to more than 250 in sector 33. These aircraft represent a mix of commercial, military, and general aviation aircraft and, for the identifiable aircraft, are classified as either large or heavy.

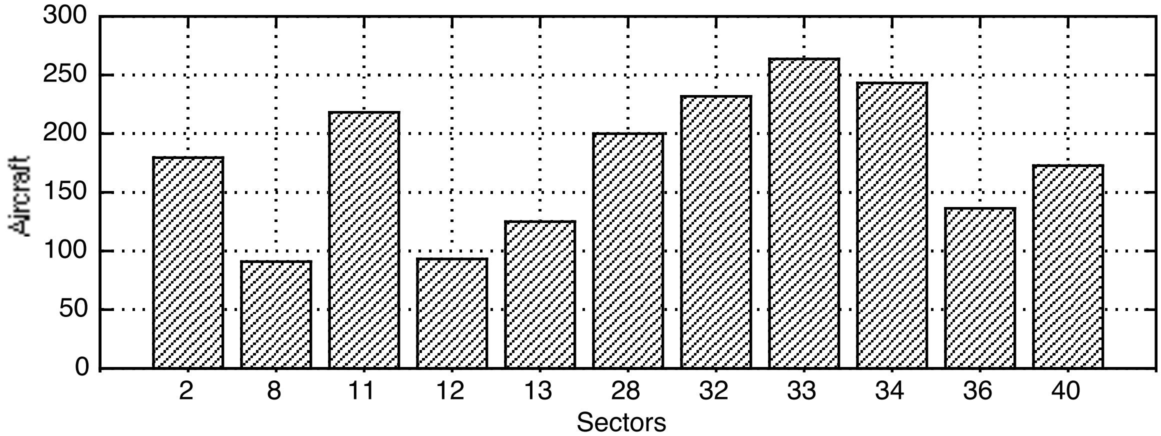

Figure 2.19 Number Of Aircraft

Figure 2.20 expands upon Figure 2.19 by computing the number of aircraft-hours of data for each sector. This is computed by accumulating the amount of time each aircraft was under the sector's control and summing over all scenarios. The bar chart is a good indicator of the volume of data that was used in this study and shows the relative differences between sectors.

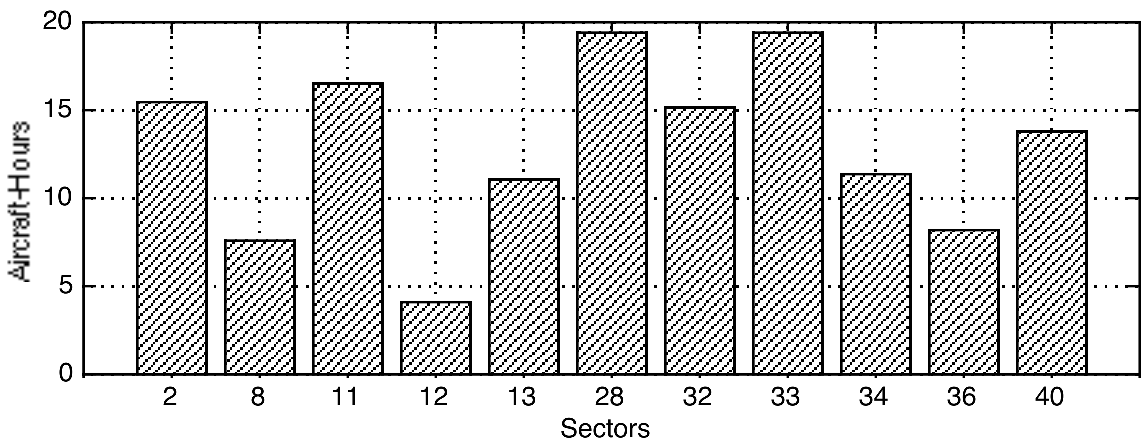

Figure 2.20 Number Of Aircraft-Hours

Using the data contained in Figure 2.19, a conflict resolution maneuver rate can be computed by dividing the total number of conflict resolutions detected in the sector by the number of aircraft in the sector. Figure 2.21 depicts the number of conflict resolution maneuvers per aircraft for each of the 11 sectors and also shows the mean number of conflict resolution maneuvers per aircraft. For sector 11, the conflict rate is approximately 0.04 which translates to approximately 1 out of 25 aircraft occupying this sector are involved in a conflict resolution maneuver. The conflict rate goes as high as 0.07 for sector 28 (1 out of 14) and as low as 0.01 for sector 34 (1 out of 100) aircraft being involved in a conflict resolution.

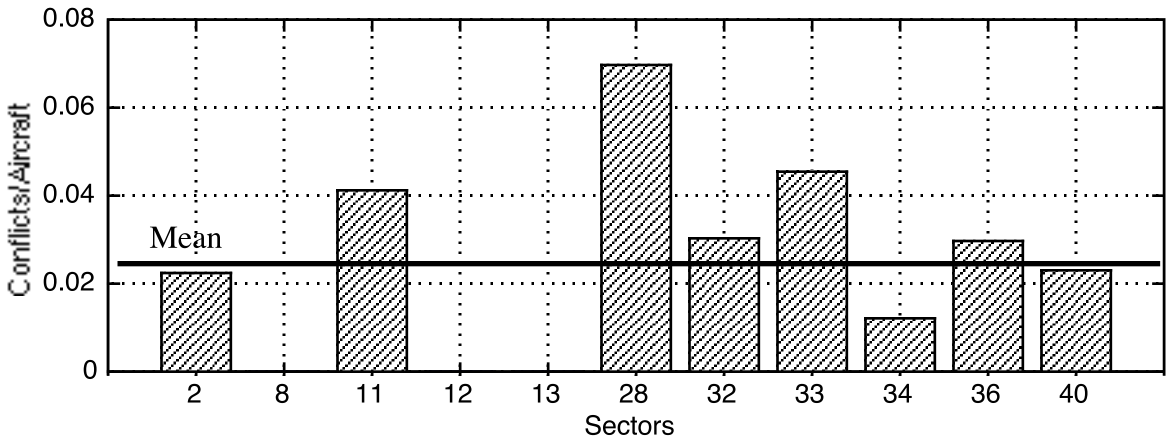

Figure 2.21 Number Of Conflict Resolutions per Aircraft

Using the data contained in Figure 2.20 the number of conflict resolutions per aircraft-hour can be computed by dividing the total number of conflict resolutions by the number of aircraft-hours of data. Figure 2.22 depicts the number of conflicts per aircraft-hour for each of the 11 sectors examined in this study. A high rate is an indicator of busy sector as is the case for sector 28 where the rate is 0.74 conflicts per aircraft-hour which translates to 1 conflict for every 1.35 aircraft-hours. A high rate would seem to indicate high pilot and controller workload.

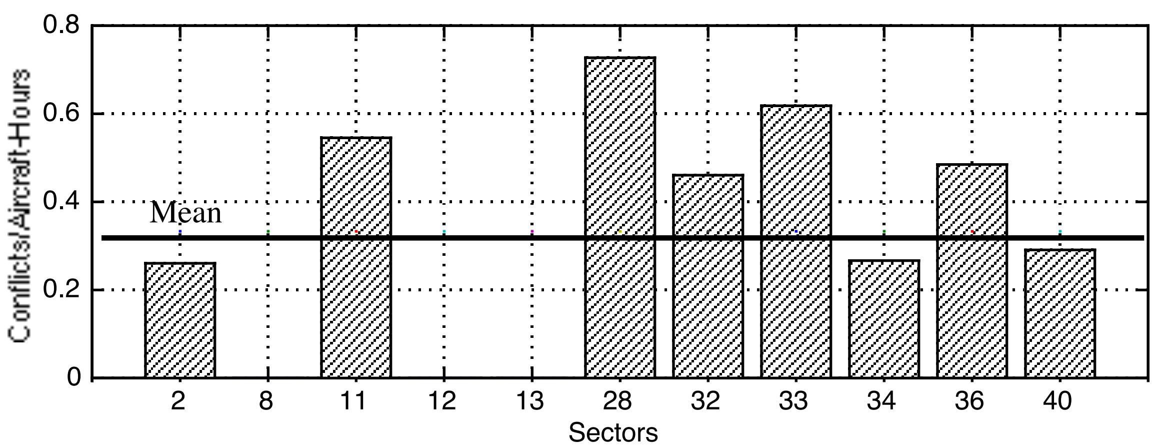

Figure 2.22 Number Of Conflict Resolutions Per Aircraft-Hour

2.5 Limitations

The FAA provided SATORI tool was used in several ways throughout this analysis. Initially, the tool was used to replay scenarios for which adequate quality voice scenarios existed. For these scenarios, conflict resolution maneuvers were easily identified and subsequently analyzed in an effort to understand the types and magnitudes of conflict resolution maneuvers. However, with this limited data set, it was evident that not all types of maneuvers were fully represented and our ability to detect other types of maneuvers was limited. Data filters, that detected altitude and heading maneuvers, were successfully developed but it was impossible to develop a reliable speed filter because aircraft speed can easily change by as much as 10% during normal flight. Aircraft speed is highly-dependent upon wind data which was not available for this study and aircraft speed will change as a result of other maneuver types as well.

The SATORI scenarios varied in length from 12 to 30 minutes with the majority of them being approximately 12 minutes in duration. The limited scenario duration's greatly diminished our ability to detect maneuvers and to measure the associated parameters with the prerequisite level of certainty to draw statistically significant conclusions. This, combined with a lack of flight plan data and lack of knowledge of existing ATM constraints, made the task of detecting conflict maneuvers, and measuring all the associated parameters extremely difficult. In many cases, the beginning of conflict resolution maneuver may have been detected, but the scenario ended before the maneuver was completed and thus total deviation from intended path was not readily available. These cases were of limited value for this study. Alternatively, a conflict resolution maneuver may have already been nearly completed when the scenario started wherein the data filters detected the end of the conflict resolution maneuver which would tend to negatively affect our ability to determine distance and time to closest point of approach as well as the total deviation from intended path. These cases were also of limited value.
1 for every 3 aircraft-hours).

Chapter 3 Free Flight Modeling

This chapter deals with various techniques of Free Flight Modeling starting with theoretical models and ending with practical techniques in developing of Free Flight trajectories.

3.1 Theoretical Models

Two different mathematical models are presented in this section. First model [8] represents a distributed motion planning algorithm based on potential and vortex fields. Second model [9] addresses optimal (least squares) approach to collision avoidance problem.

3.1.1 Potential and Vortex Field Approach to Planar Collision Avoidance Problem with Multiple Moving Agents

Suppose we have m agents, with the i th agent represented by a circle with radius r_i and its configuration denoted by $\boldsymbol{x_i} = (x_i, y_i)$. The target location of the i th agent $\boldsymbol{x_{ti}} = (x_{ti}, y_{ti})$ is represented by an attractive potential function:

$$U_a(\boldsymbol{x_i}, \boldsymbol{x_{ti}}) = \frac{1}{2}\left(\boldsymbol{x_{ti}} - \boldsymbol{x_i}\right)^2 \tag{3-1}$$

In order to achieve the target destination a force proportional to the negative gradient of the U_a needs to be applied:

$$F_a(\boldsymbol{x_i}, \boldsymbol{x_{ti}}) = -\nabla U_a(\boldsymbol{x_i}, \boldsymbol{x_{ti}}) = -\left(\boldsymbol{x_{ti}} - \boldsymbol{x_i}\right) \tag{3-2}$$

To prevent collision between agents i and j, the following spherically symmetric repulsive field $U_r(\boldsymbol{x_i}, \boldsymbol{x_{ti}})$ is associated with each agent:

$$U_r(\boldsymbol{x_i}, \boldsymbol{x_j}) = \begin{cases} -\dfrac{1}{2\delta_{rj}}\left(r_{ij} - \left(r_j + \delta_{rj}\right)\right)^2 & \text{if } r_j \le r_{ij} \le r_j + \delta_{rj} \\ 0 & \text{otherwise} \end{cases} \tag{3-4}$$

where $r_{ij} = \sqrt{\left(x_i - x_j\right)^2 + \left(y_i - y_j\right)^2}$ is the distance between the i th and j th agent, r_j is the radius of the j th agent and δ_{rj} is the influential zone of its repulsive field. The repulsive force associated with this field is:

$$F_r(\boldsymbol{x_i},\boldsymbol{x_j}) = \nabla U_r(\boldsymbol{x_i},\boldsymbol{x_{ti}}) = \left[\frac{\partial}{\partial x}\left(-\frac{1}{2\delta_{rj}}\left(r_{ij}-\left(r_j+\delta_{rj}\right)\right)^2\right), \frac{\partial}{\partial y}\left(-\frac{1}{2\delta_{rj}}\left(r_{ij}-\left(r_j+\delta_{rj}\right)\right)^2\right)\right]^T$$

$$= -\frac{2}{2\delta_{rj}}\left(r_{ij}-\left(r_j+\delta_{rj}\right)\right)\left[\frac{\partial}{\partial x}\sqrt{\left(x_i-x_j\right)^2+\left(y_i-y_j\right)^2}, \frac{\partial}{\partial y}\sqrt{\left(x_i-x_j\right)^2+\left(y_i-y_j\right)^2}\right]^T$$

$$= -\frac{1}{\delta_{rj}}\left(r_{ij}-\left(r_j+\delta_{rj}\right)\right)\frac{1}{2}\frac{1}{\sqrt{\left(x_i-x_j\right)^2+\left(y_i-y_j\right)^2}}2\left[\left(x_i-x_j\right),\left(y_i-y_j\right)\right]^T$$

$$= -\frac{1}{\delta_{rj}}\left(r_{ij}-\left(r_j+\delta_{rj}\right)\right)\frac{1}{r_{ij}}\left[\left(x_i-x_j\right),\left(y_i-y_j\right)\right]^T$$

$$= \frac{1}{\delta_{rj}}\left(\frac{r_j+\delta_{rj}}{r_{ij}}-1\right)\begin{bmatrix} x_i-x_j \\ y_i-y_j \end{bmatrix}$$

A vortex field, used to ensure that all agents turn in the same direction when encountering a conflict, is constructed around each agent tangential to the repulsive field $U_r(\boldsymbol{x_i},\boldsymbol{x_{ti}})$:

$$F_v(\boldsymbol{x_i},\boldsymbol{x_j}) = \pm\begin{bmatrix} \dfrac{\partial U_r(\boldsymbol{x_i},\boldsymbol{x_j})}{\partial y} \\ -\dfrac{\partial U_r(\boldsymbol{x_i},\boldsymbol{x_j})}{\partial x} \end{bmatrix} \tag{3-5}$$

The choice of the sign in the above vortex field expression determines the direction of the circulating field (direction of the avoidance for conflict maneuvers).

The dynamic planner for a single agent in the presence of multiple agents is obtained by superposition of participating potential and vector fields and becomes:

$$\dot{\boldsymbol{x}}_{\boldsymbol{i}} = \frac{F_a(\boldsymbol{x_i},\boldsymbol{x_{ti}})}{\left\|F_a(\boldsymbol{x_i},\boldsymbol{x_{ti}})\right\|} + \sum_j\left(k_{ri}F_r(\boldsymbol{x_i},\boldsymbol{x_j}) + k_{vi}F_v(\boldsymbol{x_i},\boldsymbol{x_j})\right) \tag{3-6}$$

where $j = 1,...m,\ i \neq j$. The contributions from repulsive and vortex fields range between [0, 1], increasing as the agent approaches the boundary of another agent. Normalization of the attractive field component makes its contribution comparable to the magnitudes of the repulsive and vortex fields. The individual contributions are then weighted by the k_{ri}, k_{vi} and resulting vector is again normalized and scaled by k_{di}, a constant proportional to the desired velocity of the i th agent. The velocity of i th agent is then:

$$\boldsymbol{v_i} = k_{di} \frac{\dot{\boldsymbol{x}}_i}{\|\dot{\boldsymbol{x}}_i\|} \tag{3-7}$$

The velocity vector in terms of its components is defined in the following way:

$$\boldsymbol{v_i} = \left[v_{xi}, v_{yi}\right]^T = \left[V_i \cos\psi_i, V_i \sin\psi_i\right]^T \tag{3-8}$$

where $V_i = |\boldsymbol{v_i}| = \sqrt{v_{xi}^2 + v_{yi}^2}$ and $\psi_i = \cos^{-1}\frac{v_{xi}}{\sqrt{v_{xi}^2 + v_{yi}^2}} = \sin^{-1}\frac{v_{yi}}{\sqrt{v_{xi}^2 + v_{yi}^2}}$

To calculate the aircraft trajectory the following equations are employed:

$$\begin{aligned} x_i(t+\Delta t) &= x_i(t) + \Delta t V_i \cos\psi_i \\ y_i(t+\Delta t) &= y_i(t) + \Delta t V_i \sin\psi_i \end{aligned} \tag{3-9}$$

Figure 3.1 shows the 2-D collision avoidance trajectories generated using MATLAB code presented in Appendix D.

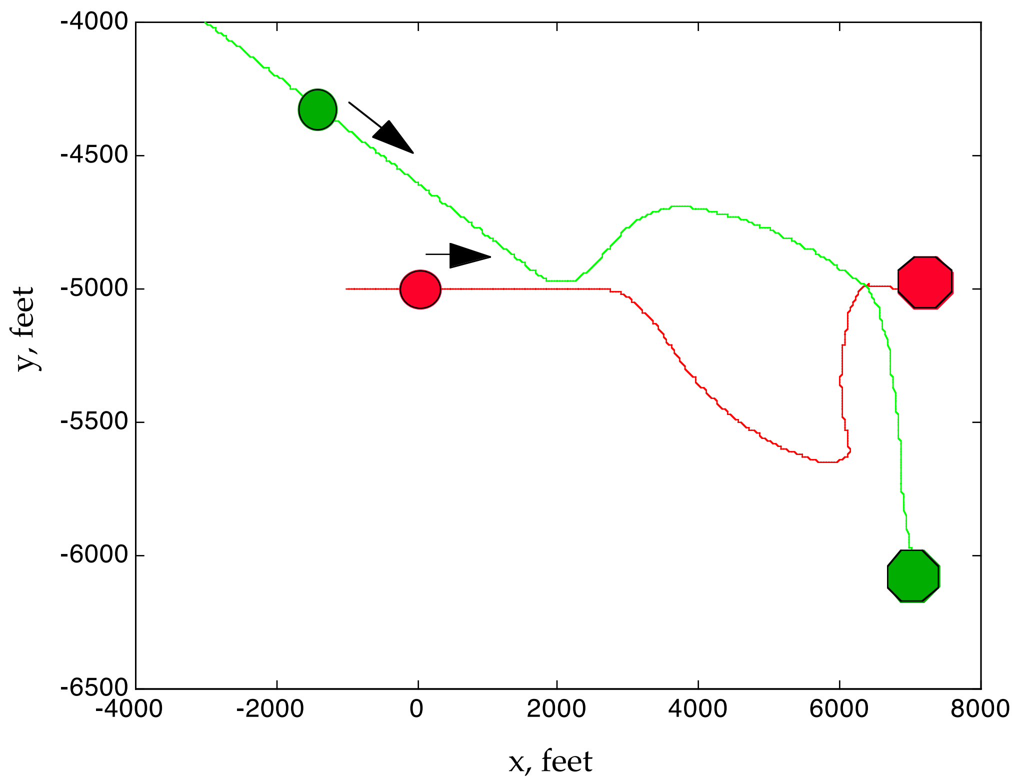

Figure 3.1 2-D Collision Avoidance Trajectories

3.1.2 Potential and Vortex Field Approach to 3-D Collision Avoidance Problem with Multiple Moving Agents and

Spherical Protection and Alert Zones

This case is an extension of the previous 2-D case. We are adding the third coordinate z, so current and target configuration of the i th agent becomes $\boldsymbol{x_i} = (x_i, y_i, z_i)$ and $\boldsymbol{x_{ti}} = (x_{ti}, y_{ti} z_{ti})$ respectively.

The distance between agents i and j is now defined by,

$$r_{ij} = \sqrt{\left(x_i - x_j\right)^2 + \left(y_i - y_j\right)^2 + \left(z_i - z_j\right)^2} \tag{3-10}$$

The repulsive force for this case is given by,

$$\begin{aligned} F_r(\boldsymbol{x_i}, \boldsymbol{x_j}) &= \nabla U_r(\boldsymbol{x_i}, \boldsymbol{x_{ti}}) \\ &= \left[\frac{\partial}{\partial x}, \frac{\partial}{\partial y}, \frac{\partial}{\partial z}\right]^T \cdot \left(-\frac{1}{2\delta_{rj}}\left(r_{ij} - \left(r_j + \delta_{rj}\right)\right)^2\right) \\ &= \frac{1}{\delta_{rj}}\left(\frac{r_j + \delta_{rj}}{r_{ij}} - 1\right)\begin{bmatrix} x_i - x_j \\ y_i - y_j \\ z_i - z_j \end{bmatrix} \end{aligned} \tag{3-11}$$

Finally, a vortex field is represented by,

$$F_v(\boldsymbol{x_i}, \boldsymbol{x_j}) = \pm \begin{bmatrix} \dfrac{\partial U_r(\boldsymbol{x_i}, \boldsymbol{x_j})}{\partial z} \\ -\dfrac{\partial U_r(\boldsymbol{x_i}, \boldsymbol{x_j})}{\partial y} \\ \dfrac{\partial U_r(\boldsymbol{x_i}, \boldsymbol{x_j})}{\partial x} \end{bmatrix} \tag{3-12}$$

Velocity vector in terms of its components is defined in the following way:

$$\boldsymbol{v_i} = \left[v_{xi}, v_{yi}, v_{zi}\right]^T = \left[V_i \cos\psi_i \cos\gamma_i, V_i \sin\psi_i \cos\gamma_i, V_i \sin\gamma_i\right]^T$$

where $V_i = |\boldsymbol{v_i}| = \sqrt{v_{xi}^2 + v_{yi}^2 + v_{zi}^2}$ and

$$\gamma_i = \sin^{-1}\frac{v_{zi}}{\sqrt{v_{xi}^2 + v_{yi}^2 + v_{zi}^2}}, \psi_i = \frac{v_{xi}}{\sqrt{v_{xi}^2 + v_{yi}^2 + v_{zi}^2}\cos\left(\sin^{-1}\dfrac{v_{zi}}{\sqrt{v_{xi}^2 + v_{yi}^2 + v_{zi}^2}}\right)} \tag{3-13}$$

To calculate the 3-D trajectory the following equations are employed:

$$\begin{aligned}
x_i(t+\Delta t) &= x_i(t) + \Delta t V_i \cos\psi_i \cos\gamma_i \\
y_i(t+\Delta t) &= y_i(t) + \Delta t V_i \sin\psi_i \cos\gamma_i \\
z_i(t+\Delta t) &= z_i(t) + \Delta t V_i \sin\gamma_i
\end{aligned} \qquad (3\text{-}14)$$

Figure 3.2 shows the 3-D collision avoidance trajectories generated using MATLAB code presented in Appendix D.

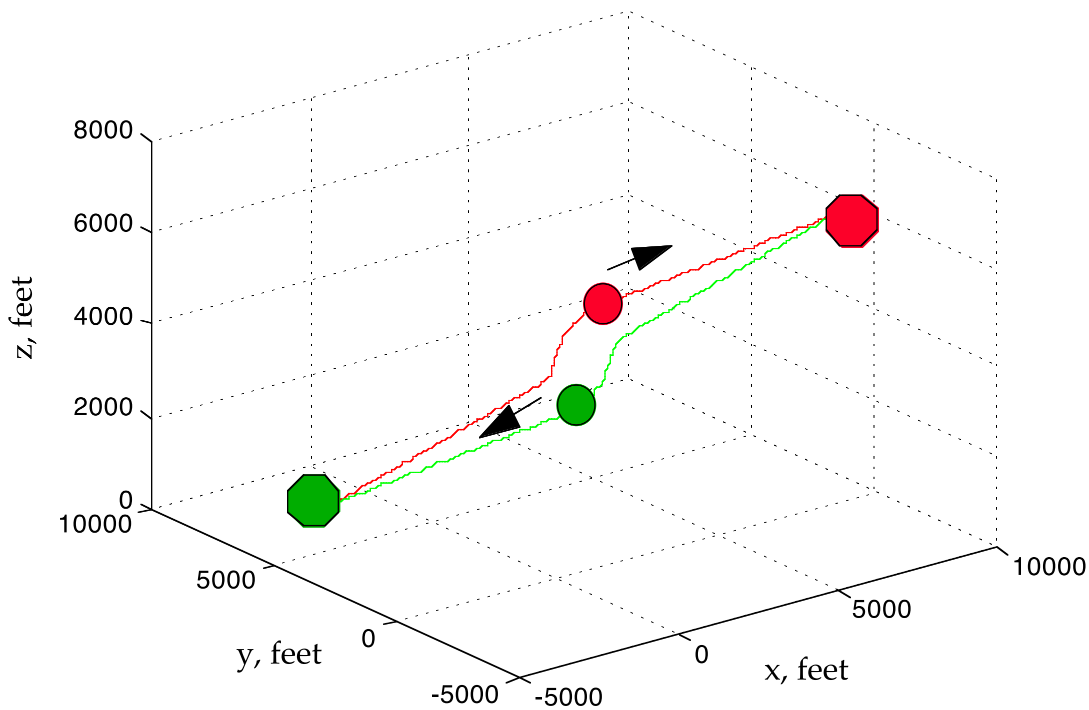

Figure 3.2 3-D Collision Avoidance Trajectories

3.1.3 Optimal (Least Squares) Approach to 3-D Collision Avoidance Problem with Multiple Moving Agents

Mathematical Description

The following system of equation describes 3-D aircraft position:

$$\begin{aligned}
x_{i+1}^{(k)} &= x_i^{(k)} + \Delta t \cdot V_{i,i+1}^{(k)} \cdot \cos\psi_{i,i+1}^{(k)} \cdot \cos\gamma_{i,i+1}^{(k)} \\
y_{i+1}^{(k)} &= y_i^{(k)} + \Delta t \cdot V_{i,i+1}^{(k)} \cdot \sin\psi_{i,i+1}^{(k)} \cdot \cos\gamma_{i,i+1}^{(k)} \\
h_{i+1}^{(k)} &= h_i^{(k)} + \Delta t \cdot V_{i,i+1}^{(k)} \cdot \sin\gamma_{i,i+1}^{(k)}
\end{aligned} \qquad (3\text{-}15)$$

Where,

$x_{i+1}^{(k)}$ is the x - coordinate of k - th aircraft at the end of solution interval

$y_{i+1}^{(k)}$ is the y - coordinate of k - th aircraft at the end of solution interval

$h_{i+1}^{(k)}$ is an altitude of k - th aircraft at the end of solution interval

$x_{i+1}^{(k)}$ is the x - coordinate of k - th aircraft at the beginning of solution interval

$y_{i+1}^{(k)}$ is the y - coordinate of k - th aircraft at the beginning of solution interval

$h_{i+1}^{(k)}$ is an altitude of k - th aircraft at the beginning of solution interval

$\psi_{i,i+1}^{(k)}$ is the heading (trajectory) angle of k - th aircraft over solution interval

$\gamma_{i,i+1}^{(k)}$ is the climb angle of the k - th aircraft over solution interval

Δt is the solution interval

Definition of angles is given in Figure 3.3 below.

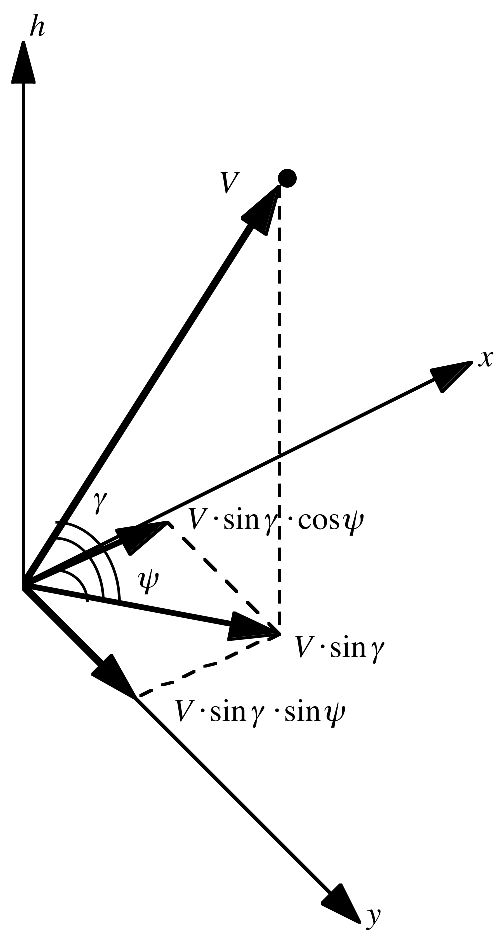

Figure 3.3 Definition of Angles

In level flight (in route flight) climb angle γ is equal to zero and (3-15) simplifies to the 2-D case.

$$
\begin{aligned}
x_{i+1}^{(k)} &= x_i^{(k)} + \Delta t \cdot V_{i,i+1}^{(k)} \cdot \cos\psi_{i,i+1}^{(k)} \\
y_{i+1}^{(k)} &= y_i^{(k)} + \Delta t \cdot V_{i,i+1}^{(k)} \cdot \sin\psi_{i,i+1}^{(k)} \\
h_{i+1}^{(k)} &= h_i^{(k)}
\end{aligned}
\tag{3-16}
$$

Note, that in this case we have two control parameters: $V_{i,i+1}^{(k)}$ and $\psi_{i,i+1}^{(k)}$. These control parameters are considered to be constant over solution interval Δt.

The system of equations (3-16) describes, basically, the en-route trajectory of an aircraft. For this case, we can consider $V_{i,i+1}^{(k)} = V_{cruise}^{(k)} = const$ over the whole in route flight, provided that there is no conflict in the airspace between aircraft. For the same case (en route, no conflict) $\psi_{i,i+1}^{(k)}$ is the set of constants, predefined by the flight program.

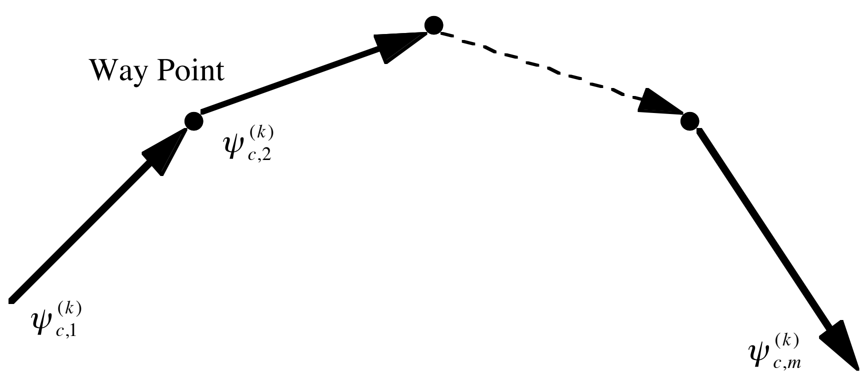

Figure 3.4 Way Points

Thus, for this particular case, equations (3-16) can be further simlified and rewritten in the following form:

$$
\begin{aligned}
x_{i+1}^{(k)} &= x_i^{(k)} + \Delta t \cdot V_{cruise}^{(k)} \cdot \cos\psi_{c,j}^{(k)} \\
y_{i+1}^{(k)} &= y_i^{(k)} + \Delta t \cdot V_{cruise}^{(k)} \cdot \sin\psi_{c,j}^{(k)} \\
h_{i+1}^{(k)} &= h_i^{(k)}
\end{aligned}
\tag{3-17}
$$

Controls and Control Rates Limitations

Since we consider a physical system, certain control and control rates limitations should apply:

$$
\begin{aligned}
&V_{\min}^{(k)} \le V_{i,i+1}^{(k)} \le V_{\max}^{(k)} \\
&-\frac{\pi}{2} \le \psi_{i,i+1}^{(k)} \le \frac{\pi}{2} \\
&-\frac{\pi}{2} \le \gamma_{i,i+1}^{(k)} \le \frac{\pi}{2} \\
&\left|\frac{V_{i,i+1}^{(k)} - V_{i-1,i}^{(k)}}{\Delta t}\right| \le a_{\max}^{(k)} \\
&\left|\frac{\psi_{i,i+1}^{(k)} - \psi_{i-1,i}^{(k)}}{\Delta t}\right| \le \dot{\psi}_{\max}^{(k)} \\
&\left|\frac{\gamma_{i,i+1}^{(k)} - \gamma_{i-1,i}^{(k)}}{\Delta t}\right| \le \dot{\gamma}_{\max}^{(k)}
\end{aligned}
\tag{3-18}
$$

Numerical Example (Case of 2 Aircraft)

- Simulation Data

Table 3.1 shows a sample problem to test this model. Parameters in this table describe original (intended) 2-D trajectories of two aircraft. Parameter m is used to assign the aircraft priority in the conflict resolution. Larger number m corresponds to the aircraft with higher priority, i.e. in this case to the aircraft that will not be maneuvered and preserve original (intended) trajectory while resolving the conflict.

0Table 3.1 Simulation Input Data

Simulation Parameter	Aircraft #1	Aircraft #2
x_{i0}, miles	0	10
y_{i0}, miles	0	20
V_{i0}, mph	500	600
ψ_{i0}, deg	10	-15
$V_{i\min}$, mph	450	550
$V_{i\max}$, mph	550	650
$\psi_{i\min}$, deg	-180	-180
$\psi_{i\max}$, deg	180	180
R_a, miles	10	10
m	2	1

The simulation start time is $t_0 = 0$ s and the end time is $t_f = 450$ sec. The simulation step size is $\Delta t = 10$ sec.

• <u>Simulation Results</u>

The MATLAB code, used to generate simulation results, is presented in Appendix D.

Figure 3.5 shows speed time history for both aircraft with and without conflict resolution. Aircraft #1 in both cases preserves original speed of 500 mph (735 ft/sec on the plot) since it has higher priority. Aircraft #2 accelerates first to 650 mph (at about 100 s), than decelerates to 550 mph (at about 300 s), than it finally restores original speed of 600 mph (875 ft/sec on the plot at about 400 s).

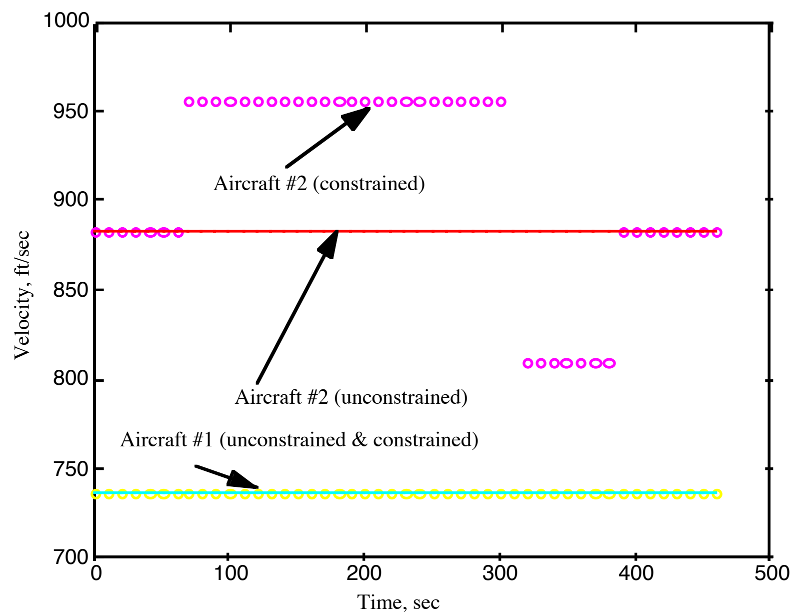

Figure 3.5 Speed vs. Time Plot

Figure 3.6 shows heading angle time history for both aircraft with and without conflict resolution. Aircraft #1 in both cases preserves original heading of 10 deg since it has higher priority. Aircraft #2 first changes its heading to about 0 deg (at 100 s), than gradually changes its heading from 0 deg to –40 deg within next 200 s, than it restores its original heading of –15 deg during next 100 s.

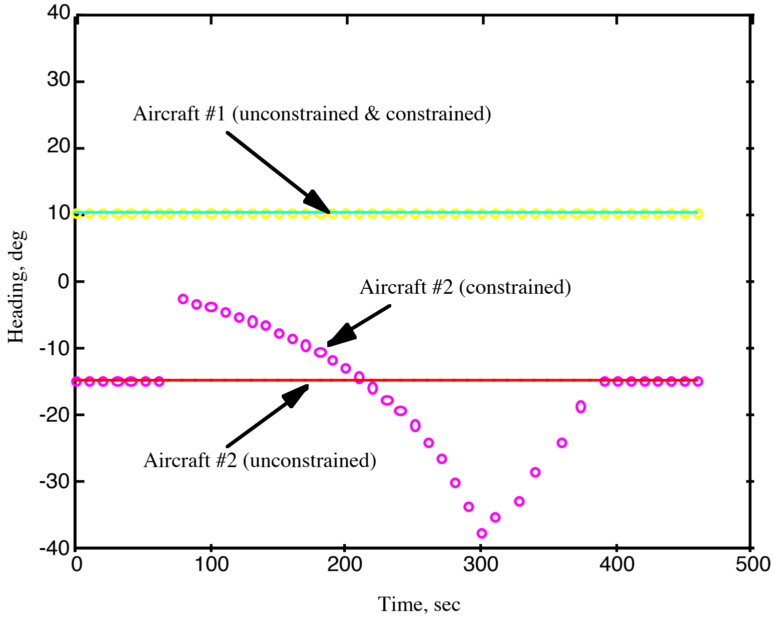

Figure 3.6 Heading vs. Time Plot

Figure 3.7 shows planar trajectories for 2 conflicting aircraft. Aircraft #1 preserves its original trajectory, while Aircraft #2 deviates from its original trajectory due to conflict resolution and restores its original trajectory after conflict has been resolved.

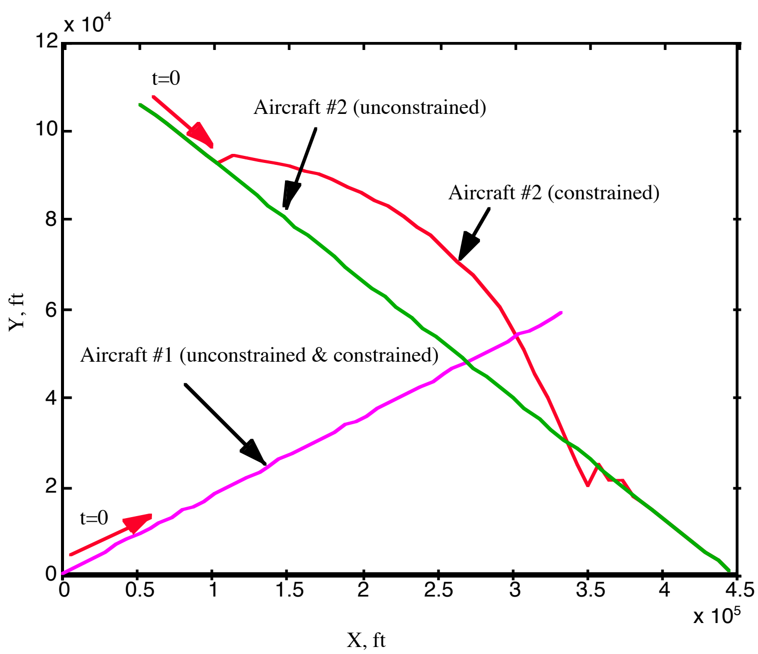

Figure 3.7 Planar Trajectories for 2 Conflicting Aircraft

Figures 3.8 and 3.9 illustrate the horizontal distance between two conflicting aircraft with and without collision avoidance maneuver performed by Aircraft #2. The separation that should be preserved is equal to alert zone diameter of 20 nmi. Figure 3.8 shows that without conflict resolution two aircraft can come as close as 16 nmi. On the other hand, when conflict resolution is performed, aircraft are preserving the minimum separation of 20 nmi throughout the duration of the simulation.

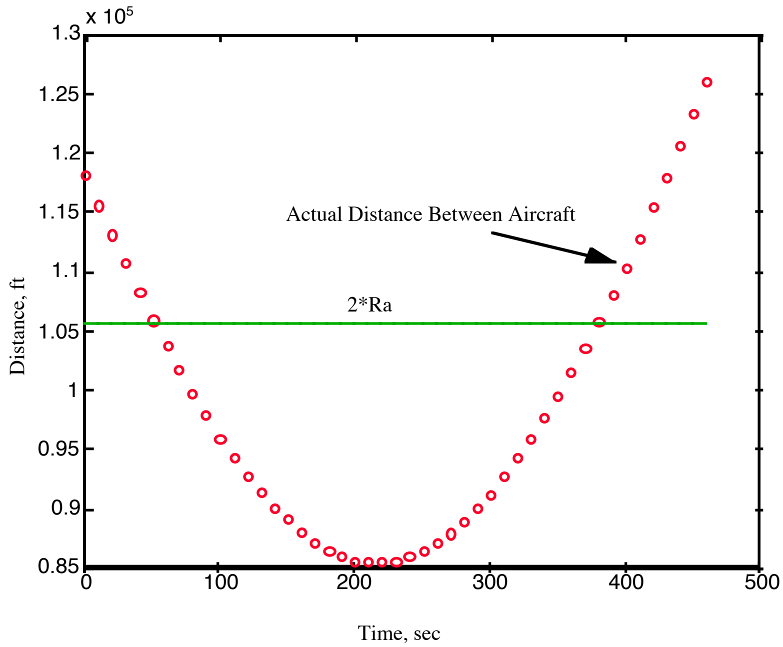

Figure 3.8 Distance between 2 Aircraft (Without Collision Avoidance)

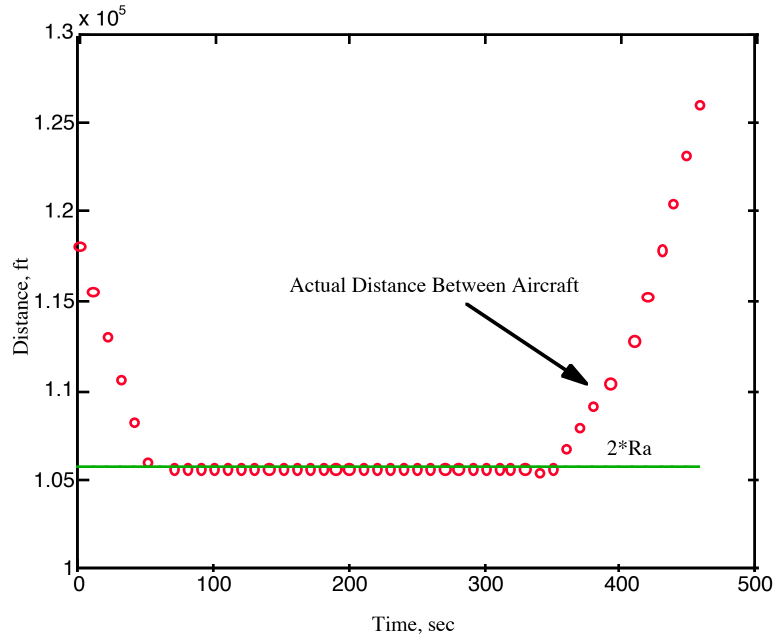

Figure 3.9 Distance between 2 Aircraft (With Collision Avoidance)

Conflict Resolution Strategies

- <u>Strategy I</u>

Description: Speed up to $V_{\max}^{(k)}$ or slow down to $V_{\min}^{(k)}$, $\psi^{(k)}$ remains the same, and $\gamma^{(k)} = 0$.

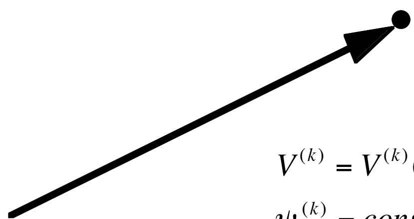

$$V^{(k)} = V^{(k)}(t)$$
$$\psi^{(k)} = const$$
$$\gamma^{(k)} = 0$$

Equations of motion:

$$\begin{aligned} x_{i+1}^{(k)} &= x_i^{(k)} + \Delta t \cdot V_{i,i+1}^{(k)} \cdot \cos\psi_{c,j}^{(k)} \\ y_{i+1}^{(k)} &= y_i^{(k)} + \Delta t \cdot V_{i,i+1}^{(k)} \cdot \sin\psi_{c,j}^{(k)} \\ h_{i+1}^{(k)} &= h_i^{(k)} \end{aligned} \qquad (3\text{-}19)$$

Maneuver complexity: Low.

- <u>Strategy II</u>

Description: Change $\psi^{(k)}$ maintaining the same $V_{cruise}^{(k)}$ and $\gamma^{(k)} = 0$.

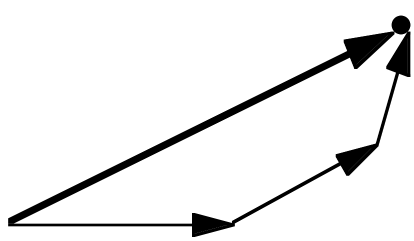

$$V^{(k)} = const$$
$$\psi^{(k)} = \psi^{(k)}(t)$$
$$\gamma^{(k)} = 0$$

Equations of motion:

$$\begin{aligned} x_{i+1}^{(k)} &= x_i^{(k)} + \Delta t \cdot V_{cruise}^{(k)} \cdot \cos\psi_{i,i+1}^{(k)} \\ y_{i+1}^{(k)} &= y_i^{(k)} + \Delta t \cdot V_{cruise}^{(k)} \cdot \sin\psi_{i,i+1}^{(k)} \\ h_{i+1}^{(k)} &= h_i^{(k)} \end{aligned} \qquad (3\text{-}20)$$

Maneuver complexity: Low.

- <u>Strategy III</u>

Description: Change $\psi^{(k)}$and $V^{(k)}$, $\gamma^{(k)} = 0$.

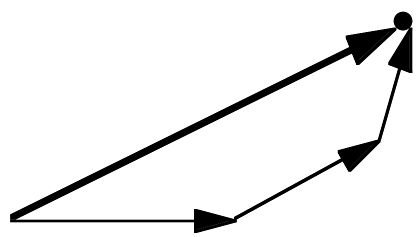

$$V^{(k)} = V^{(k)}(t)$$
$$\psi^{(k)} = \psi^{(k)}(t)$$
$$\gamma^{(k)} = 0$$

Equations of motion:

$$\begin{aligned} x_{i+1}^{(k)} &= x_i^{(k)} + \Delta t \cdot V_{i,i+1}^{(k)} \cdot \cos\psi_{i,i+1}^{(k)} \\ y_{i+1}^{(k)} &= y_i^{(k)} + \Delta t \cdot V_{i,i+1}^{(k)} \cdot \sin\psi_{i,i+1}^{(k)} \\ h_{i+1}^{(k)} &= h_i^{(k)} \end{aligned} \tag{3-21}$$

Maneuver complexity: Medium.

- <u>Strategy IV</u>

Description: Change $\gamma^{(k)}, V^{(k)} = const$, $\psi^{(k)} = const$.

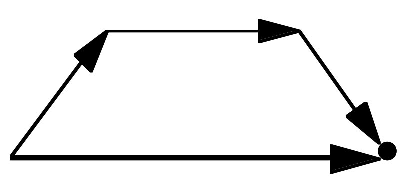

$$V^{(k)} = const$$
$$\psi^{(k)} = const$$
$$\gamma^{(k)} = \gamma^{(k)}(t)$$

Equations of motion:

$$\begin{aligned} x_{i+1}^{(k)} &= x_i^{(k)} + \Delta t \cdot V_{cruise}^{(k)} \cdot \cos\psi_{c,j}^{(k)} \cdot \cos\gamma_{i,i+1}^{(k)} \\ y_{i+1}^{(k)} &= y_i^{(k)} + \Delta t \cdot V_{cruise}^{(k)} \cdot \sin\psi_{c,j}^{(k)} \cdot \cos\gamma_{i,i+1}^{(k)} \\ h_{i+1}^{(k)} &= h_i^{(k)} + \Delta t \cdot V_{cruise}^{(k)} \cdot \sin\gamma_{i,i+1}^{(k)} \end{aligned} \tag{3-22}$$

Maneuver complexity: Medium.

- <u>Strategy V</u>

Description: Change $\gamma^{(k)}$, $V^{(k)}$. $\psi^{(k)} = const$.

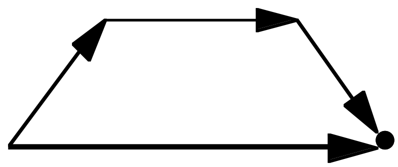

$$V^{(k)} = V^{(k)}(t)$$
$$\psi^{(k)} = const$$
$$\gamma^{(k)} = \gamma^{(k)}(t)$$

Equations of motion:

$$\begin{aligned}
x_{i+1}^{(k)} &= x_i^{(k)} + \Delta t \cdot V_{i,i+1}^{(k)} \cdot \cos\psi_{c,j}^{(k)} \cdot \cos\gamma_{i,i+1}^{(k)} \\
y_{i+1}^{(k)} &= y_i^{(k)} + \Delta t \cdot V_{i,i+1}^{(k)} \cdot \sin\psi_{c,j}^{(k)} \cdot \cos\gamma_{i,i+1}^{(k)} \\
h_{i+1}^{(k)} &= h_i^{(k)} + \Delta t \cdot V_{i,i+1}^{(k)} \cdot \sin\gamma_{i,i+1}^{(k)}
\end{aligned} \tag{3-23}$$

Maneuver complexity: High.

- <u>Strategy VI</u>

Description: Change $\gamma^{(k)}$, $V^{(k)}$. $\psi^{(k)} = const$.

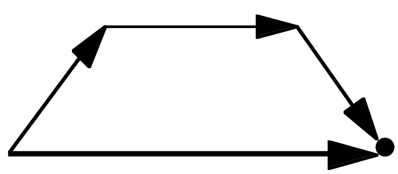

$$V^{(k)} = const$$
$$\psi^{(k)} = \psi^{(k)}(t)$$
$$\gamma^{(k)} = \gamma^{(k)}(t)$$

Equations of motion:

$$\begin{aligned}
x_{i+1}^{(k)} &= x_i^{(k)} + \Delta t \cdot V_{cruise}^{(k)} \cdot \cos\psi_{i,i+1}^{(k)} \cdot \cos\gamma_{i,i+1}^{(k)} \\
y_{i+1}^{(k)} &= y_i^{(k)} + \Delta t \cdot V_{cruise}^{(k)} \cdot \sin\psi_{i,i+1}^{(k)} \cdot \cos\gamma_{i,i+1}^{(k)} \\
h_{i+1}^{(k)} &= h_i^{(k)} + \Delta t \cdot V_{cruise}^{(k)} \cdot \sin\gamma_{i,i+1}^{(k)}
\end{aligned} \tag{3-24}$$

Maneuver complexity: High.

- <u>Strategy VII</u>

Description: Change $\gamma^{(k)}$, $V^{(k)}, \psi^{(k)}$.

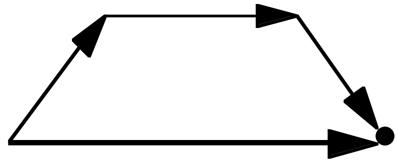

$$V^{(k)} = V^{(k)}(t)$$
$$\psi^{(k)} = \psi^{(k)}(t)$$
$$\gamma^{(k)} = \gamma^{(k)}(t)$$

Equations of motion:

$$\begin{aligned}
x_{i+1}^{(k)} &= x_i^{(k)} + \Delta t \cdot V_{i,i+1}^{(k)} \cdot \cos\psi_{i,i+1}^{(k)} \cdot \cos\gamma_{i,i+1}^{(k)} \\
y_{i+1}^{(k)} &= y_i^{(k)} + \Delta t \cdot V_{i,i+1}^{(k)} \cdot \sin\psi_{i,i+1}^{(k)} \cdot \cos\gamma_{i,i+1}^{(k)} \\
h_{i+1}^{(k)} &= h_i^{(k)} + \Delta t \cdot V_{i,i+1}^{(k)} \cdot \sin\gamma_{i,i+1}^{(k)}
\end{aligned} \tag{3-25}$$

Maneuver complexity: Very High.

3.2 Practical Implementation

The previous section describes mathematical and physical approaches to conflict resolution involved in Free Flight modeling. These models can be useful if applied to a small number of aircraft. Otherwise, the computational time, required to resolve the conflicts in the system, is going to be very high. More efficient algorithms are needed in order to process the realistic sets of hundreds and thousands of aircraft. One such algorithm, developed by CSSI, Inc., is outlined in this section.

The most essential part of determining any analysis of changes to the NAS is the development of schedules and associated trajectories reflective of actual demand under new operational concepts being evaluated (e.g., free flight). The schedule gives the basic loading factors at the sources and sinks of the NAS, the airports. The trajectories provide the rest of the loading by providing the path flown or to be flown from which assignments to the NAS components can be made.

The temporal mapping determines where and when a path intersects a NAS component or essentially is a demand on that resource. This four dimensional mapping capability includes the x, y, z, t of both component pierce and departure. Temporal mapping will enable analysis of the loads placed on NAS recourses (i.e., equipment and personnel) associated with new operational concepts.

Once the temporal mapping is done, the NARIM [10] simulation capabilities can be brought to bear. The temporal mapping derived from the schedule and trajectory demand profiles are modeled against capacity parameters representative of NAS resources. The simulation is capable of accurately reflecting control actions that are typically implemented to ensure that procedures are not violated and that NAS resources are not over saturated. Analysis of simulation results yields sector and resource loading data, as well as identification and characterization of potential conflicts.

Since data validity effects the ultimate acceptability of the results, Enhanced Traffic Management System (ETMS) data [13] is used as the data source for schedules and trajectories. ETMS provides the most accurate and comprehensive data source for NAS demand and flight status under current operations. ETMS data covers every IFR aircraft in the NAS and provides track updates for each aircraft approximately every five minutes.

Flight profiles which reflect the flexibility afforded to the user under Free Flight are generated with the Optimum Aircraft Trajectory Generator (OPGEN) [11], [12]. OPGEN produces 4-D flight trajectories based on winds aloft and Special Use Airspace (SUA) status (i.e., access). OPGEN optimizes the overall cost factor by allowing for minimum fuel-burn rates and reduced flight times considering time-variable wind aloft and SUA avoidance based on hours of activation.

Six different route structures were generated using OPGEN. These route structures consist of a baseline and five different variations representing systematic reduction in restrictions, one of the primary objective of Free Flight.

1) Current NAS Operations.

This scenario represents the baseline. It is constructed with RT [13] messages to reflect user preferences under current concept of operations and to preclude reflecting controller intervention actions.

2) Wind-Optimized Routing with Hemispherical Rules.
This scenario reflects removal of the reliance on ground-based NAVAIDs (such as enabled by GPS) but retains current directional flight levels imposed to avoid excessive controller workload (i.e., avoid excessive head-on type conflicts). The flight tracks for these routes are generated using OPGEN and gridded winds aloft and avoid active SUA. The altitude for these routes is filed flight altitude and thus satisfy the following criteria required under the current concept of operations:

Westbound Flight Levels	Eastbound Flight Levels
18,000′ to FL290 - 2000′ beginning at 18,000′ at or above FL290 - 4000′ beginning at FL310	18,000′ to FL290 - 2000′ beginning at FL190 at or above FL290 - 4000′ beginning at FL290

3) Wind-Optimized Routing with Reduced Vertical Separation Minimum (RVSM).

This is an extension of scenario 2 with the exception of flight level. While scenario 2 altitudes are filed altitudes and thus reflect 2000’ vertical separation above FL280 and directional flight levels, altitudes for this scenario are assigned based upon the altitude which satisfies the following criteria and is closest to the filed flight altitude:

Westbound Flight Levels	Eastbound Flight Levels
2000′ beginning at 18,000′	2000′ beginning at FL190

4) Wind-Optimized Profiles with Hemispherical Rules (Cardinal).

This scenario is similar to scenario 2 with the exception that the flight levels in this scenario are aircraft performance based as opposed to reflecting the filed altitude. Cardinal flight altitudes apply, thus the altitudes for these routes satisfy the following criteria:

Westbound Flight Levels	Eastbound Flight Levels
18,000′ to FL290 - 2000′ beginning at 18,000′ at or above FL290 - 4000′ beginning at FL310	18,000′ to FL290 - 2000′ beginning at FL190 at or above FL290 - 4000′ beginning at FL290

5) Wind-Optimized Profiles with RVSM.

This scenario is similar to scenario 4 with the exception that the flight levels in this scenario include RVSM and thus satisfy the following criteria:

Westbound Flight Levels	Eastbound Flight Levels
2000′ beginning at 18,000′	2000′ beginning at FL190

6) Wind-Optimized Profiles without Hemispherical Rules (Cruise-Climb).

This scenario reflect full 4-D en route trajectory optimization on the part of the users. Thus, trajectories are not constrained by flight level, current cardinal altitude rules or RVSM, and reflect full cruise-climb both in the terminal environment and en route.

Chapter 4 Dynamic Density Analysis

The concept of Free Flight as defined in “Final Report of RTCA Task Force 3: Free Flight Implementation,“ dated October 26, 1995 is based heavily on a metric called dynamic density. The premise as outlined in the Task Force 3 report is that when the dynamic density exceeds a predetermined threshold, flight restrictions may be imposed, otherwise free flight is possible. One of the recommendations of the FAA’s “Free Flight Action Plan” prepared for the Government/Industry Free Flight Implementation Group is that methodologies and tools be developed to predict dynamic density. While there are currently several research efforts associated with developing a suitable metric for dynamic density, at this time there is not one that is generally accepted.

This chapter of thesis examines dynamic density for the NAS under current operations and two variations of the Free Flight concept of operations [14]. The primary metrics or traditional indicators to be used are:

- aircraft counts
- aircraft proximity events

These metrics will be compared with relevant dynamic density measures currently being investigated by NASA and FAA research efforts.

4.1 Literature Review

Literature review pertaining to dynamic density uncovered four significant research efforts associated with metrics and methods for measuring dynamic density. Three of these research activities are being done either by NASA or under NASA funding, the fourth is being sponsored by the FAA. Of the three NASA-sponsored activities, one is related to developing a metric for estimating display processing difficulty based on traffic factors. This metric would then be used to estimate the cognitive processing difficulty associated with structured and unstructured traffic patterns. There was not a great deal of information available regarding this metric or the methodology.

Another NASA research activity is being conducted by Dr. Irene Laudeman at NASA Ames Research Center. The dynamic density metric developed under this task incorporates nine traffic factors, uses two-minute time increments and a twenty-minute projection of future aircraft positions. The metric is very sensitive to trajectory prediction accuracy and uses inputs from the CTAS system for aircraft position and conflict prediction information. As a part of recent validation effort, they computed dynamic density for operational sectors at the Denver ARTCC while collecting observations of controller activity. The nine activity measures consisted of 4 communication measures and 5 radar scope related activities. The validation data collected will be used to determine what weights (if any) provide the best fit of the data. At the time this analysis was conducted, the metric was simply a sum of the nine traffic factors

Another NASA sponsored research effort was that performed by Wyndemere [15]. This task identified various factors of an air traffic situation that impact cognitive complexity of control and developed a model designed to evaluate the perceived complexity of an air traffic situation. The overall complexity measure developed uses eleven individual factors. The study included controller interviews to determine the relative weighting of the contributing factors. Controllers rated each complexity factor individually and then by combinations of pairs of factors. The study also included evaluating the complexity of air traffic, as measured by the algorithm developed, for today's concept of operations and for free flight. The result of this analysis was quite different from previous analyses that used only airspace density and proximity event occurrence rates as metrics. The comparison indicated a large increase in complexity, as measured by the new algorithm, for free flight as compared to current operations. The conclusion drawn by the researchers is that measures of density and conflict event occurrence rates do not adequately capture the overall complexity of ATC and further that physical processes alone are not enough to allow a full understanding of the complexity of ATC.

An FAA sponsored dynamic density research effort was conducted by Drs. K. Smith, S.F. Scallen, W. Knecht, and P.A. Hancock [16]. The research identified an index that focuses on separation, since separation was noted as the single most important factor in estimating collision risk. The Reference paper first presents an algorithm for the more general aircraft pair. This calculation uses three parameters; the distance between the aircraft pair, a normalization constant, and a weighting parameter, a, which is empirically determined and used to weight the contribution of closer aircraft while diminishing the impact of more distant aircraft. The calculation was expanded to capture the interaction between a single aircraft and multiple aircraft targets. The sensitivity of the dynamic density metric as a function of the weighting parameter a was presented. The point illustrated is that smaller values of a tend to blur information about the different aircraft, while larger values of a tend to suppress the effects of distant aircraft. This further illustrates the empirical nature of selecting an appropriate value of a. The calculation was finally expanded to consider all pairings of aircraft at the same altitude to yield a global index of traffic density.

For this analysis the Kip Smith and Irene Laudeman metrics as well as the aforementioned traditional indicators were incorporated. A detailed description of the metrics used in this study is presented in the next chapter.

4.2 Dynamic Density Metrics Description

Aircraft Counts:

This number represents the number of aircraft physically present within the sectors (cells) boundaries at a given time.

$$D_t = N_t \tag{4-1}$$

N_t - count of all aircraft currently in the sector (cell)

Proximity Events Counts:

To calculate the number of proximate aircraft pairs the same methodology described in the Section 2.4.2 was used.

$$D_t = \left\{ N_{d(t)<10}, N_{d(t)<15}, N_{d(t)<20} \right\} \tag{4-2}$$

$N_{d(t)<10}, N_{d(t)<15}, N_{d(t)<20}$ - number of aircraft pairs not separated by altitude with lateral separation less than 10, 15 and 20 nmi. respectively.

The following altitude separation bands were used in this study:

- for flight levels below FL290 - 700 ft;
- for flight levels above FL290 - 1700 ft.

Kip Smith Metric:

This metric is the product of an FAA sponsored dynamic density research effort conducted by Drs. K. Smith, S.F. Scallen, W. Knecht, and P.A. Hancock. The research identified an index that focuses on separation as the single most important factor in estimating collision risk.

$$K_t = \sum_{i=1}^{N-1} \sum_{j=i+1}^{N} \frac{1}{\left(\frac{d_{ij}(t)}{c} \right)^a} \tag{4-3}$$

N - number of aircraft
d_{ij} - distance between two aircraft not separated by altitude
c - normalization constant, equal to 5 nmi., the minimum allowable lateral separation by current FAA regulations
a - weighting parameter, set to 3 for a reasonable balance between the relative contributions of close and distant aircraft

Laudeman Metric:

This metric is the result of research activity conducted by Dr. Irene Laudeman at NASA Ames Research Center. The dynamic density metric developed under this task incorporates nine traffic factors, uses two-minute time increments and a twenty-minute projection of future aircraft positions.

$$\begin{aligned} D_t &= N_t + N_{\Delta h(t-2,t)} + N_{\Delta V(t-2,t)} + N_{\Delta \psi(t-2,t)} + N_{out(t-2,t)} \\ &+ N_{\varepsilon(t)<5,d(t+20)>5} + N_{\varepsilon(t)\in(5,10),d(t+20)>5} + N_{d(t)<25,d(t+20)<5} \\ &+ N_{d(t)\in(25,40),d(t+20)<5} + N_{d(t)\in(40,70),d(t+20)<5} \end{aligned} \tag{4-4}$$

N_t - count of all aircraft currently in the sector (cell)
$N_{\Delta h(t-2,t)}$ - count of aircraft found to have changed altitude during previous two minutes
$N_{\Delta V(t-2,t)}$ - count of aircraft found to have changed speed during previous two minutes
$N_{\Delta \psi(t-2,t)}$ - count of aircraft found to have changed heading during the previous two minutes
$N_{out(t-2,t)}$ - count of aircraft whose speed is +/- 150 knots of mean aircraft speed in
sector
$N_{\varepsilon(t)<5,d(t+20)>5}$ - count of aircraft (not predicted to be in conflict) whose Euclidean distance is < 5 nmi.
$N_{\varepsilon(t)\in(5,10),d(t+20)>5}$ - count of aircraft (not predicted to be in conflict) whose Euclidean distance is between 5 and 10 nmi.
$N_{d(t)<25,d(t+20)<5}$ - count of aircraft predicted to be in conflict with current range <25nmi.
$N_{d(t)\in(25,40),d(t+20)<5}$ - count of aircraft predicted to be in conflict with current range between 25 and 40 nmi.
$N_{d(t)\in(40,70),d(t+20)<5}$ - count of aircraft predicted to be in conflict with current range between 40 and 70 nmi.

Threshold for altitude change: 750 ft over 2 min interval.
Threshold for speed change: 10 knots over 2 min interval.
Threshold for heading change: 10 degrees over 2 min interval.

In this analysis, along with the absolute value of this metric, its normalized version was introduced. The normalized Laudeman metric is the ratio of count of all aircraft in the sector (cell) and absolute value of this metric. Since aircraft count is one of the nine components of Laudeman metric, the normalized Laudeman metric ranges from 0 to 1. Small values of this metric then indicate high level of activity in the sector (cell).

4.3 Methodology

The methodology that was used for this analysis involved using several of the existing NARIM analysis tools and the development of a new tool, the Dynamic Density Metric Analysis Tool (DDMAT) (see Appendix C). The NARIM ETMS Parser was used to generate the baseline scenario corresponding to current operations. Two variations of the free flight concept of operations were subsequently generated using another NARIM analysis tool, OPGEN. The two free flight variants are:

- Wind-optimized routing without hemispherical rules (referred to in the remainder of this chapter as “Wind Optimized (Cruise-Climb)” and
- Wind-optimized routing with hemispherical rules (referred to in the remainder of this chapter as “Wind Optimized (Cardinal Rules)”.

To reduce the computational load while still allowing a comprehensive analysis, the scope of the analysis was limited to a single center, Atlanta and the associated sectors contained within the center. The scenarios contain 18 hours of traffic data corresponding to 6:00 AM to 11:59 PM EST for April 6, 1996.

The DDMAT consists of three major components: a preprocessor, a dynamic density computational element, and a graphical post processor. The preprocessor is essentially used as a coarse filter to reduce the demand scenario to the area of interest which is expressed as the minimum bounding rectangle around the center, and time of interest. The preprocessor creates a specially formatted file that can be quickly loaded by the dynamic density computational element. Any flight that passes through the area of interest at any time during the 18 hour time window is included in this file. Since the Laudeman metric includes aircraft that are predicted to be in conflict within a series of specified ranges, the minimum bounding rectangle was slightly expanded in order to capture aircraft that could be outside the Center but still near the boundary and would therefore be required to properly compute the value of this metric. Additionally, calculation of the Laudeman dynamic density metric assumes perfect knowledge of future aircraft positions. In this analysis the metric is calculated based on existing data as opposed to in real-time, thereby precluding the requirement to predict future aircraft position.

The dynamic density computation element is used to compute the grid count, the number of proximity events, the value of the Kip Smith dynamic density metric, and the value of the Laudeman dynamic density metric for each of the scenarios and is implemented as a series of MATLAB programs. For this study, the grid count refers to the current sectorization of Atlanta Center or a one-degree grid placed upon Atlanta Center. The dynamic density metrics are computed for cells since current sectorization will likely change during the evolution to free flight. Prior to computing the dynamic density metrics, the flight plan data is processed in order to construct a 4-D discretized flight plan for every aircraft on a 2 minute time interval. After completing this, the four metrics can be computed at every time step. The grid count is defined as the number of aircraft that are physically within the bounds of the sector or cell and are above FL240. The number of proximity events refers to the number of aircraft that fall within the prescribed altitude bands (e.g. 700 ft. below FL290 and 1700 ft. above FL290) at a distance of 10, 15, and 20 nmi. A complete description of the Kip Smith and Laudeman dynamic density metrics is included in Section 4.2.

The DDMAT post processor is used to generate a wide variety of output including the value of all metrics (traditional indicators and dynamic density metrics) vs. time for any sector or cell, the correlation between grid counts and the dynamic density metrics, and the correlation between proximity event counts and the dynamic density metrics. Additionally, the DDMAT post processor generates a summary report file containing a summary of each scenario. An example of this report file has been included in Appendix B.

Figure 4.1 depicts the 14 high altitude sectors for the Altanta Center with the sector numbers shown inside the sector. Note that sectors 42 and 43 have the same horizontal bounds but are separated by altitude as is the case for sectors 32 and 34.

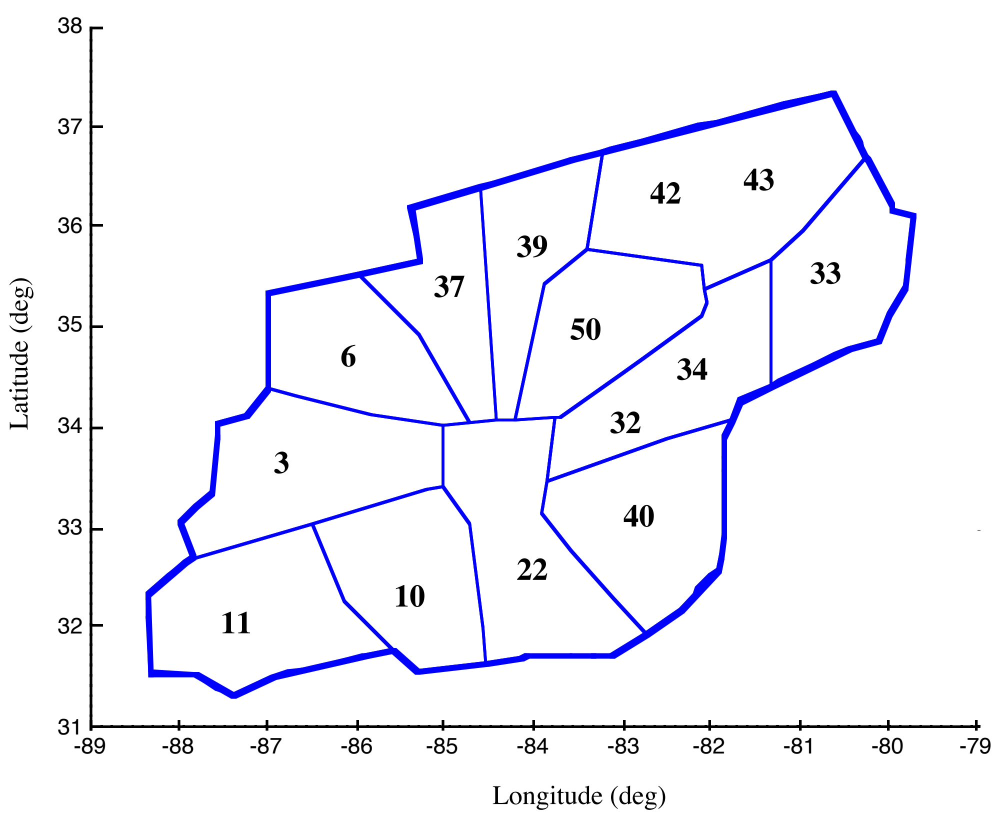

Figure 4.1 High Altitude Sectors

Figure 4.2 depicts the 7 ultra high altitude sectors for the Atlanta Center with the sector number shown inside the sector. The value of the four metrics is computed for each high and ultra high sector for the three scenarios.

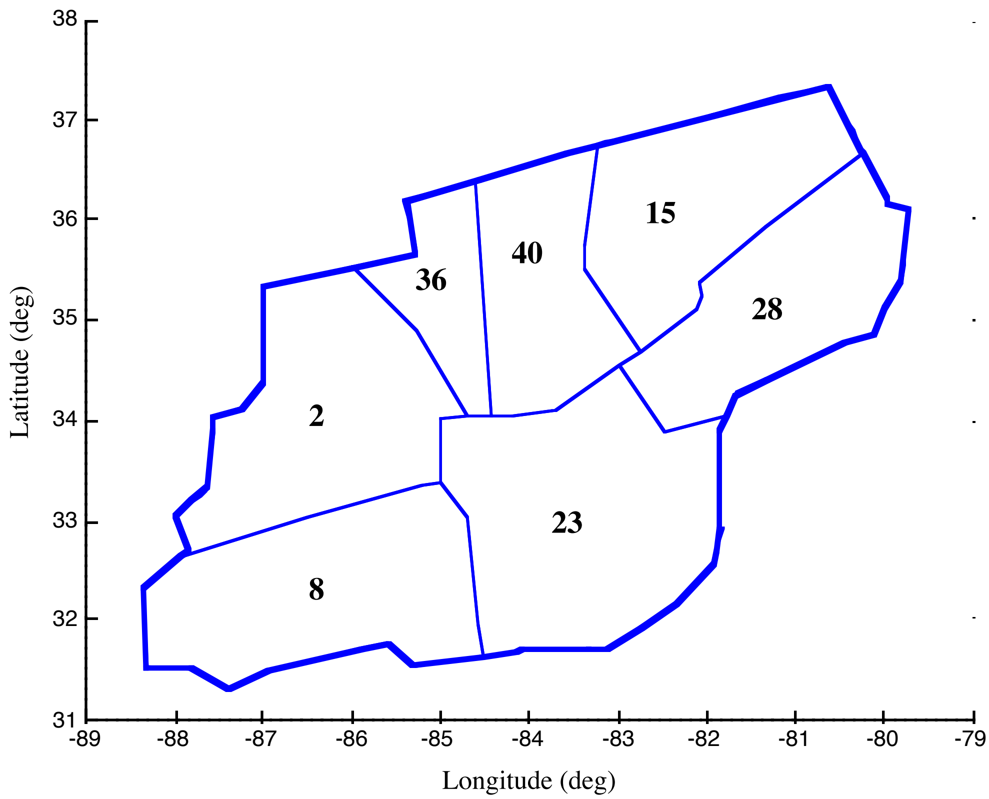

Figure 4.2 Ultra High Altitude Sectors

A one degree by one degree cell grid for Atlanta Center is depicted in Figure 4.3. There are 47 cells that encompass the Atlanta Center. The cells comprise altitudes from FL240 and higher. The value of the four metrics was also computed for each cell for all three scenarios.

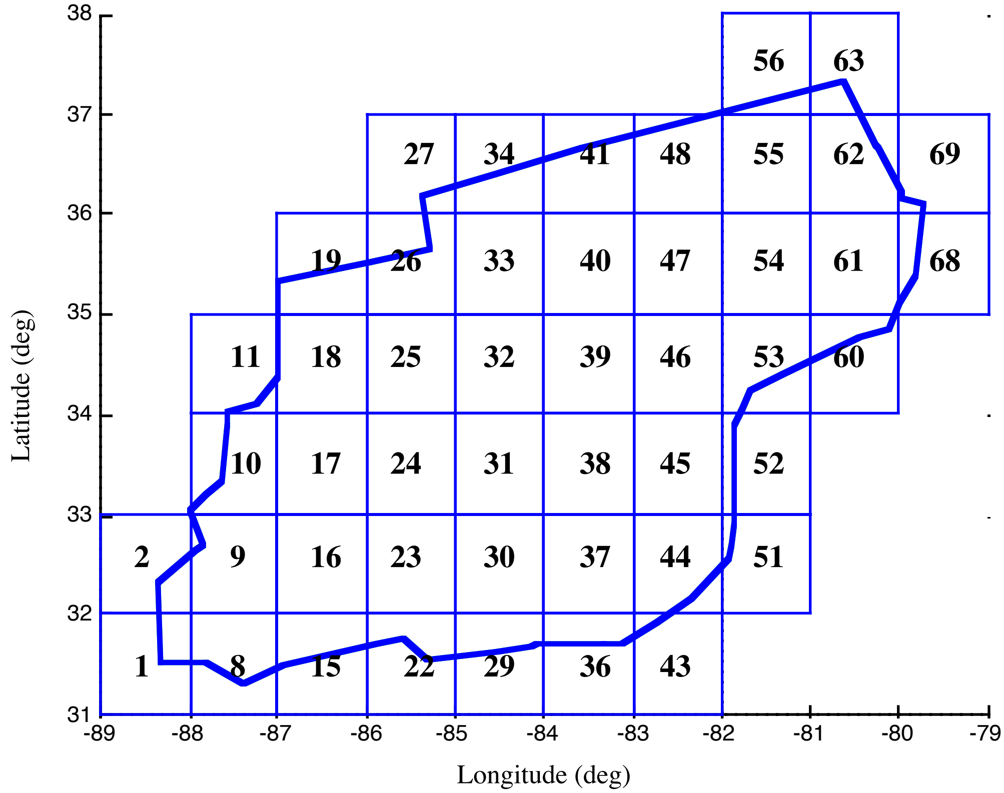

Figure 4.3 Atlanta Center, 1x1 Degree Cells

Figure 4.4 and 4.5 depict a two hour sample of traffic data for the baseline scenario and the "Wind Optimized (Cruise Climb)" scenario, respectively. These plots show the Center boundaries and the ground track for every aircraft that occupies the Center during the scenario time. The baseline traffic pattern exhibits a distinct node and link structure representing major fixes and jet routes. In contrast, Figure 4.5 clearly depicts a more distributed traffic pattern as compared to Figure 4.4. The volume of traffic is nearly identical between the two scenarios with many aircraft sharing the same ground track for the baseline scenarios as compared to the "Wind Optimized (Cruise Climb)" scenario wherein the ground tracks are unique.

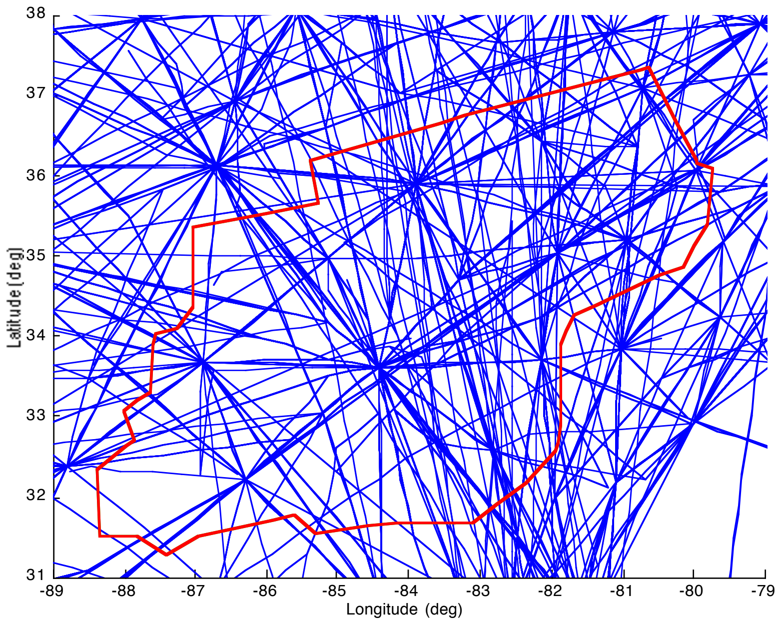

Figure 4.4 Baseline Scenario Traffic Pattern

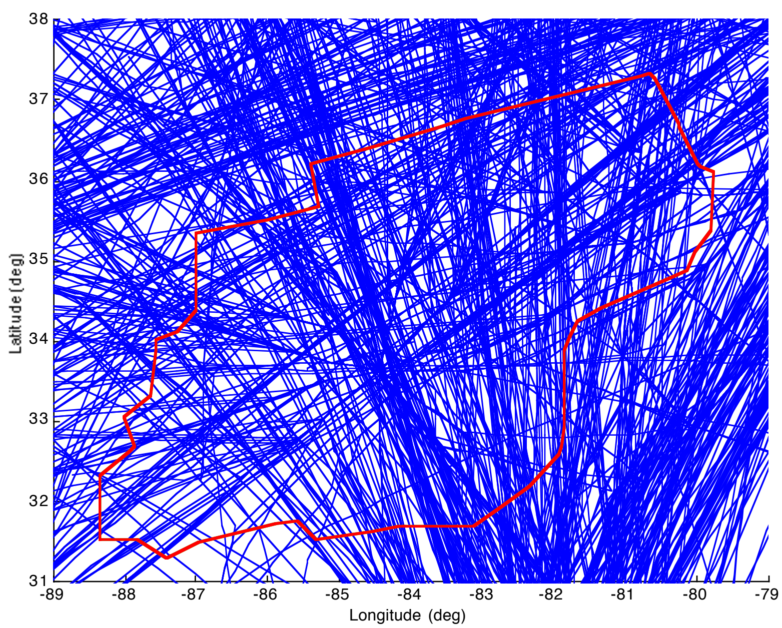

Figure 4.5 Cruise Climb Traffic Pattern

4.4 Results

The Dynamic Density Metric Analysis Tool was used to process the three scenarios previously discussed. The tool generated a wide variety of output data that will be discussed in this section of the report. The discussion will include a comparison of how the metrics vary between the three scenarios, the correlation between various metrics, a ranking of sectors and cells, and a comparison of how the monitor alert threshold varies between the scenarios.

4.4.1 Baseline Comparison

The first analysis that was performed was to compare the change in the four metrics between the baseline and the free flight variants. Table 4.1 shows the absolute number of sectors that change from the baseline by the ranges shown in column 1. For example, if the value of the metrics changed by less than 10% (i.e. either negative or positive) between the baseline and the free flight variants, the sectors of interest would be included in the "Unchanged (~10%)" row. Similarly, if the value of the metric increases from 10% to 25% from the baseline, the sector would be included in the "+25%" row. The dynamic density metrics were computed for 21 sectors and as such the sum of each column is 21.

The grid count in Table 4.1 refers to the number of unique aircraft that fall within the physical bounds of the sector. The proximity events count refers to the total number of unique proximity events between aircraft pairs that are within a 10 nmi. cutoff region. The Kip Smith entry in the table is a cumulative sum of the Kip Smith metric over the 18 hour scenarios. The Laudeman metric table entry is the mean value of the metric over the entire scenario.

By examining the table some general observations may be made. For both scenarios, the maximum observed change in the Laudeman metric is plus or minus 25% with all but one sector changing less than 10%. Table 4.1 indicates that the Laudeman metric is the least sensitive metric to changes between various scenarios. Alternatively, the Kip Smith metric shows a larger number of sectors that either increase or decrease, with nearly half decreasing between 50% and 100%.

1Table 4.1 Sector Baseline Comparison

Change From Baseline (%)	Wind Optimized (Cruise - Climb)				Wind Optimized (Cardinal Rules)			
	Grid Count	Prox. Events	Kip Smith	Laude -man	Grid Count	Prox. Events	Kip Smith	Laude -man
Unchanged (~10%)	7	3	1	20	7	4	1	20
-25%	2	2	0	0	3	1	0	1
-50%	0	5	3	0	0	7	2	0
-75%	0	1	5	0	0	0	6	0
-100%	0	0	5	0	0	1	5	0
+25%	6	2	1	1	7	2	1	0
+50%	3	1	0	0	3	1	0	0
+75%	0	1	1	0	0	2	2	0
+100%	2	2	1	0	0	1	1	0
More than +100%	1	4	4	0	1	2	3	0

Table 4.2 is constructed in a similar manner as Table 4.1 with the principal difference being that this table compares the metrics between the baseline and the free flight variants using a cell-based approach. Referring back to Figure 4.3, there were 47 cells identified in the Atlanta Center and as such, the sum of each column of this table is 47. As was the case with the sector-based analysis shown in Table 4.1, the percentage change in the Laudeman metric for all cells was within plus or minus 25%. The Kip Smith metric exhibits the largest change, with a large number of cells increasing between 75% and 100%.

Table 4.2 Cell Baseline Comparison

Change From Baseline (%)	Wind Optimized (Cruise - Climb)				Wind Optimized (Cardinal Rules)			
	Grid Count	Prox. Events	Kip Smith	Laude -man	Grid Count	Prox. Events	Kip Smith	Laude -man
Unchanged (~10%)	14	12	0	43	12	6	1	43
-25%	17	4	4	1	19	6	3	1
-50%	8	12	2	0	7	15	1	0
-75%	0	12	7	0	0	12	7	0
-100%	0	4	26	0	0	5	28	0
+25%	6	1	2	3	7	1	1	3
+50%	1	2	1	0	1	1	1	0
+75%	1	0	1	0	0	1	2	0
+100%	0	0	2	0	1	0	1	0
More than +100%	0	0	2	0	0	0	2	0

4.4.2 Metric Correlation Coefficients

An analysis of the correlation between various metrics was performed for each of the three scenarios. Table 4.3 shows the correlation for the aircraft count and proximity event count for 10, 15, and 20 nmi. with both the Laudeman and Kip Smith metrics for each of the 21 sectors. The table shows a very strong correlation (> 0.90) between the aircraft count and the Laudeman metric for all sectors. This is a result of the formula used for computing the Laudeman metric which includes a term containing the aircraft count (4-4). If the remaining terms in the equation were sufficiently small, the correlation would approach 1. There does not appear to be any strong correlation between any of the remaining metrics shown in this table. However, a few general trends can be observed. For example, the correlation between the Laudeman metric and the three proximity event counts tend to increase slightly when going from the 10 nmi. range to 15 and 20 nmi. ranges. While the correlation coefficients are statistically insignificant, the general trend does appear which is logical when you consider that as the proximity zone increases it approaches the size of the sector and essentially approaches the sector count. Alternatively, the Kip Smith metric does not appear to be strongly correlated to either aircraft counts or proximity events. The correlation between the Kip Smith metric and the aircraft count is low since the Kip Smith metric depends more on separation than aircraft count. The correlation of the Kip Smith metric seems to decrease with increasing proximity zone which is logical, again since the Kip Smith metric is based largely on separation.

Table 4.3 Baseline Scenario Correlation Coefficients

Sector	Laudeman Metric				Kip Smith Metric			
	Aircraft Counts	Prox. (10 nmi)	Prox. (15 nmi)	Prox. (20 nmi)	Aircraft Counts	Prox. (10 nmi)	Prox. (15 nmi)	Prox. (20 nmi)
2	0.93	0.24	0.37	0.41	0.19	0.79	0.47	0.31
3	0.94	0.47	0.47	0.50	0.22	0.35	0.35	0.32
6	0.94	0.46	0.43	0.44	0.08	0.26	0.21	0.19
8	0.92	0.49	0.50	0.50	0.34	0.62	0.62	0.57
10	0.93	0.42	0.50	0.55	0.23	0.53	0.42	0.37
11	0.91	0.19	0.31	0.32	0.02	0.40	0.26	0.22
15	0.95	0.38	0.53	0.52	0.36	0.94	0.60	0.55
20	0.91	0.17	0.21	0.21	0.15	0.45	0.39	0.32
22	0.95	0.45	0.49	0.51	0.16	0.31	0.29	0.22
23	0.90	0.23	0.30	0.32	0.11	0.27	0.14	0.12
28	0.93	0.38	0.35	0.48	0.18	0.46	0.54	0.43
32	0.96	0.52	0.58	0.61	0.05	0.24	0.19	0.15
33	0.91	0.32	0.35	0.37	0.19	0.30	0.26	0.27
34	0.95	0.38	0.42	0.44	0.07	0.26	0.22	0.16
36	0.92	-	-	0.21	0.41	-	-	0.89
37	0.94	0.49	0.51	0.52	0.17	0.32	0.29	0.25
39	0.94	0.53	0.57	0.56	0.16	0.22	0.17	0.20
40	0.90	0.23	0.31	0.39	0.25	0.82	0.62	0.58
42	0.93	0.29	0.24	0.27	0.18	0.29	0.33	0.30
43	0.93	0.52	0.59	0.62	0.21	0.31	0.23	0.22
50	0.95	0.50	0.54	0.53	0.28	0.43	0.33	0.27
Mean	0.93	0.41	0.43	0.44	0.19	0.46	0.38	0.33

Table 4.4 and 4.5 are constructed in a similar manner as Table 4.3 but show the correlation coefficients for the “Wind Optimized (Cruise Climb)” scenario, and the correlation coefficients for the “Wind Optimized (Cardinal Rules)” scenario, respectively. In the “Wind Optimized (Cardinal Rules)” scenario, aircraft are required to follow hemispherical rules (i.e. directional flight levels). The aircraft are slightly more constrained than the aircraft in the ‘Wind Optimized (Cruise Climb)” scenario but not nearly has much as the baseline. Both free flight scenarios exhibit the same patterns in the correlation coefficients as the baseline.

Table 4.4 Wind Optimized (Cruise-Climb) Correlation Coefficients

Sector	Laudeman Metric				Kip Smith Metric			
	Aircraft Counts	Prox. (10 nmi)	Prox. (15 nmi)	Prox. (20 nmi)	Aircraft Counts	Prox. (10 nmi)	Prox. (15 nmi)	Prox. (20 nmi)
2	0.92	0.33	0.40	0.45	0.03	0.35	0.26	0.19
3	0.94	0.41	0.47	0.53	0.16	0.30	0.30	0.23
6	0.93	0.46	0.45	0.45	0.08	0.25	0.20	0.15
8	0.90	0.45	0.47	0.47	0.25	0.59	0.46	0.38
10	0.93	0.48	0.50	0.51	0.16	0.44	0.42	0.32
11	0.91	0.11	0.19	0.32	0.01	0.43	0.32	0.24
15	0.96	0.51	0.66	0.66	0.27	0.47	0.41	0.39
20	0.90	0.23	0.30	0.25	0.16	0.74	0.41	0.33
22	0.95	0.49	0.53	0.55	0.21	0.48	0.43	0.43
23	0.92	0.25	0.25	0.25	0.20	0.56	0.43	0.34
28	0.93	0.49	0.54	0.52	0.29	0.57	0.44	0.29
32	0.95	0.49	0.50	0.51	0.10	0.18	0.14	0.09
33	0.93	0.42	0.45	0.45	0.14	0.31	0.20	0.16
34	0.95	0.31	0.31	0.39	0.12	0.18	0.14	0.11
36	0.96	0.29	0.42	0.54	0.15	0.35	0.21	0.14
37	0.93	0.36	0.42	0.44	0.09	0.34	0.22	0.17
39	0.94	0.48	0.54	0.56	0.11	0.29	0.20	0.15
40	0.95	0.30	0.31	0.40	0.22	0.68	0.48	0.45
42	0.92	0.17	0.19	0.26	0.16	0.38	0.31	0.28
43	0.94	0.45	0.49	0.53	0.19	0.28	0.17	0.12
50	0.94	0.62	0.60	0.60	0.32	0.38	0.36	0.32
Mean	0.94	0.39	0.43	0.46	0.17	0.41	0.31	0.26

Table 4.5 Wind Optimized (Cardinal Rules) Correlation Coefficients

Sector	Laudeman Metric				Kip Smith Metric			
	Aircraft Counts	Prox. (10 nmi)	Prox. (15 nmi)	Prox. (20 nmi)	Aircraft Counts	Prox. (10 nmi)	Prox. (15 nmi)	Prox. (20 nmi)
2	0.92	0.32	0.37	0.34	0.04	0.32	0.25	0.19
3	0.94	0.41	0.49	0.55	0.17	0.31	0.30	0.23
6	0.93	0.40	0.41	0.42	0.03	0.19	0.16	0.12
8	0.90	0.51	0.53	0.52	0.27	0.58	0.47	0.39
10	0.93	0.48	0.52	0.52	0.16	0.43	0.41	0.31
11	0.91	0.12	0.20	0.32	0.01	0.44	0.32	0.25
15	0.95	0.42	0.60	0.60	0.32	0.74	0.53	0.47
20	0.89	0.22	0.25	0.27	0.15	0.50	0.21	0.19
22	0.94	0.48	0.52	0.53	0.20	0.48	0.43	0.43
23	0.91	0.17	0.17	0.14	0.32	0.84	0.70	0.57
28	0.93	0.47	0.52	0.48	0.30	0.56	0.43	0.29
32	0.95	0.48	0.50	0.50	0.10	0.18	0.14	0.09
33	0.92	0.41	0.44	0.44	0.14	0.31	0.19	0.16
34	0.95	0.33	0.32	0.40	0.12	0.18	0.14	0.11
36	0.96	0.08	0.30	0.34	0.06	0.99	0.23	0.17
37	0.92	0.36	0.42	0.44	0.07	0.32	0.22	0.18
39	0.94	0.47	0.56	0.55	0.10	0.28	0.19	0.14
40	0.92	0.19	0.23	0.23	0.14	0.61	0.35	0.30
42	0.92	0.18	0.18	0.23	0.16	0.38	0.31	0.28
43	0.93	0.46	0.50	0.54	0.19	0.28	0.17	0.12
50	0.93	0.60	0.59	0.59	0.31	0.38	0.36	0.31
Mean	0.93	0.36	0.41	0.43	0.17	0.45	0.32	0.26

Table 4.6 shows the effect of increasing proximity alert zone size on the correlation coefficients of the different metrics. It is constructed by counting the number of sectors where the correlation coefficient either increases, decreases, or stays the same for the Laudeman and Kip Smith metrics as compared to the proximity event alert zone size. The table shows that, on average, the correlation increases with increasing alert zone sizes for the Laudeman metric. Conversely, the table shows that the correlation between Kip Smith metric and the proximity event alert zone decreases with increasing alert zone size. The average correlation coefficient for the three proximity event alert zone sizes also supports this conclusion. These results apply to all three scenarios with the principal difference being the number of sectors that either increase or decrease. Virtually all of the sectors' correlation coefficients (i.e. 16-21) decrease with increasing alert zone size for the Kip Smith metric which is a direct result of this metric diminishing the contribution of conflict pairs with greater separation. The Laudeman and Kip Smith metrics tend to disagree in their respective correlation coefficients in regard to proximity event alert zone sizes.

Table 4.6 Proximity Count Correlation

Scenario	Type	Laudeman		Kip Smith	
		10 to 15	15 to 20	10 to 15	15 to 20
Baseline	+	16	15	2	1
Baseline	-	3	3	16	19
Baseline	nc	2	3	3	1
Cruise-Climb	+	18	13	0	0
Cruise-Climb	-	1	2	20	20
Cruise-Climb	nc	2	6	1	1
Cardinal Rules	+	17	11	0	0
Cardinal Rules	-	2	4	21	20
Cardinal Rules	nc	2	6	0	1

4.4.3 Ranking

Tables 4.7 and 4.8 provide a ranking of sectors and cells respectively for the various dynamic density metrics. A higher sector or cell ranking indicates a higher value of the associated metric for the sector or cell. The rankings have been performed for the baseline scenario shown under the "BL" column, wind optimized (cruise climb) under the "CC" column, and the wind optimized (cardinal rules) under the "CD" column. The rankings range from 1 to 21, with 21 being the highest and 1 the lowest. Performing the sector and cell ranking is useful for comparing the relative dynamic density of sectors and cells across all metrics and scenarios. For example, sector 22 has a very high ranking for all of the metrics. Sector 22 rankings range from 16 to 21 with most in the 20-21 range. The sector 22 (shown in bold) rankings for aircraft counts, the number of proximity events, and the Kip Smith metric fall between 20 and 21. In contrast, the Laudeman metric is somewhat lower for all three scenarios, ranging between 16 and 20. Sectors 32 and 34 have a very high ranking for all three scenarios using the Laudeman metric but have significantly lower rankings for the remaining metrics. In the case of sector 32, ZTL's primary departure sector for Atlanta Hartsfield International Airport, this is logical since the Laudeman metric considers altitude transitions, which would be prevalent in this sector.

On the opposite end of the spectrum, sector 36 rankings are consistently low for all of the metrics and scenarios. They range from 1 to 7 with a majority being in the 1 to 2 range. These numbers indicate that sector 36 (shown in bold) probably has a lower average dynamic density than other sectors examined in the Atlanta Center. One interesting observation is that sector ranking by a dynamic density measure is relatively consistent across scenarios. That is, the ranking of a sector by any metric (e.g. aircraft count, Laudeman) does not vary significantly across scenarios (e.g. BL, CC, CD).

Table 4.7 Ranking Of Sectors

Sector	Aircraft Count			Prox. (10 nmi)			Kip Smith			Laudeman		
	BL	CC	CD	BL	CC	CD	BL	CC	CD	BL	CC	CD
2	4	8	7	4	11	11	4	12	12	6	8	10
3	20	16	16	17	16	15	12	13	13	19	16	16
6	14	18	18	13	19	17	14	16	15	13	18	18
8	3	2	1	2	1	4	8	9	9	10	7	7
10	12	12	12	15	18	18	19	18	18	18	17	17
11	10	9	10	10	9	10	7	5	7	11	6	6
15	6	5	6	7	10	6	3	6	6	3	2	2
20	11	11	11	11	3	7	10	10	10	12	10	9
22	**21**	**20**	**20**	**21**	**21**	**21**	**21**	**21**	**21**	**16**	**20**	**19**
23	9	10	9	10	4	2	5	1	1	2	5	5
28	7	1	3	6	6	8	16	4	5	5	4	4
32	13	15	14	12	15	16	17	15	16	21	21	21
33	19	13	13	14	12	12	18	17	17	7	13	13
34	5	3	4	3	2	5	9	14	14	20	19	20
36	**1**	**4**	**2**	**1**	**7**	**1**	**1**	**7**	**3**	**1**	**1**	**1**
37	16	14	15	18	14	14	15	8	8	15	12	12
39	15	17	17	19	17	19	13	19	19	14	11	11
40	2	7	5	5	8	3	2	2	2	8	3	3
42	8	6	8	8	5	9	6	3	4	4	9	8
43	18	19	19	16	13	13	11	11	11	9	15	15
50	17	21	21	20	20	20	20	20	20	17	14	14

Table 4.8 summarizes the ranking for the various dynamic density metrics for each scenario and uses the 47 cells previously discussed. In this table, the ranking ranges from 1 to 47 with a 1 indicating a very low value of the dynamic density metric and a 47 being a very high value of the dynamic density. The table shows that cell 39 contains a very high value of the dynamic density metric for all scenarios and metrics. The ranking varies from 38 to 47 indicating a very busy volume of airspace. This particular cell is nearby the Atlanta Hartsfield International Airport and processes a large volume of that airports arrival and departures. Additionally, cell 39 is collocated with sector 50 which had a very high ranking for each of the dynamic density metrics as shown in Table 4.7. For the cell-based ranking, it was not possible to identify a cell that had consistently a very low ranking for all metrics. For example, cell number 22 contains several rankings in the 1 to 6 range but also includes a ranking for the Kip Smith metric of 27 for the baseline scenario. The rankings for cell number 51 vary from 1 to 47 which indicates that, in general, the metrics do not agree. While sector rankings across scenarios seemed relatively consistent for any dynamic density measure, this does not appear the case for cell rankings. That is the ranking by any of the different metrics varied considerably between scenario (e.g. BL, CC, CD). This might be due to the fact that the shift in flight tracks from the baseline to the free flight variants might be constrained to their original sector but shift between cells since cells on average are considerably smaller than sectors.

2Table 4.8 Ranking Of Cells

Cell	Aircraft Count			Prox. (10 nmi)			Kip Smith			Laudeman		
	BL	CC	CD	BL	CC	CD	BL	CC	CD	BL	CC	CD
1	1	4	4	1	2	2	1	8	7	22	30	27
2	9	5	5	20	15	10	10	3	17	36	13	15
8	2	3	3	4	4	5	5	10	8	28	27	28
9	5	7	7	8	12	8	3	20	21	15	11	11
10	11	6	6	6	5	9	4	4	4	10	12	12
11	8	21	20	16	30	23	6	24	18	8	31	30
15	3	1	1	2	1	1	2	15	13	30	36	36
16	23	18	18	32	23	25	22	11	12	39	34	34
17	18	11	11	27	9	11	23	17	16	40	35	35
18	13	22	23	9	21	19	13	30	20	37	40	40
19	12	12	13	28	8	12	15	12	2	24	28	32
22	**4**	**2**	**2**	**3**	**6**	**3**	**27**	**1**	**1**	**1**	**2**	**2**
23	24	17	17	18	24	22	26	13	14	41	41	41
24	6	9	9	5	13	14	8	34	35	45	46	46
25	33	34	34	30	27	28	33	28	29	44	45	45
26	19	37	37	10	29	31	12	29	31	32	26	24
27	34	38	39	37	34	37	44	27	34	17	17	17
29	29	8	8	11	14	16	20	16	15	2	7	7
30	28	15	15	13	10	15	31	32	30	29	42	42
31	31	23	22	38	3	4	34	2	3	9	3	3
32	26	29	27	17	18	13	36	6	5	34	37	39
33	39	35	35	36	35	33	30	41	40	35	29	29
34	16	27	28	22	32	26	39	21	22	31	25	26
36	15	33	33	14	28	24	9	35	36	16	14	14
37	27	47	46	24	38	39	11	40	41	46	44	44
38	7	14	14	7	11	6	19	5	24	18	22	22
39	**38**	**44**	**44**	**44**	**47**	**47**	**47**	**47**	**47**	**47**	**47**	**47**
40	44	39	38	42	45	45	25	43	43	33	32	31
41	30	32	32	25	39	38	18	31	32	4	6	5
43	46	45	45	46	44	40	35	33	33	38	33	33
44	20	16	16	12	7	7	38	23	25	6	4	4
45	14	13	12	33	22	29	17	9	9	26	16	16
46	41	42	42	31	42	42	21	45	45	43	43	43
47	21	40	40	23	43	44	16	25	26	20	23	25
48	10	24	24	19	19	20	14	18	11	14	8	8
51	47	31	31	47	37	35	46	46	46	11	1	1
52	43	26	26	43	26	30	42	19	19	25	18	18
53	25	20	21	21	16	17	29	22	23	27	10	10
54	42	41	41	39	41	41	45	26	28	12	19	19
55	32	36	36	29	36	34	7	14	10	3	20	21
56	35	30	30	40	33	36	41	39	39	13	9	9
60	36	19	19	34	20	21	24	44	44	19	39	38
61	37	28	29	35	25	27	32	7	6	7	15	13
62	40	46	47	41	16	46	40	36	37	23	24	23

63	45	43	43	45	40	43	28	37	27	21	5	6
68	17	10	10	26	17	18	43	42	42	42	38	37
69	22	25	25	15	31	32	37	38	38	5	21	20

4.4.4 Monitor Alert Threshold Comparisons

The percentage of time that each sector exceeds a specified percentage (e.g. 25%, 50%, 75%, 100%) of the sectors monitor alert threshold is shown in Table 4.9. This table provides an important indicator of how this current workload indicator would be affected for the different operational concepts. The last row in the table shows the number of sectors that exceed a given percentage of the MAT. For example, 20 sectors exceed 25% their MAT value from 1.2% to 82.6% of the time for the baseline scenario. In the two free flight variants, all sectors exceed 25% of their MAT value from 0.4% to 80.2% of the time.

As the exceedance criteria is increased, the number of sectors that exceed the threshold decreases. With a 50% MAT value, the number of sectors exceeding this value ranges from 13 to 18. With a 100% MAT value, only 3 sectors exceed this value in the baseline and 4 exceed the value in the two free flight variants. The total time exceeding the value is very small for these cases.

Table 4.9 contains 3 sectors that exceed 100% MAT during each of the three scenarios. These sectors, 22, 32, and 43, are also ranked very high as shown in Table 4.9. Conversely, sector 36 exceeds the 25% MAT value for a small percentage of the time and is ranked very low as shown in Table 4.9. Therefore, at least in these isolated cases, the dynamic density metrics evaluated appear to correspond relatively well with the current workload indicator, exceedance of MAT.

Table 4.9 MAT Summary

Sector	MAT	25 % MAT			50% MAT			75% MAT			100% MAT		
		BL	CC	CD	BL	CC	CD	BL	CC	CD	BL	CC	CD
3	18	49.6	43.2	42.4	18.2	12.0	11.9	1.5	0.9	1.1	-	-	-
6	18	34.6	36.9	37.6	2.3	4.3	4.8	-	-	-	-	-	-
10	18	33.5	28.3	28.2	3.9	3.7	3.7	0.4	0.2	0.2	-	-	-
11	18	10.6	8.3	9.1	-	0.4	0.4	-	-	-	-	-	-
20	18	14.3	18.2	19.6	-	0.6	0.9	-	-	-	-	-	-
22	16	82.6	79.4	80.2	58.3	50.2	51.3	25.0	18.5	20.6	4.3	1.9	2.8
32	16	61.5	61.9	62.2	19.8	20.7	20.7	4.1	3.9	3.9	0.6	0.2	0.2
33	16	53.7	42.0	42.0	10.9	8.2	8.2	0.6	0.6	0.6	-	-	-
34	18	11.3	13.0	13.2	-	1.1	1.1	-	-	-	-	-	-
37	18	37.4	29.8	29.4	7.4	2.8	3.0	0.4	-	-	-	-	-
39	17	40.7	31.5	31.9	10.0	5.2	6.7	0.7	0.2	0.4	-	-	-
42	17	8.5	8.9	8.7	0.7	1.1	0.9	-	-	-	-	-	-
43	17	35.9	35.0	35.0	11.3	9.6	10.2	3.5	3.7	3.5	0.7	0.4	0.2
50	18	45.9	55.2	56.1	13.3	22.0	22.2	1.1	3.2	3.7	-	0.6	0.6
8	18	5.9	6.7	5.2	0.6	0.2	0.2	-	-	-	-	-	-
2	18	3.2	13.0	8.2	-	0.7	0.2	-	-	-	-	-	-
36	18	-	1.9	0.4	-	-	-	-	-	-	-	-	-
40	18	1.2	9.3	1.7	-	-	-	-	-	-	-	-	-
15	18	6.5	12.8	11.5	-	1.5	-	-	-	-	-	-	-
28	18	8.0	6.3	6.1	-	-	-	-	-	-	-	-	-
23	18	19.3	34.4	22.6	1.1	7.2	3.5	-	-	-	-	-	-
Total Sectors (non-zero)		20	21	21	13	18	17	9	8	8	3	4	4

Chapter 5 Cockpit Display of Traffic Information (CDTI) Requirements Analysis

One class of decision support tools currently under research and development by NASA and the FAA are cockpit displays of traffic information (CDTI). These displays are highlighted as a midterm need in the implementation of Free Flight by the recent meetings of the RTCA Taskforce 3 [17] and they are in the NASA AATT development plan as a functionally inherent in the Hazard Avoidance Planner to be developed by AATT's Aircraft Systems and Operations subelement [18]. The purpose of this analysis is to assess the requirements for CDTI to support free flight operations in the en route environment.

5.1 Literature Review

The literature review uncovered numerous research and development efforts dating back to flight tests of CDTI for approach conducted by NASA in 1979 [19]. In this implementation, CDTI display range varied from 1 to 32 miles. The CDTI research efforts reviewed indicate numerous different CDTI range requirements ranging from 10 to 160 nmi. Display range is limited by display size and the literature reviewed seemed to agree that for general aviation applications the maximum display size was 4 inches in diameter due to limited cockpit real-estate.

NASA also recently conducted research on pilots performing self separation using CDTI(s) with variable display ranges [18]. The map ranges of CDTI(s) used in the study could be set by the pilot at 10, 20, 40, 80, or 160 nmi. This study indicated that pilots spent more time operating at the larger (160 nmi) display range in low density conditions, and more time at the smaller (80 nmi or 40 nmi) display ranges when operating in high density conditions. The rationale provided was the reduced range gave better information regarding proximate aircraft and their relative position as compared with the larger display range (i.e., 160 nmi).

RTCA SC-186 is beginning to develop a Minimum Operational Performance Standards (MOPS) for CDTI [17], and has issued a preliminary subset of a MOPS containing guidance information for some near term applications (such as CDTI for basic GA situational awareness and enhanced VFR operations).

5.2 Methodology and Results

This analysis [19] was conducted in 2 parts, the first part entailed a high-level analysis of en route display requirements on a national level. The second part of the analysis was a higher fidelity analysis of display requirements performed for a single en route Center.

5.2.1 National Airspace Analysis

Table 5.1 and Figure 5.1 describe 20 contiguous ARTCCs used in National Airspace analysis.

Table 5.1 Contiguous ARTCCs

ARTCC	Name	Location	Approximate Area (nmi sq.)
ZAB	Albuquerque	Albuquerque, New Mexico	179,240
ZTL	Atlanta	Hampton, Georgia	91,357
ZBW	Boston	Nashua, New Hampshire	111,770
ZAU	Chicago	Aurora, Illinois	75,450
ZOB	Cleveland	Oberlin, Ohio	67,337
ZDV	Denver	Longmont, Colorado	200,860
ZFW	Fort Worth	Euless, Texas	122,620
ZHU	Houston	Houston, Texas	275,220
ZID	Indianapolis	Indianapolis, Indiana	70,529
ZJX	Jacksonville	Hilliard, Florida	144,750
ZKC	Kansas City	Olathe, Kansas	133,010
ZLA	Los Angeles	Palmdale, California	135,190
ZME	Memphis	Memphis, Tennessee	106,770
ZMA	Miami	Miami, Florida	356,680
ZMP	Minneapolis	Farmington, Minnesota	285,970
ZNY	New York	Ronkonkoma, New York	76,145
ZOA	Oakland	Fremont, California	130,660

ZLC	Salt Lake City	Salt Lake City, Utah	312,330
ZSE	Seattle	Auburn, Washington	194,360
ZDC	Washington	Leesburg, Virginia	120,160

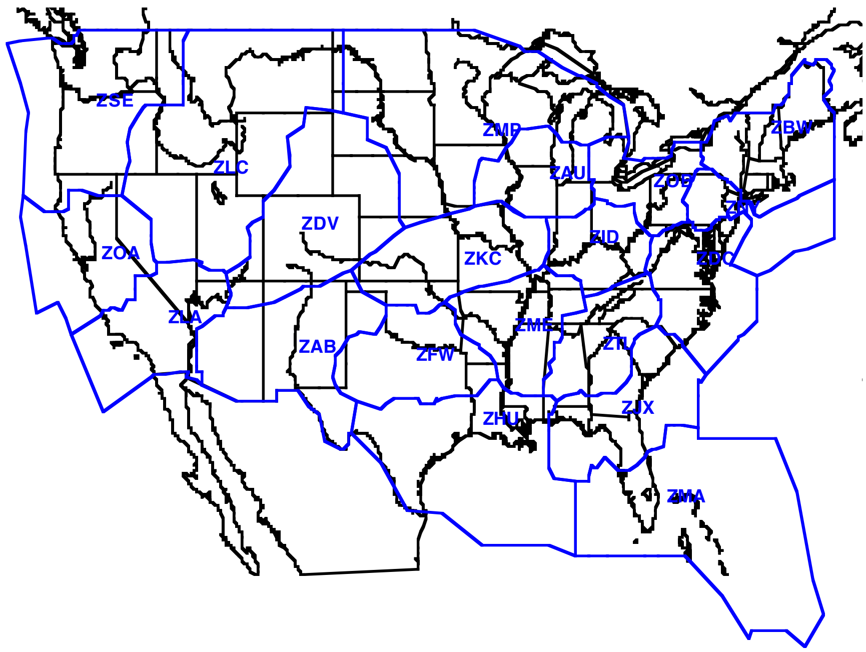

Figure 5.1 Contiguous ARTCCs

Figures 5.2-5.5 show mean, maximum, relative mean and relative maximum aircraft counts for 1/4/96 (Baseline) by ARTCCs. Relative mean and maximum are calculated by dividing mean and maximum counts by the areas of respective ARTCCs.

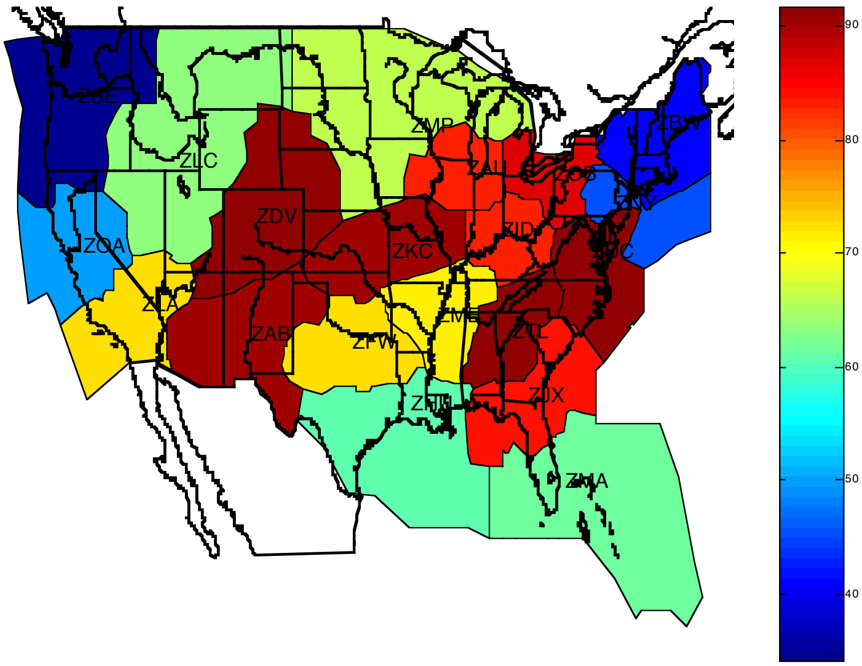

Figure 5.2 Mean Aircraft Count (Baseline)

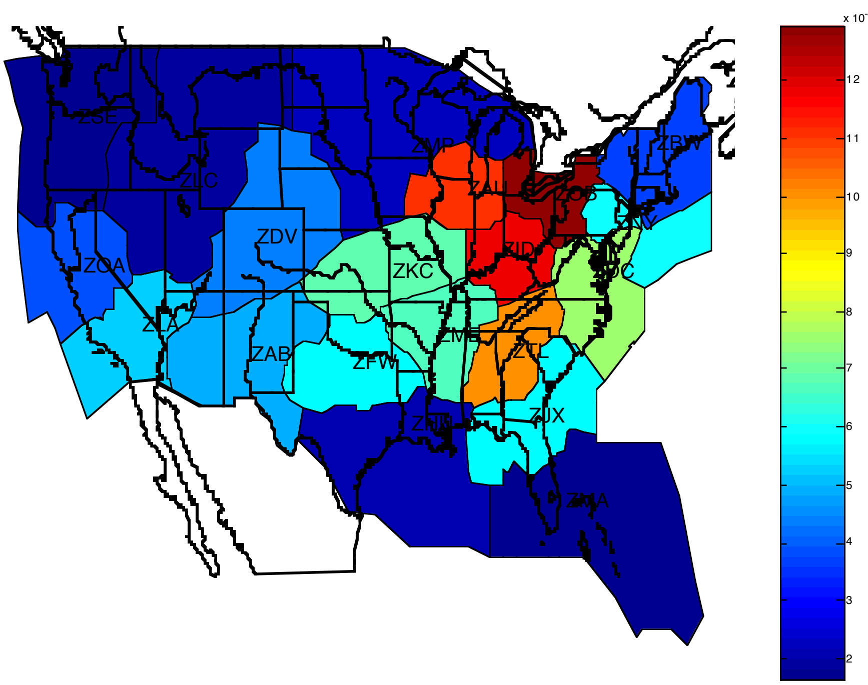

Figure 5.3 Relative Mean Aircraft Count (Baseline)

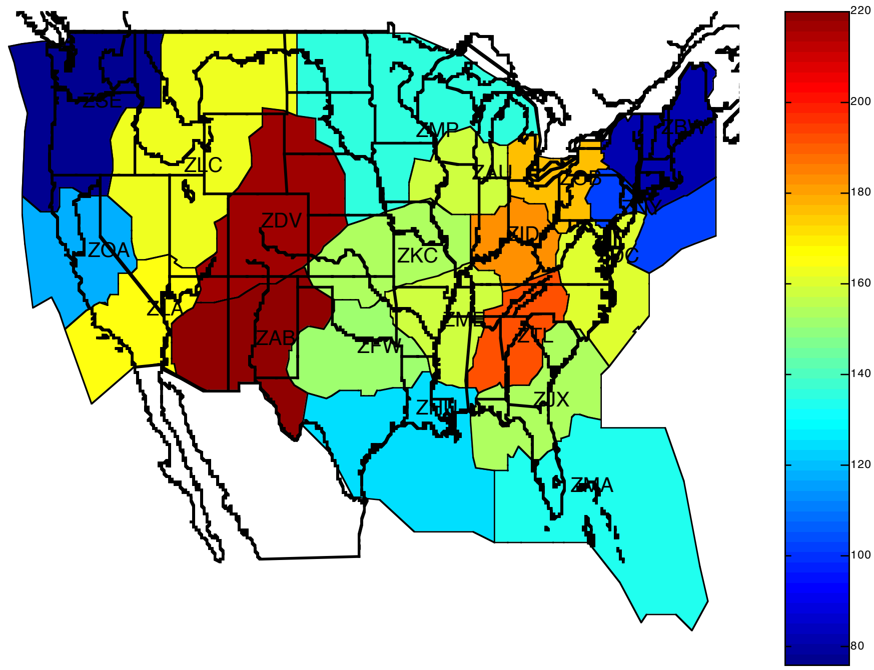

Figure 5.4 Maximum Aircraft Count (Baseline)

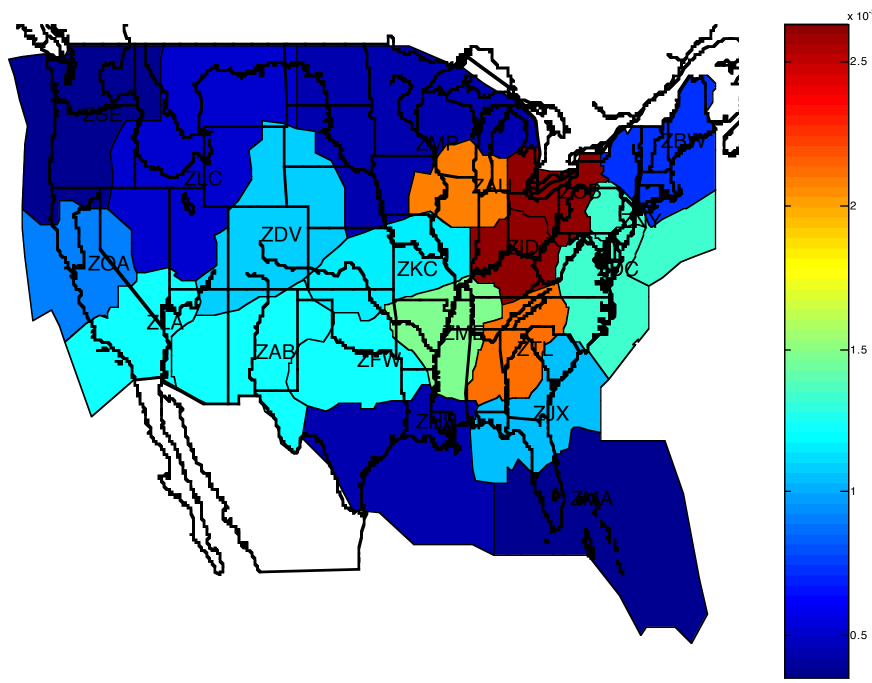

Figure 5.5 Relative Maximum Aircraft Count (Baseline)

Figure 5.6 shows deviations from baseline scenario of mean aircraft counts for cruise-climb variation of Free Flight. The results are presented for four different days of 1996. While almost all centers show a consistent decrease in mean aircraft counts for cruise-climb as opposed to baseline scenario, only one center (ZDV) manifests the opposite trend.

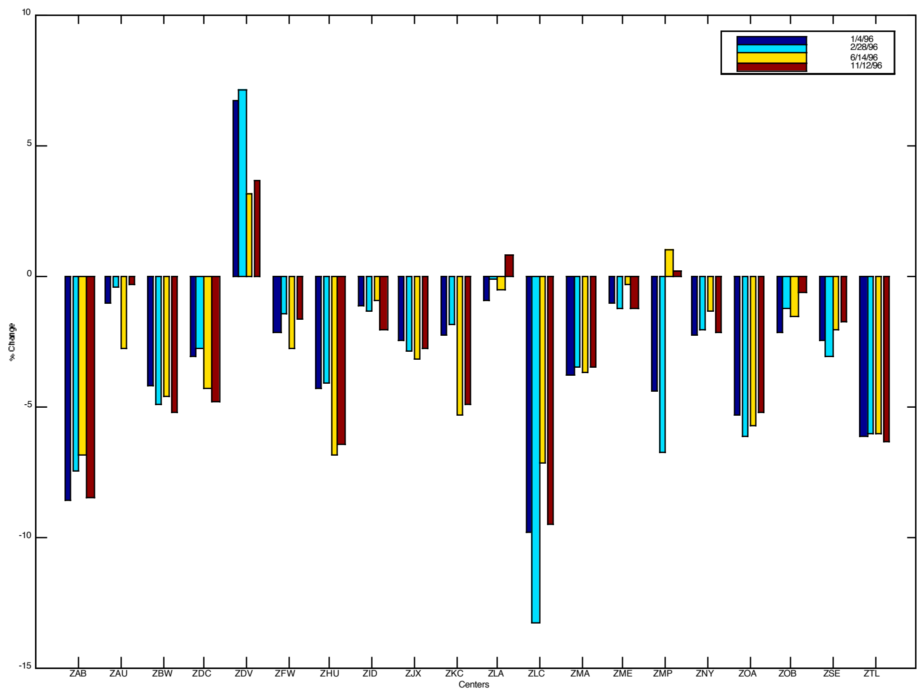

Figure 5.6 Mean Aircraft Count Deviation

5.2.2 High Fidelity Analysis

This analysis was performed on a single center (Atlanta) for a seven-hour time period (8:00 AM - 3:00 PM Atlanta time) for five different days (1/4/96, 2/28/96, 4/6/96, 6/14/96, and 11/12/96); using three scenarios that reflected baseline and two free flight variants:

- user-preferred trajectories with hemispherical rules (cardinal);
- user-preferred without hemispherical rules (cruise-climb).

This is a high fidelity analysis of display requirements using a CDTI display range (see Figure 5.7) that more closely approximated that described in the draft ADS-B MASPS.

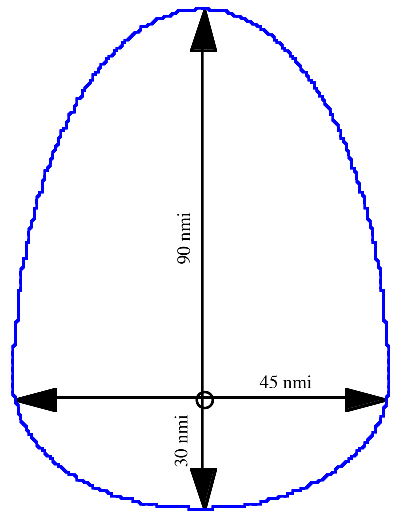

Figure 5.7 CDTI Display Range

Equations used to describe the position of display in time along with illustrative graphic in Figure 5.8 are presented below.

$$
\begin{aligned}
&\theta \in (0,\pi):\\
&x(t) = x_o(t) + 45\cdot\cos(\theta)\cdot\cos(\alpha(t)) + 90\cdot\sin(\theta)\cdot\sin(\alpha(t))\\
&y(t) = y_o(t) - 45\cdot\cos(\theta)\cdot\sin(\alpha(t)) + 90\cdot\sin(\theta)\cdot\cos(\alpha(t))\\
&\theta \in (\pi,2\pi):\\
&x(t) = x_o(t) + 45\cdot\cos(\theta)\cdot\cos(\alpha(t)) + 30\cdot\sin(\theta)\cdot\sin(\alpha(t))\\
&y(t) = y_o(t) - 45\cdot\cos(\theta)\cdot\sin(\alpha(t)) + 30\cdot\sin(\theta)\cdot\cos(\alpha(t))
\end{aligned}
\tag{5-1}
$$

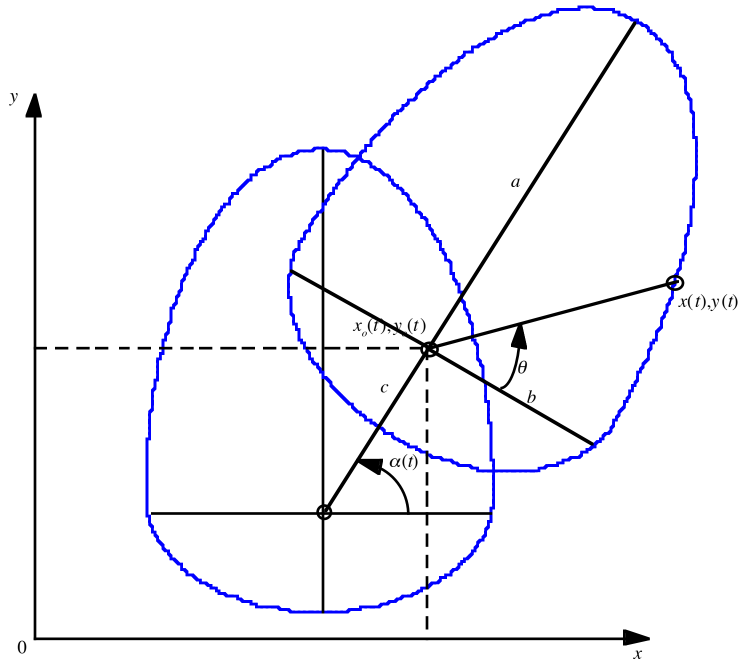

Figure 5.8 CDTI Display Kinematics

A virtual CDTI display was super-imposed over each aircraft and the position of each updated at two-second intervals as illustrated in Figure 5.9.

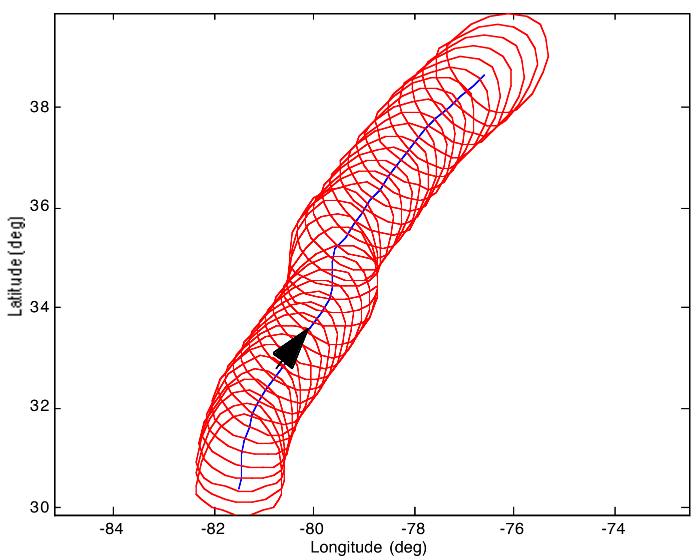

Figure 5.9 Aircraft and CDTI Display Track History for DAL378 (Baseline)

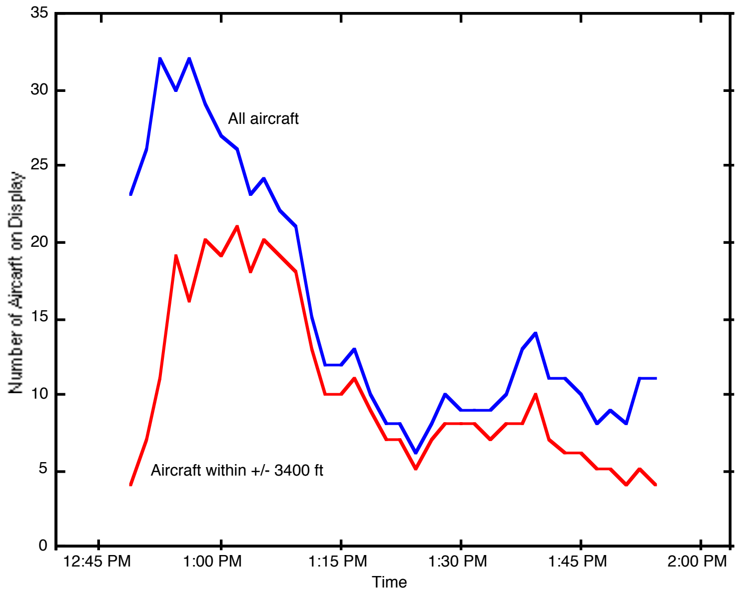

Figure 5.10 Time History of Displayed Aircraft for DAL378 (Baseline)

The number of other aircraft that fell within this area was determined by looking at each aircraft at each two-second position update. The number of aircraft within the CDTI display was maintained for each aircraft for the duration of the scenario. Two counts of display requirements were maintained:

- display requirements disregarding the altitude difference between aircraft;
- display requirements based on the count of aircraft within 3400 feet vertically.

Figure 5.11 shows the maximum display requirement for all aircraft over the scenario duration (4/6/96). The abscissa is the display requirement in terms of the maximum number of displayed aircraft. The ordinate is the number of aircraft which correspond to this display. Three scenarios and two different operational scenarios are shown in Figure 5.11. The three scenarios are:

- Baseline (B);
- Cardinal Flight Levels (CD);
- Cruise-Climb (CC).

The two operational assumptions are:

- all aircraft above FL240 within the range of display must be displayed;
- only aircraft above FL240 that are both within the range of display and within +/- 3400 feet vertically must be displayed.

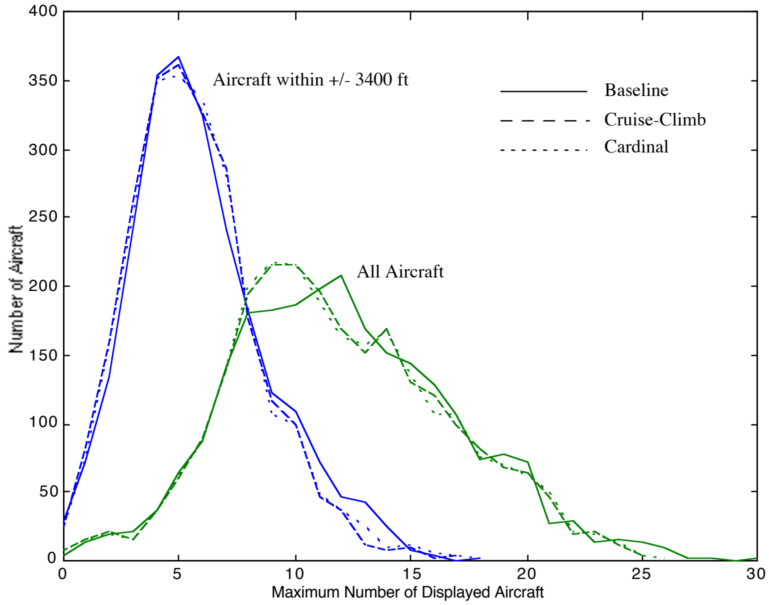

Figure 5.11 Display Requirements and Impacted Users

Figure 5.11 illustrates logical conclusion that display requirements without altitude filtering are much greater than display requirements with altitude filtering. What is also illustrated in Figure 5.11 and shown in Table 5.2 is that the number of aircraft that must be displayed for a given range are very consistent across the different days and different concepts of operations.

Table 5.2 CDTI Requirements Summary

Day	AC Total			Max w/o Filter			Max with Filter			Mean w/o Filter			Mean with Filter		
	B	CC	CD	B	CC	CD	B	CC	CD	B	CC	CD	B	CC	CD
1/4	2381	2367	2368	30	25	26	18	17	18	12.1	11.9	11.9	5.9	5.6	5.7
2/28	2421	2399	2405	28	26	26	20	18	18	12.5	12.4	12.4	6.7	6.4	6.4
4/6	2158	2132	2136	32	28	28	21	19	20	12.3	11.6	11.6	6.8	6.2	6.3
6/14	2329	2313	2316	24	26	26	17	15	16	10.9	11.1	11.0	6.0	5.9	5.9
11/12	2361	2327	2328	30	29	29	17	17	17	11.9	11.6	11.7	6.3	5.9	6.0

Based on results shown in Table 5.2, maximum CDTI requirements vary from 24 to 32 (without altitude filtering) and from 15 to 21 (with altitude filtering).

Chapter 6 Conclusions and Recommendations

The move towards Free Flight is already underway via, for example, the expanded National Route Program (NRP), the Central Pacific oceanic program, and future communications, navigation, surveillance, and air traffic management technologies. NRP is designed to be a phased approach, to ultimately permit aircraft flying above 29,000 feet to select their own routes as alternatives to published preferred IFR routes, thereby removing the restrictions and constraints currently imposed on these users. In March 1996, the expanded NRP included all flights in the U.S. above 33,000 feet. In the western U.S., NRP currently includes all flights above 31,000 feet. The FAA estimates that NRP saved aviation industry $40 million in 1994 by allowing pilots to fly more optimal routes. In the airspace over the Central Pacific, advanced satellite voice and data communications are being used to provide faster and more reliable transmissions to enable reductions in vertical, lateral and longitudinal separation, more direct flights and tracks, and faster altitude clearances.

In the long term, technologies to improve conflict identification and resolution, data transmission and display, and direct exchange among aircraft, airline operation centers, controllers, and pilots are needed. Some of these technologies include:

- Global Positioning System;
- Wide Area Augmentation System;
- Traffic Alert and Collision Avoidance System;
- Two-way data link;
- Automatic Dependent Surveillance-Broadcast;
- Aeronautical Telecommunication Network;
- Decision support systems including Final Approach Spacing Tools, enhanced traffic flow management tools, Conflict Probe/Resolution and Surface Management Advisor Program.

These and other on-going FAA programs are being adjusted to expedite the implementation of the Free Flight.

6.1 Conclusions

The purpose of Controller Conflict Resolution Baseline Study was to analyze typical controller conflict resolution actions to determine the types of resolutions typically made under today's concept of operations, and the resultant deviation from intended path in order to establish a conflict resolution baseline. Over 55 hours of scenario data was examined using a variety of analysis tools and resulted in the identification of 57 conflict pairs. For each a conflict pair, the controller issued either a heading change, a temporary or new altitude, a parallel offset, or a temporary speed-control as part of the conflict resolution maneuver. While many of these maneuver types can be combined to create more complex resolution strategies, this analysis, for the most part, ignored these cases because of the lack of essential aircraft intent information.

For each of the 57 conflict pairs identified, a variety of analysis was performed. This included measuring the conflict geometry, identifying and measuring the maximum deviation from intended path, and removing the conflict resolution maneuver by creating a pseudo-track based upon estimated aircraft intent and performance. Of the 57 conflict pairs identified, 32% of these cases would have resulted in a loss of separation if the controller had not intervened. The time to closest point of approach (CPA) was computed by taking the difference between the time at CPA and the time that the conflict resolution maneuver is started. The average time to CPA, as observed in this study, was approximately 3.0 minutes. The minimum average CPA was 7.0 nmi with the conflict resolution maneuver and 1.0 nmi with the conflict resolution maneuver removed. For maneuvers classified as parallel offsets, the observed average maximum horizontal offset was 7.4 nmi and the average additional distance flown was 4.6 nmi. The average vector involved a 22 degree heading change. For all altitude maneuvers identified, the controller attempted to assign the aircraft to an adjacent altitude band requiring only a small change in flight level. If the aircraft was climbing or descending when the conflict was detected, the resolution typically involved holding the aircraft at an intermediate flight level so as not to conflict with other aircraft. For speed control maneuvers, the percentage change in speed varied from -4.7% to +2.5% of the original speed. However, a majority of these cases were incomplete and the percentage change in speed could not be computed. The average conflict resolution duration was approximately 6 minutes.

The final type of analysis that was performed on these data involved computing the rate of conflict resolution maneuver occurrence and is expressed as the number of conflict resolution maneuvers per aircraft and the number of conflict resolution maneurvers per aircraft-hour. The conflict resolution maneuver rate of occurrence is dependent upon the number of aircraft and the number of conflicts. This rate varied significantly from 0.01 for sector 34 (1 out of 100) to 0.07 (1 out of 14) for sector 28 with an average of approximately 0.04 (1 out of 25). The number of conflict resolution maneuvers per aircraft-hour varied from 0.25 (1 for every 4 aircraft-hours) to 0.74 (1 for every 1.35 aircraft-hours) with a mean of 0.33 (1 for every 3 aircraft-hours).

The Dynamic Density analysis represents a first attempt at evaluating alternative dynamic density metrics and measurement techniques under current and possible future concepts of operations. The study did not perform an exhaustive analysis of the suitability of these dynamic density metrics or of the impact of transitioning to a new concept of operations. However, the analysis did provide a comparison of two candidate dynamic density metrics with traditional indicators under current and future concepts of operations. Further, the study provides a methodology for evaluating proposed dynamic density measurement techniques under numerous concepts of operations and, once a metric has been agreed upon, a methodology for more exhaustive analysis of the impacts of new concepts of operations.

This analysis demonstrates that in the current formulation of both dynamic density metrics, neither metric completely captures the complexity of the air traffic situation. The Kip Smith metric is good at capturing information associated with aircraft separation (i.e., proximity events) but does not include any terms that account for complexity of control that might be associated with aircraft climbing or descending or operating at significantly different speeds. While the Laudeman metric includes this information, at the time of our study each term was equally weighted. Therefore, the final value of the metric tended to minimize the effect of these factors.

From CDTI analysis it was concluded that on average, Maximum Instantaneous Aircraft Count (MIAC) goes down in Free Flight, suggesting that controllers will be handling fewer aircraft at the worst moments of the day. This is beneficial to the controllers working the average existing sector. Nevertheless a few sectors do experience an increase in MIAC in the experimental scenarios.

It is expected that user benefits will increase for direct or wind-optimized routes. Under examined scenarios, the reduction in median flying distance ranged from 0.54 to 1.0 percent. These are notable benefits when applied to the large number of aircraft that fly every day.

6.2 Recommendations

One near-term enhancement that could quite easily be performed for Dynamic Density analysis would be to add the weighting coefficients that NASA has derived for the Laudeman metrics and re-evaluate the results.

The next logical step would be to extend the analysis using the remaining NARIM scenarios that were developed as a part of the FY97 NARIM program. While several days should probably be examined for each scenario to increase the level of confidence associated with the individual metrics and metric correlation, other ongoing NARIM studies have indicated a large degree of stability across days and thus multiple days may not actually be necessary and thus this suggestion should be considered in light of a more detailed assessment of the findings of those studies. The scope of the analysis should be expanded to include additional Centers selected to evaluate the metrics where the dynamic density is expected to be both low and high. Additional dynamic density measurement techniques should be added as deemed appropriate by NASA and the FAA. And finally, since the transition to Free Flight is likely to occur over several years, the analysis should be extended with demand scenarios that include the demand growth that has been forecast to occur during this transition period.

Sector throughput is expected to increase in Free Flight as aircraft cut corners, thereby passing through more sectors. This suggests that resectorization may be required. Otherwise, the increased throughput (with decrease in sector occupancy times) will require an increase in the number of point-outs or transfers of communication and control. Should data link be available, transfer of communications could be accomplished in a more automated fashion, possibly reducing controller communication time.

Bibliography

1. "Statement of FAA Administrator David R. Hinson on the Nation's ATC System." FAA News, Washington, DC, June 17, 1995.

2. Embt, D., Suchkov, A., Rodgers, M., Colligan, W., "Controller Conflict Resolution Baseline Study.", CSSI, Inc., October 1997.

3. Federal Aviation Administration, "SATORI: Situation Assessment through the Recreation of Incidents.", DOT/FAA/AM-93-12, Office of Aviation Medicine, Washington, DC.

4. Federal Aviation Administration, "Air Traffic Control.", FAA Order 7110.65J, 1995.

5. Federal Aviation Administration, "Airman's Information Manual.", 1997.

6. Federal Aviation Administration, "Atlanta Sector Charts.", 1995.

7. Federal Aviation Administration, "National Air Traffic Training Program En Route Study Guide.", 1995.

8. Kosecka, J., Tomlin, C., Pappas, G., Sastry, S., "Generation of Conflict Resolution Maneuvers for Air Traffic Management.", Department of Electrical Engineering and Computer Sciences, University of California at Berkeley.

9. Athans, Michael, Falb, Peter L., "Optimal Control. An Introduction to the Theory and Its Applications.", McGraw-Hill Book Company, 1968.

10. Bradford, S., Colligan, W., "National Airspace Resource Investment Model Needs Analysis and Operational Concept Report.", Report to the National Aeronautics and Space Administration, April 1996.

11. Mondoloni, Stephane L., "Development of an Enroute Conflict Resolution Rulebase for the Reorganized Air Traffic Control Mathematical Simulator (RAMS).", CSSI, Inc., December 1997.

12. Mondoloni, Stephane L., Weiss, William E., Politano, Arturo L., "Multi-Center GPS Direct Routes Analysis.", ASD430-97-002, July 1997.

13. Martin Marietta Energy Systems, "CONUS NAS Data Access Tool (CONDAT).",1994.

14. Suchkov, A., Embt, D., Colligan, W., "Dynamic Density Study.", CSSI, Inc., December 1997.

15. Wyndemere, Inc., “An Evaluation of Air Traffic Control Complexity.”, Final Report for Contract Number NAS2-14284, October 1996.

16. Smith, K., et al, “An Index of Dynamic Density.”

17. RTCA SC186, “ADS-B Minimum Aviation System Performance Specifications.”, Draft Version 6.2.

18. Lozito, Sandra, “Free Flight and Self-Separation from the Flight Deck Perspective.

19. Colligan, W., Rodgers, M., “Cockpit Display of Traffic Information (CDTI) Requirements Study.”, CSSI, Inc., December 1997.

20. Using MATLAB®., Version 5, The Mathworks, Inc., December 1996.

21. Using MATLAB® Graphics., Version 5, The Mathworks, Inc., December 1996.

Appendix A Conflict Analysis Resolution Display System (CARDS)

CARDS was developed using version 5.1 of MATLAB® [20], which is distributed by Mathworks, Inc.. MATLAB is a high-performance language used for technical computing. It integrates computation, visualization, and programming into an easy-to-use environment. Problems can be formulated using traditional mathematical notation. Mathematical operations can then be easily performed on the data such as computing a derivative, estimating the variance in a data set, or comparing the difference between two vectors. Results can then be expressed in familiar mathematical notation or displayed graphically where appropriate. MATLAB is particularly well suited for performing matrix operations on data sets and uses highly-optimized subroutines. MATLAB comes with many libraries containing functions used during common analysis tasks including general purpose commands, statistical commands, matrix functions, data analysis, differential equations, 2-D and 3-D graphing and plotting, and file input and output. Separate toolboxes can be purchased that contain libraries of highly-specialized functions for specific analysis tasks such as optimization, signal processing, control system design, and simulation. In addition to providing an efficient easy to use command language, MATLAB provides data base structures which allow data to be hierarchically formatted as well as tools for building a graphical user interface (GUI) [21]. CARDS was quickly developed by leveraging off from these features. CARDS represents the combination of a GUI, a structured database, and a library of functions that were developed to manipulate the individual data elements contained in the database.

A.1 Data Structures

There are five different data structures used for storing and loading externally generated data into CARDS. The first data structure stores flight related information such as aircraft id, aircraft type, origin, destination, and time history. The time history is essentially a time sequenced array of data for the individual aircraft. This array contains the heading, ground speed, assigned altitude, reported altitude, latitude, longitude, as well as information about the current controller for every radar-hit contained in the SATORI (see Appendix B) data. To allow the manipulation and comparison of aircraft tracks, the time has been adjusted such that all aircraft in the scenario have data elements for every time unit starting from the scenario start time and extending to the scenario end time. To fully populate individual aircraft time histories frequently requires assigning cells with an artificial value of "NaN" when data does not exist. By performing this operation, any combination of aircraft can be compared or plotted within a scenario. Figure A-1 depicts the flight information data structure, which is the most complex data structure used in CARDS. A separate flight information data structure was created for each of the 25 SATORI scenarios.

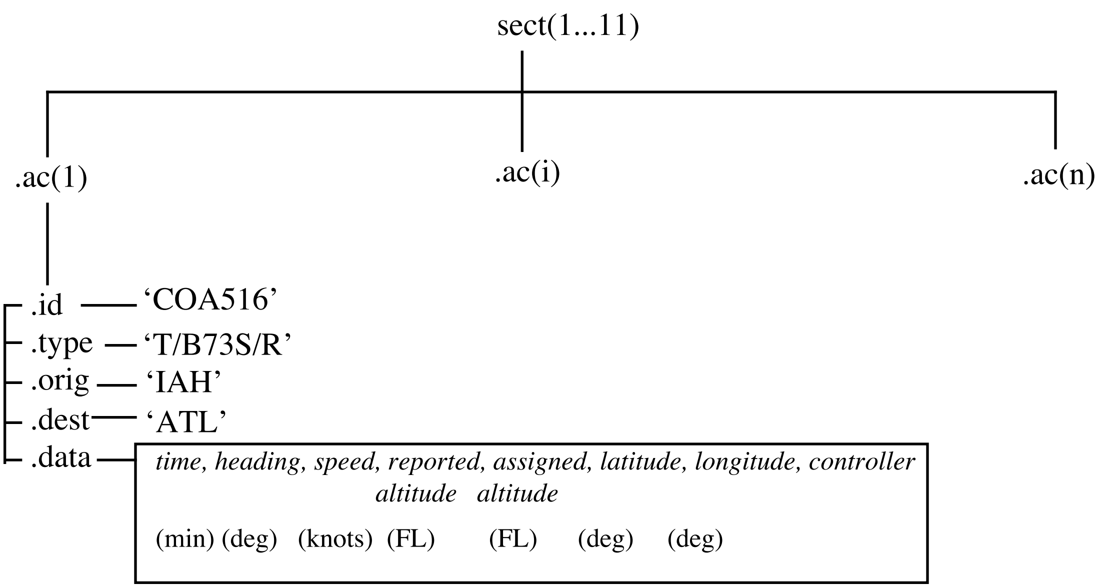

Figure A-1 Flight Information Data Structure

In addition to the flight information data structure an airspace fixes data structure was developed that contains the major fixes, VOR's and DME's for the entire ARTCC. For each fix the name, description, latitude, and longitude was included and is depicted in Figure A-2. This data structure is used within CARDS to aid in detecting aircraft route changes.

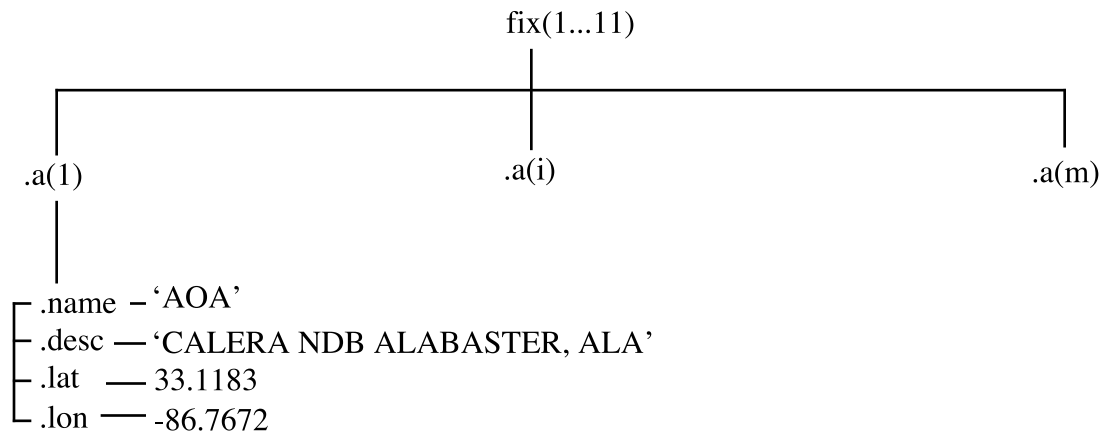

Figure A-2 Airspace Fixes and Information Data Structure

Figures A-3 and A-4 depict the data structures that contain aircraft that were detected by the data filters (see Section 2.3.2) as aircraft that were potentially moved as part of a conflict resolution maneuver. Figure A-3 depicts the data structure containing the id’s of aircraft that were potentially moved as part of an altitude conflict resolution maneuver. A separate data structure was created for each of the 25 SATORI scenarios.

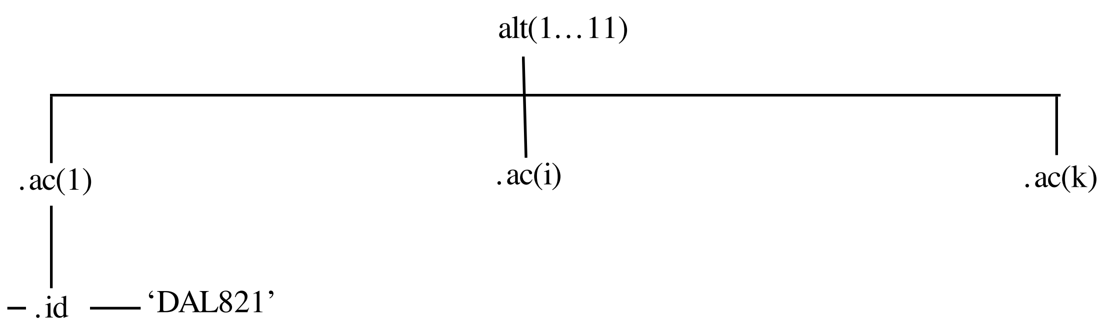

Figure A-3 Candidate Altitude Maneuvered Aircraft Data Structure

Figure A-4 shows the data structure containing the id’s of aircraft that were potentially moved as part of a vector or heading change conflict resolution maneuver. A separate data structure was created for each of the 25 SATORI scenarios.

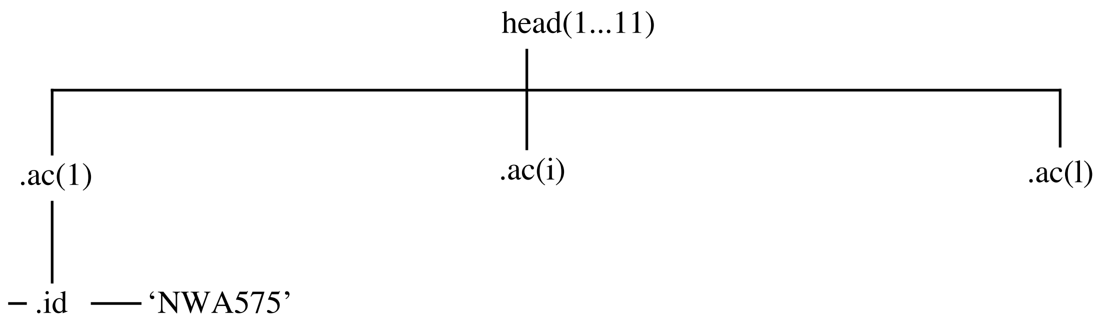

Figure A-4 Candidate Heading Maneuvered Aircraft Data Structure

The final data structure that was developed for CARDS contains the locations of high intensity precipitation information as shown in Figure A-5. The data structure is grouped by sector to minimize the potential overhead associated with displaying a large number of precipitation cells. Each precipitation cell contains the latitude and longitude of the cell and the scenario time that the cell was activated. The precipitation data used in SATORI has an ARTCC dependent time duration which was 120 seconds for our scenarios. The CARDS tool only provides the capability of displaying cells for a specific sector without regard to cell activation time. Additionally, the analysis performed with CARDS ignored aircraft that were potentially constrained by precipitation cells because of the complex interaction of precipitation cells and aircraft flight paths.

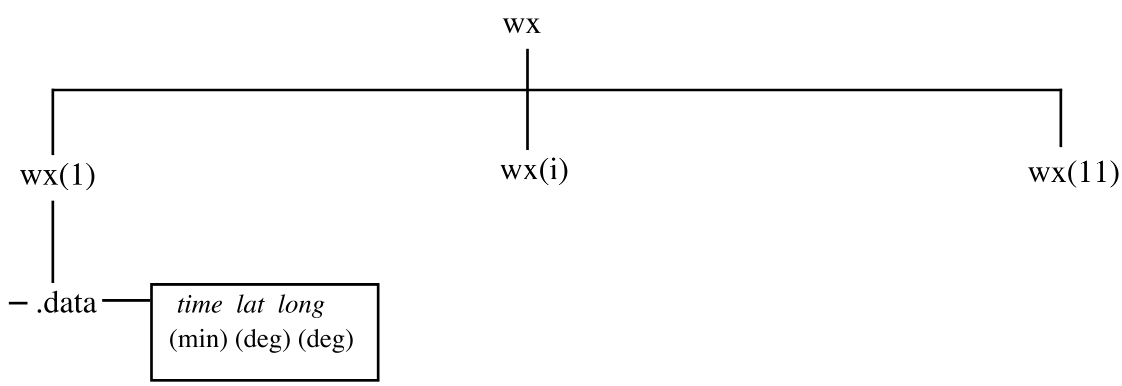

Figure A-5 Weather Information Data Structure

A.2 Graphical User Interface

A brief description of the Graphical User Interface to the CARDS tool is presented below. At the Main Menu a user can load scenario data and select a sector for analysis from the Atlanta Center sector map as shown in Figure A-6. Pressing the “Sector Info” button will bring up a new screen that contains information pertinent to the selected sector.

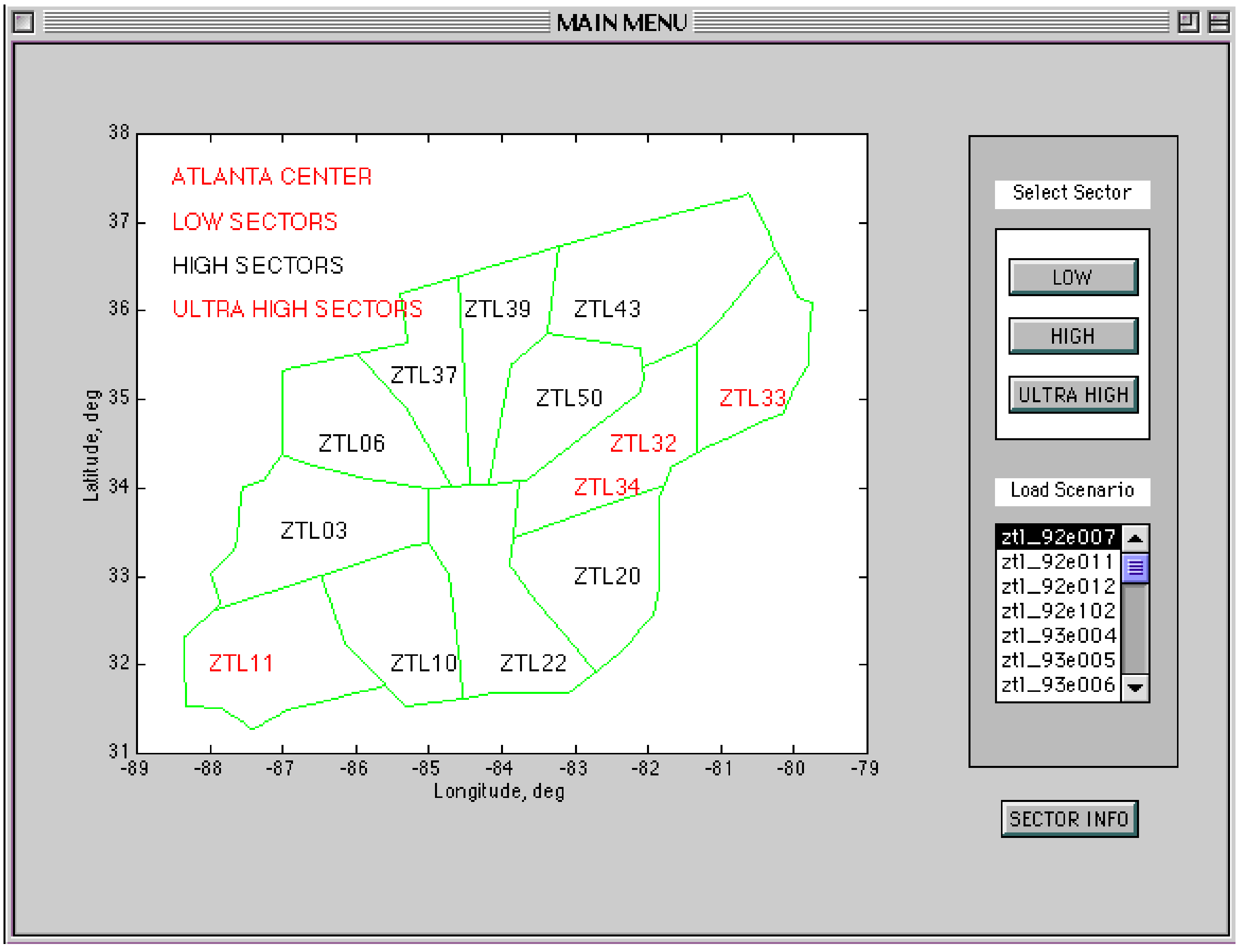

Figure A-6 Main Menu Screen

Sector Info displays information about the current scenario, sector, scenario start time, and scenario end time as shown in Figure A-7. The figure also displays a list of all aircraft ids, ids of aircraft that were detected as possible heading changes, and ids of aircraft that were detected as possible altitude changes. Since we were unable to develop a reliable speed data filter, there are no aircraft ids listed under the Speed Filter column. From this screen the user selects the desired aircraft for further investigation from the Aircraft List and then presses the "Generate Plots" button.

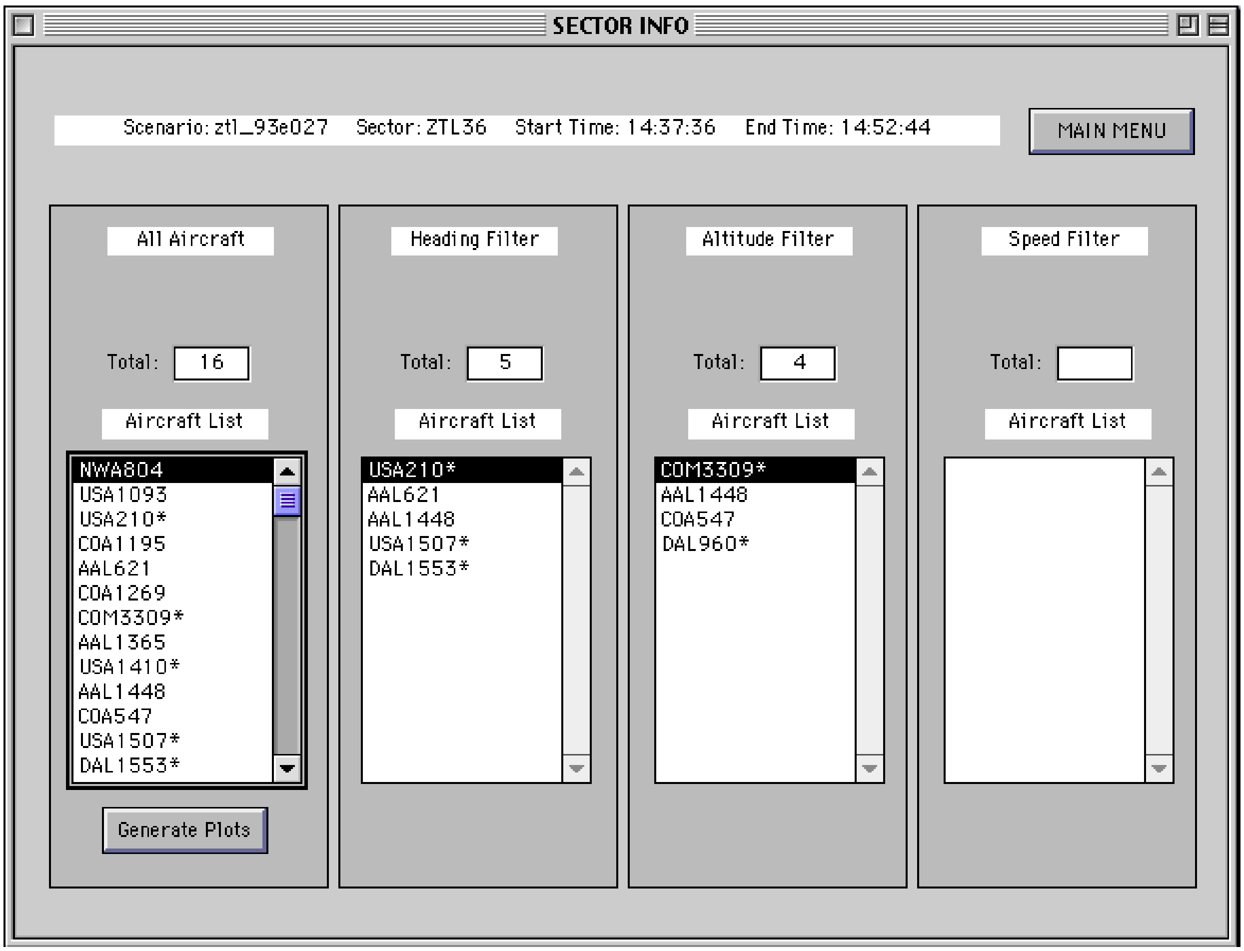

Figure A-7 Sector Information Screen

Figure A-8 displays the time histories of heading, reported and assigned altitude, ground speed, and a plot of the latitude vs. longitude for the aircraft selected. Based on these plots a preliminary decision can be made as to whether this aircraft was maneuvered. From this screen a user can return to the previous screen, “Sector Info”, or proceed with further analysis by pressing the “Airspace Constraints” button which will activate the closest point of approach tool implemented in CARDS.

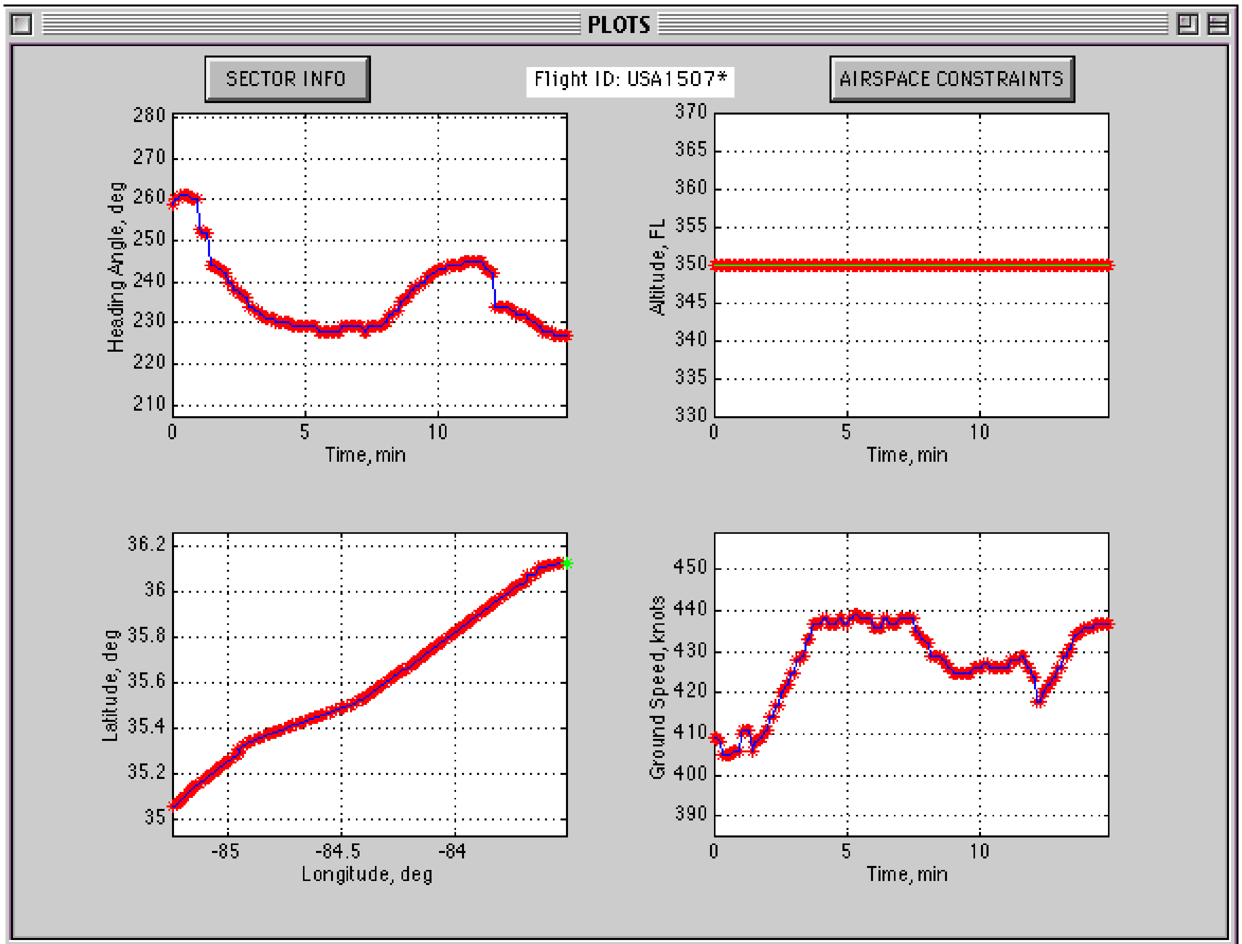

Figure A-8 Aircraft Time History Screen

Figure A-9 depicts the Airspace Constraints Menu which is used for analyzing CPA's. The CPA tool requires the user to input a maximum horizontal distance filter and a maximum altitude distance filter. The tool then computes the CPA for all aircraft contained in the sector. If the CPA falls within both the horizontal and vertical bands specified, it's CPA is shown in the histogram. If there are five aircraft whose minimum CPA's with other aircraft in the sector fall within these bands, then there will be a total of 10 conflict pairs (e.g. 5*(5-1)/2) shown in the histogram. The dashed bars represent a conflict pair between the aircraft being investigated and other aircraft. The solid bars represent all other aircraft pairs. Figure A-9 shows as example where the horizontal filter was set to 25 nmi and the vertical filter was set to ± 6000 ft. By pressing the "Show Traffic" button a histogram of the proximate aircraft will be generated. The total number of proximate aircraft detected was 15 with only 4 associated with the aircraft under investigation. The CPA's for this aircraft are shown in the 16, 17, 19, and 20 nmi bins. The user can return to the previous menu by pressing the Sector Info button, or generate a latitude vs. longitude plot and/or an altitude profile plot showing the aircraft being investigated and the aircraft shown with dashed bars by pressing the "Show Plots" button. A separate plot is created for each plot option.

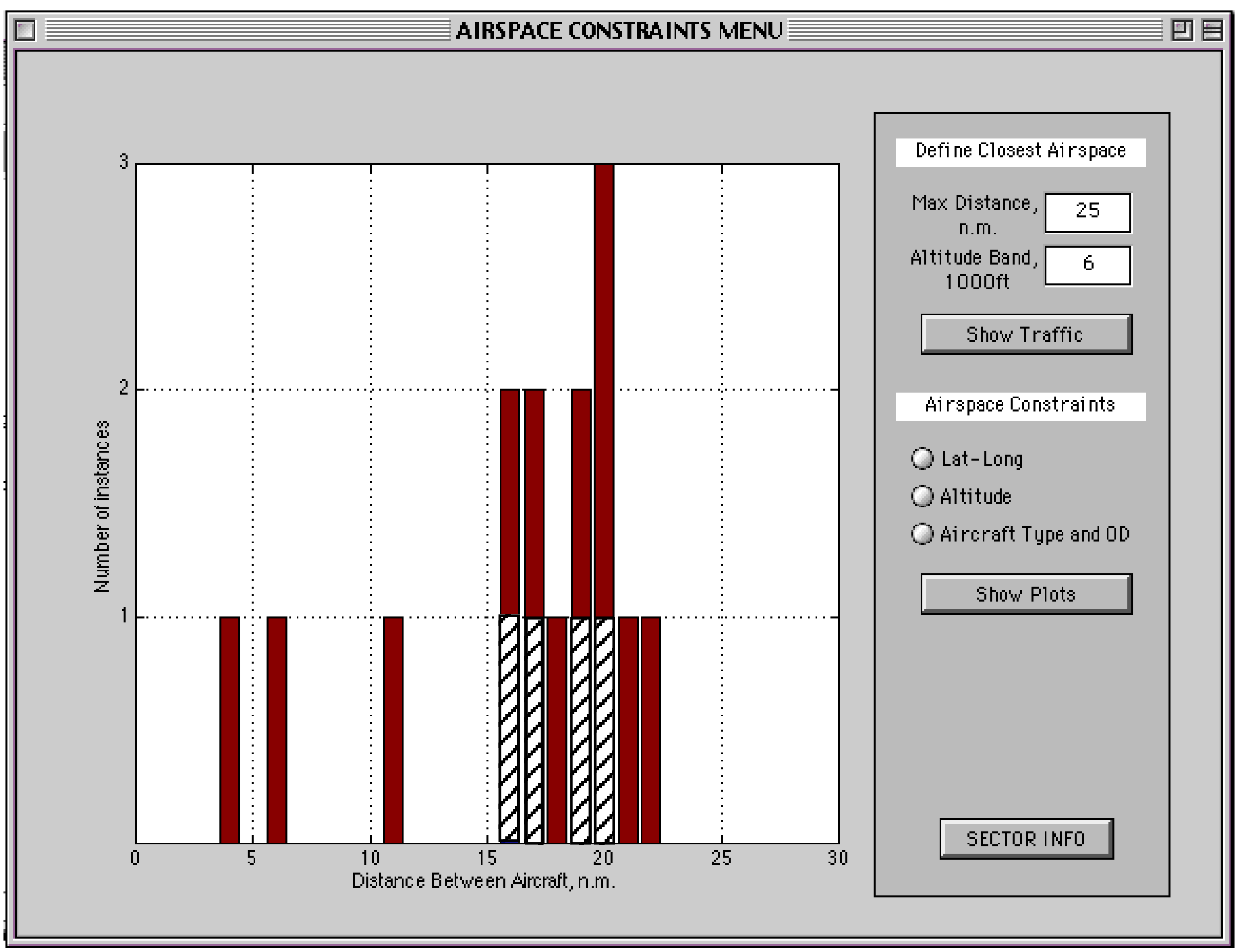

Figure A-9 Airspace Constraints Menu Screen

A table showing the aircraft type and origin and destination information can be created by selecting the “Aircraft Type and OD” plot option.

Figure A-10 shows a latitude versus longitude plot depicting the horizontal tracks of flight id USA1507 with it’s associate time history as previously shown on Figure A-9. The plot also shows the four neighboring aircraft that were detected by the CPA tool as also shown on Figure A-9. There are several airspace constraints that can be displayed including sector boundaries, weather cells, fixes, aircraft type, origin, destination and major airports many of which can be toggled on or off. CARDS also allows the Jrings (5 nmi separation rings), as shown in SATORI, to be displayed. Based on the horizontal distance calculation described above, the distance between any two points on the latitude-longitude plot can be calculated and displayed. Tracks may also be extrapolated by time or distance using this screen.

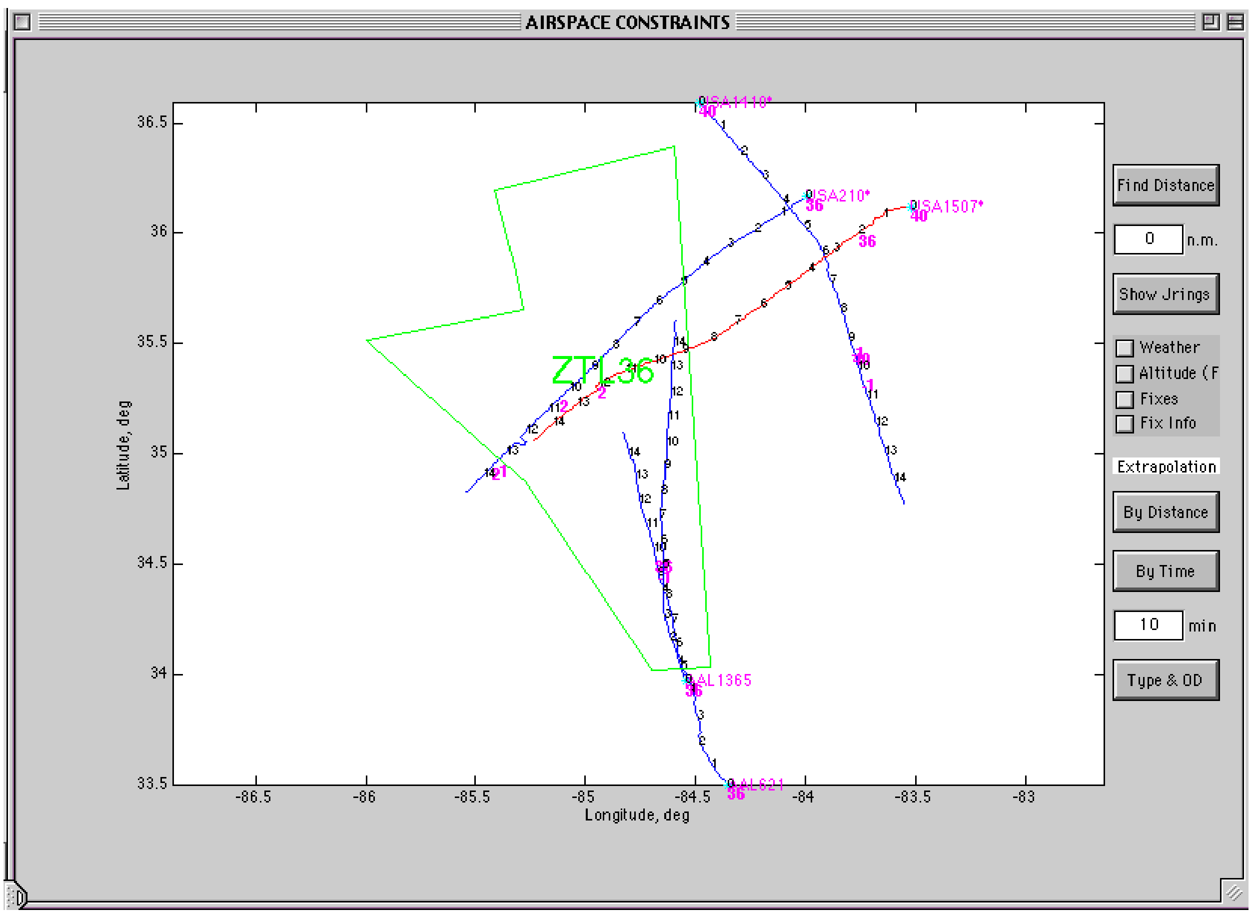

Figure A-10 Airspace Constraints Screen

A.3 Formulas

To calculate the closest point of approach between two aircraft requires calculating the horizontal distance between two aircraft given their positions which are expressed in latitude and longitude. This calculation was performed by employing the equations of spherical trigonometry. The angles and sides notation involved in the horizontal distance derivation is shown in Figure A-9.

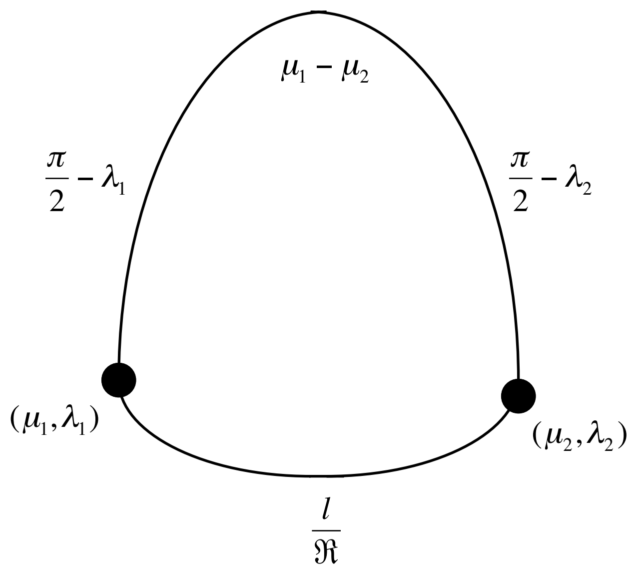

Figure A-11 Angles and Sides Notation

Using law of cosines for sides we can write:

$$\cos\left(\frac{l}{\Re}\right) = \cos\left(\frac{\pi}{2} - \lambda_1\right) \cdot \cos\left(\frac{\pi}{2} - \lambda_2\right) + \sin\left(\frac{\pi}{2} - \lambda_1\right) \cdot \sin\left(\frac{\pi}{2} - \lambda_2\right) \cdot \cos(\mu_1 - \mu_2) \qquad \text{(A-1)}$$

From where,

$$l = \Re \cdot \cos^{-1}\left(\cos\left(\frac{\pi}{2} - \lambda_1\right) \cdot \cos\left(\frac{\pi}{2} - \lambda_2\right) + \sin\left(\frac{\pi}{2} - \lambda_1\right) \cdot \sin\left(\frac{\pi}{2} - \lambda_2\right) \cdot \cos(\mu_1 - \mu_2)\right) \qquad \text{(A-2)}$$

Where,

l – the distance between two aircraft (nmi)

$\Re$ = 3437 nmi – radius of the Earth

λ – aircraft latitude (rad)

μ – aircraft longitude (rad)

The distance between two aircraft is calculated for every position contained in the data set. The minimum of these distances is then calculated and stored as the proximity if both aircraft are within the same altitude band. If we consider a sector with n aircraft, an $n \times n$ matrix of proximities can be constructed. Each entry in this matrix represents the minimum distance (i.e. CPA) between aircraft i and aircraft j. The matrix is symmetric and the entries along the main diagonal are zero. If the proximity point falls outside the altitude band under consideration, the entry is ignored and replaced with an artificial value (e.g. -1). A maximum CPA may also be ignored by replacing entries with an artifical value if their respective CPA exceeds a user-defined threshold.

Track Extrapolation by Time

In this case the user defines the starting point for extrapolation by selecting the corresponding point on the track. The user also defines for how long he or she wishes to extrapolate the track by inputting an appropriate time.

Extrapolation is implemented by using the following equations:

$$\begin{aligned}
\lambda_i &= \lambda^* + \left(\overline{V} \cdot \sin\left(\frac{\pi}{2} - \overline{\psi}\right) \cdot \Delta t \cdot (i-1)\right) \cdot \frac{1}{60} \\
\mu_i &= \mu^* + \left(\overline{V} \cdot \cos\left(\frac{\pi}{2} - \overline{\psi}\right) \cdot \Delta t \cdot (i-1)\right) \cdot \frac{1}{60 \cdot \cos(\lambda_i)} \qquad \text{(A-3)} \\
t_i &= t^* + \Delta t \cdot (i-1)
\end{aligned}$$

Where,

λ^* – latitude at starting point

μ^* – longitude at starting point

t^* – starting time for extrapolation

$\overline{V}$ – average speed (based on 6 prior to extrapolation records, including starting point)

$\overline{\psi}$ – average heading (based on 6 prior to extrapolation records, including starting point)

The extrapolated track will be displayed as a dashed line on the same plot with original track. Having both of the tracks displayed on the same plot along with the capability of calculating the horizontal distance between any two points on the plot is useful for performing track analysis.

Track extrapolation by distance

In this case, the user selects the start point and the end point of the desired track. Depending on their relative location, the following equations are employed to calculate the extrapolated track:

$$
\begin{aligned}
\lambda_i &= \lambda_{start} \pm \Delta\lambda \cdot (i-1) \\
\mu_i &= \mu_{start} \pm \Delta\mu \cdot (i-1) \\
t_i &= t_{start} + \Delta t \cdot (i-1)
\end{aligned}
\tag{A-4}
$$

Where latitude and longitude increments as well as time step are selected such that the boundary conditions are met at the end of extrapolated track. The final time for extrapolation in this case is calculated by taking a ratio of the distance, flown by aircraft along the extrapolated track, and an average speed along the extrapolated track. Average speed is calculated in the same way as it was described for the case of extrapolation by time.

Appendix B — Situation Assessment through the Re-creation of Incidents (SATORI)

The Situation Assessment through the Re-creation of Incidents (SATORI) tool was developed by the FAA's Civil Aeromedical Institute (CAMI), located in Oklahoma City. The tool was originally developed to provide a means of investigating the situational dynamics associated with operational errors wherein loss of separation occurs. The tool facilitates the investigation and determination of the causal factors leading to the operational error which subsequently supports the identification of training needs or system deficiencies.

SATORI operates on a UNIX workstation which is configured to resemble a Plan View Display (PVD). SATORI replays the radar data recorded at En Route Air Traffic Control facilities through representations of a PVD, and the Continuous Readout Update Display (CRD). The re-creation synchronizes the graphic display of these data with digitized voice containing the associated verbal interactions between pilots and the controller. SATORI attempts to re-create the display exactly as the controller would have seen it with the associated functionality. Many of these features that are available to the controller are also useful for performing analysis. These include; the ability to display sector boundaries, routes, fixes, airports, terrain, high and low intensity weather, aircraft, and aircraft data blocks. Figure B-1 is an example of the SATORI setup screen which is used to control many of the display features.

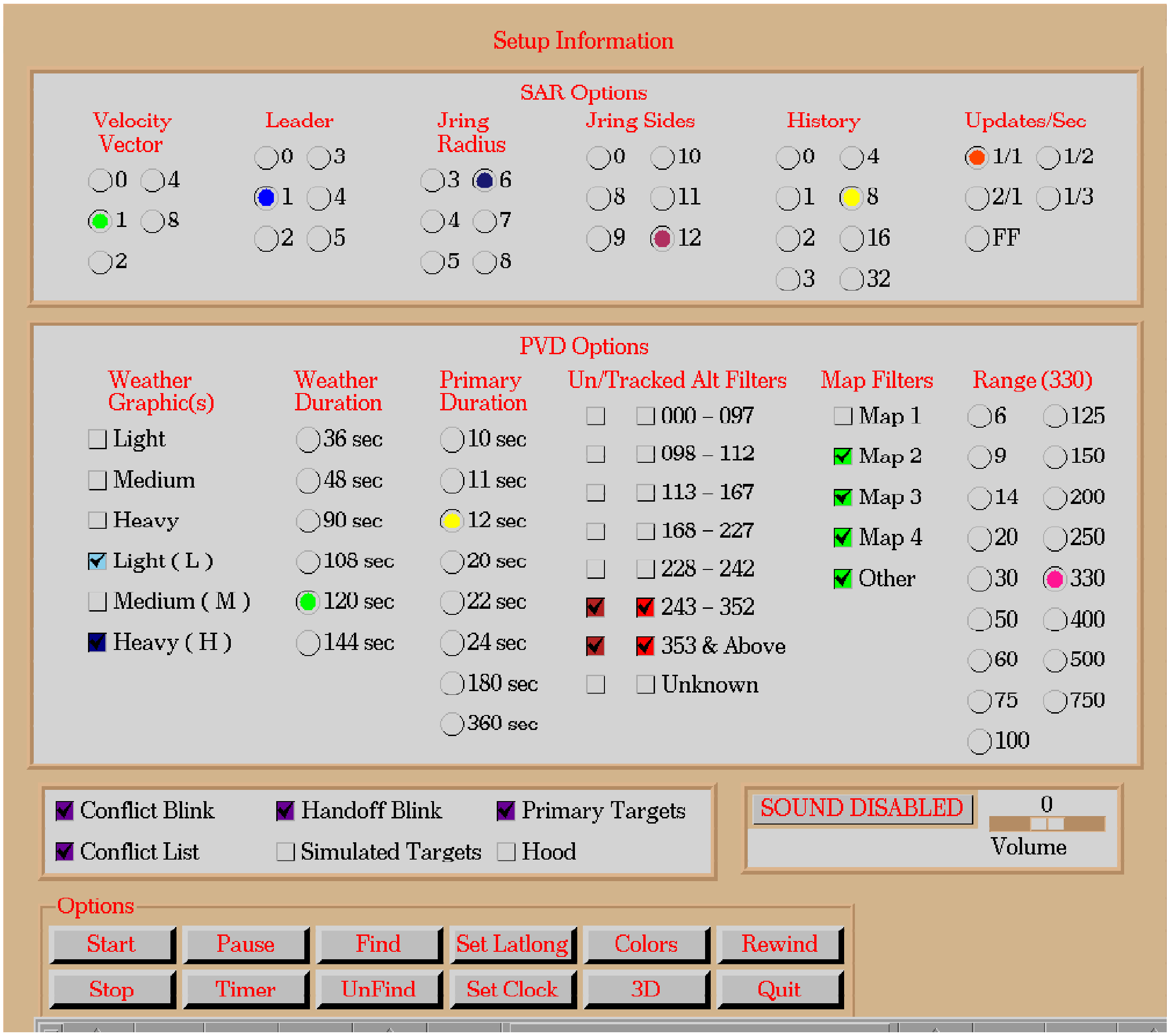

Figure B-1 SATORI Setup Information

Figure B-2 is an example of the SATORI PVD and CRD output displays. The figure shows several sectors contained in the Atlanta ARTCC; however, the PVD display is configured for sector 36 and the only aircraft under the control of sector 36 are displayed. Basic map operations such as recentering and zooming are also provided by SATORI. Additionally, individual aircraft can be queried to obtain information such as assigned altitude, reported altitude, heading, speed, beacon code, current sector, and position. The distance between aircraft can be measured by selecting the distance option and double-clicking the mouse on the respective aircraft.

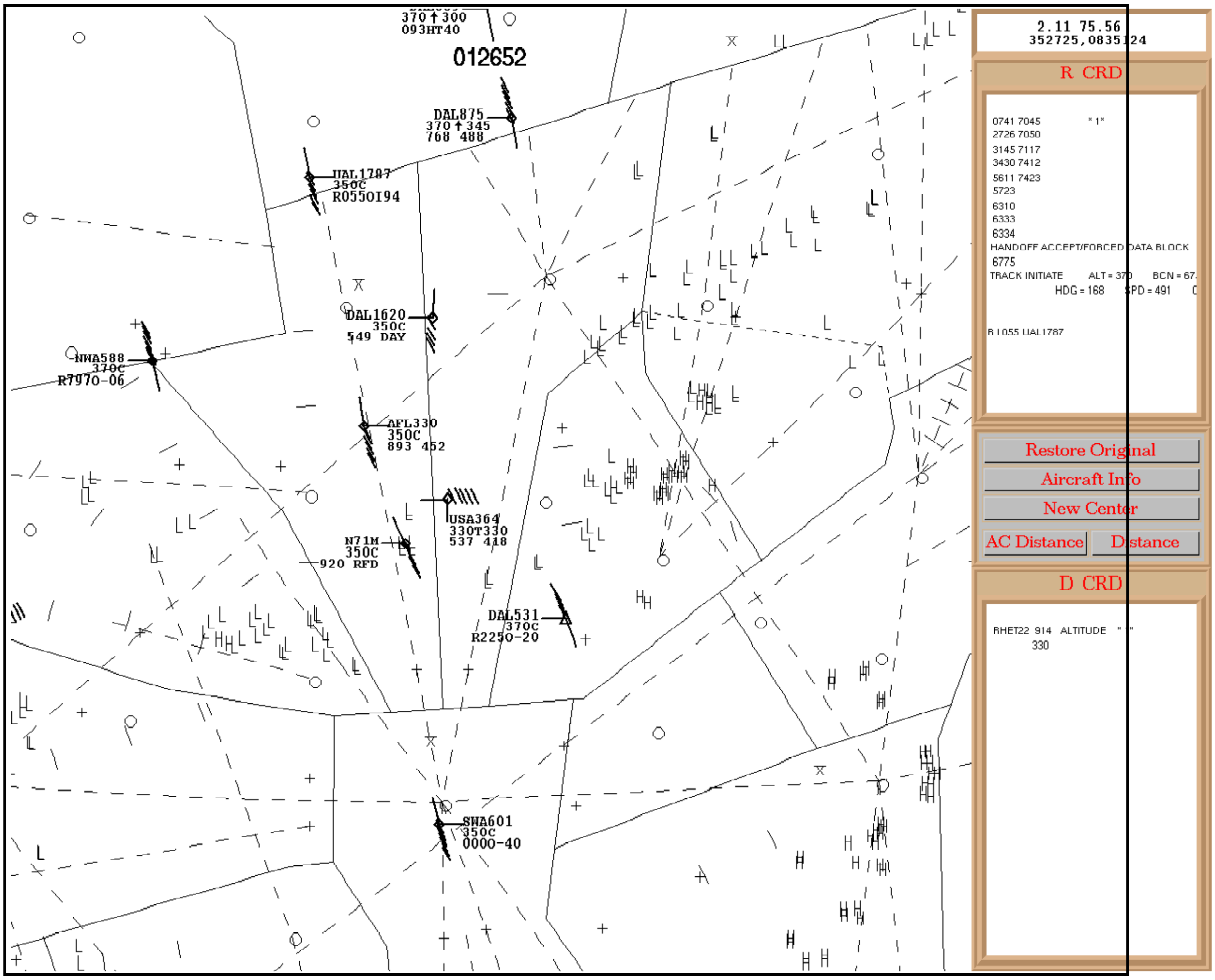

Figure B-2 SATORI Screen Display

Appendix C

Dynamic Density Metric Analysis Tool (DDMAT) Report File

Column 1	sector (cell) id
Column 2	total number of aircraft (Baseline)
Column 3	total number of aircraft (Wind Optimized (Cruise-Climb))
Column 4	total number of aircraft (Wind Optimized (Cardinal))
Column 5	total number of proximity events with 10 nmi alert zone (Baseline)
Column 6	total number of proximity events with 10 nmi alert zone (Wind Optimized (Cruise-Climb))
Column 7	total number of proximity events with 10 nmi alert zone (Wind Optimized (Cardinal))
Column 8	cumulative Kip Smith x 0.001 (Baseline)
Column 9	cumulative Kip Smith x 0.001 (Wind Optimized (Cruise-Climb))
Column 10	cumulative Kip Smith x 0.001 (Wind Optimized (Cardinal))
Column 11	mean normalized Laudeman (Baseline)
Column 12	mean normalized Laudeman (Wind Optimized (Cruise-Climb))
Column 13	mean normalized Laudeman (Wind Optimized (Cardinal))

<u>Sectors</u>

--1	(--2	---3	----4)	(--5	---6	----7)	(------8	------9	-----10)	(-----11	-----12	-----13)
3	(471	451	454)	(58	47	43)	(2.12	1.20	1.00)	(0.52	0.52	0.52)
6	(401	456	474)	(49	54	49)	(3.53	2.06	1.78)	(0.53	0.51	0.51)
10	(384	390	388)	(51	52	49)	(5.20	2.38	2.38)	(0.52	0.52	0.52)
11	(262	280	281)	(14	16	14)	(0.29	0.07	0.07)	(0.68	0.70	0.70)
20	(311	350	366)	(19	11	11)	(1.37	0.59	0.59)	(0.58	0.61	0.62)
22	(628	600	619)	(169	135	138)	(14.83	14.79	14.79)	(0.48	0.46	0.46)
32	(399	431	433)	(47	44	45)	(4.38	1.90	1.90)	(0.46	0.46	0.45)
33	(460	413	413)	(49	32	32)	(4.70	2.30	2.30)	(0.60	0.58	0.58)
34	(157	176	176)	(6	10	10)	(1.00	1.51	1.51)	(0.44	0.46	0.46)
37	(407	429	443)	(70	34	37)	(3.74	0.23	0.23)	(0.58	0.58	0.58)
39	(406	454	470)	(86	48	54)	(2.34	4.54	4.54)	(0.58	0.58	0.59)
42	(198	233	233)	(11	12	13)	(0.17	0.04	0.04)	(0.60	0.63	0.62)
43	(456	482	484)	(55	33	34)	(1.43	0.67	0.68)	(0.57	0.56	0.56)
50	(453	623	637)	(105	134	132)	(8.62	10.45	10.44)	(0.54	0.57	0.57)
8	(139	158	125)	(4	9	7)	(0.85	0.51	0.51)	(0.66	0.67	0.64)
2	(146	271	209)	(6	27	14)	(0.02	1.04	0.98)	(0.70	0.66	0.61)
36	(65	197	142)	(0	15	2)	(0.00	0.22	0.02)	(0.89	0.92	0.93)
40	(137	249	192)	(7	15	4)	(0.01	0.02	0.01)	(0.73	0.78	0.75)
15	(163	216	199)	(9	17	10)	(0.02	0.12	0.06)	(0.84	0.85	0.86)
28	(190	157	155)	(8	14	12)	(4.27	0.05	0.05)	(0.78	0.75	0.75)
23	(238	335	276)	(15	11	3)	(0.08	0.01	0.01)	(0.67	0.75	0.72)

<u>Cells</u>

--1	(--2	---3	----4)	(--5	---6	----7)	(------8	------9	-----10)	(-----11	-----12	-----13)
1	(114	198	202)	(3	4	5)	(0.01	0.03	0.03)	(0.75	0.76	0.76)
2	(380	285	287)	(37	15	10)	(0.40	0.01	0.08)	(0.69	0.80	0.80)
8	(205	191	195)	(8	5	6)	(0.17	0.03	0.03)	(0.73	0.77	0.76)
9	(298	306	300)	(13	12	8)	(0.08	0.14	0.14)	(0.77	0.82	0.81)
10	(388	289	292)	(12	6	8)	(0.13	0.02	0.02)	(0.80	0.81	0.81)
11	(360	429	417)	(33	32	26)	(0.29	0.23	0.09)	(0.80	0.75	0.75)
15	(252	186	188)	(5	3	2)	(0.05	0.04	0.04)	(0.73	0.70	0.69)
16	(512	410	409)	(50	25	27)	(1.40	0.04	0.04)	(0.68	0.72	0.71)
17	(464	348	351)	(42	11	10)	(1.41	0.07	0.06)	(0.68	0.70	0.71)
18	(424	429	437)	(22	21	18)	(0.69	0.41	0.11)	(0.69	0.68	0.68)

19	(405	366	378)	(42	8	10)	(0.73	0.04	0.01)	(0.74	0.77	0.75)
22	(253	186	190)	(7	6	5)	(1.80	0.01	0.01)	(0.86	0.87	0.87)
23	(519	403	404)	(34	27	24)	(1.78	0.04	0.04)	(0.66	0.65	0.65)
24	(328	320	322)	(11	12	11)	(0.36	0.69	0.63)	(0.57	0.54	0.54)
25	(591	551	552)	(47	29	28)	(2.43	0.38	0.41)	(0.59	0.56	0.56)
26	(497	581	571)	(28	31	30)	(0.51	0.39	0.42)	(0.72	0.77	0.77)
27	(591	596	608)	(63	36	43)	(4.54	0.34	0.53)	(0.75	0.79	0.79)
29	(569	313	313)	(29	12	13)	(1.07	0.05	0.05)	(0.84	0.84	0.83)
30	(566	396	397)	(31	11	11)	(2.27	0.42	0.42)	(0.73	0.64	0.63)
31	(577	438	436)	(65	4	5)	(2.50	0.01	0.01)	(0.80	0.87	0.86)
32	(553	508	485)	(33	17	10)	(2.64	0.02	0.02)	(0.72	0.69	0.68)
33	(691	564	556)	(61	36	34)	(2.13	1.53	1.33)	(0.70	0.76	0.76)
34	(441	472	486)	(39	34	27)	(3.16	0.16	0.14)	(0.73	0.77	0.76)
36	(438	542	541)	(31	29	26)	(0.39	0.76	0.75)	(0.76	0.80	0.80)
37	(556	729	722)	(41	42	46)	(0.43	1.35	1.36)	(0.55	0.59	0.59)
38	(341	393	385)	(12	11	6)	(0.95	0.02	0.20)	(0.75	0.78	0.77)
39	(677	709	710)	(101	98	100)	(9.90	8.01	8.01)	(0.51	0.53	0.52)
40	(741	606	607)	(86	57	55)	(1.69	1.88	1.85)	(0.72	0.75	0.75)
41	(572	535	536)	(41	45	45)	(0.93	0.41	0.46)	(0.83	0.84	0.85)
43	(848	716	715)	(106	55	48)	(2.53	0.45	0.50)	(0.69	0.75	0.75)
44	(503	399	400)	(29	6	6)	(2.96	0.21	0.22)	(0.81	0.85	0.86)
45	(426	374	374)	(53	22	28)	(0.88	0.03	0.03)	(0.74	0.80	0.79)
46	(707	649	653)	(47	51	51)	(1.28	1.91	1.91)	(0.63	0.62	0.62)
47	(505	623	624)	(39	52	53)	(0.86	0.26	0.27)	(0.75	0.78	0.77)
48	(384	451	453)	(35	19	18)	(0.69	0.08	0.04)	(0.78	0.83	0.83)
51	(987	530	530)	(158	39	39)	(5.97	1.98	1.98)	(0.79	0.87	0.87)
52	(734	461	461)	(99	28	28)	(3.48	0.10	0.10)	(0.74	0.79	0.79)
53	(547	427	427)	(37	15	15)	(1.90	0.17	0.17)	(0.73	0.82	0.82)
54	(717	642	639)	(71	50	50)	(5.04	0.31	0.31)	(0.79	0.78	0.78)
55	(589	565	568)	(43	37	35)	(0.30	0.04	0.03)	(0.83	0.78	0.78)
56	(597	526	520)	(79	34	39)	(3.47	1.07	1.31)	(0.79	0.83	0.83)
60	(639	412	414)	(58	20	20)	(1.69	1.88	1.88)	(0.75	0.69	0.69)
61	(657	493	489)	(60	27	27)	(2.28	0.02	0.02)	(0.81	0.80	0.80)
62	(693	725	733)	(80	73	71)	(3.39	0.80	0.80)	(0.75	0.77	0.77)
63	(812	661	661)	(102	47	52)	(1.88	0.87	0.29)	(0.75	0.85	0.85)
68	(444	338	338)	(41	16	16)	(4.23	1.56	1.56)	(0.65	0.69	0.69)
69	(511	452	453)	(31	32	32)	(2.70	1.01	1.01)	(0.83	0.78	0.78)

Appendix D MATLAB Programs

Only programs used in Free Flight modeling are presented in this appendix. Programs, used to create different analysis tools and GUIs, are not presented due to their excessive size (order of thousands of lines). These programs are stored on Compact Discs and available through CSSI, Inc.

D.1 Potential and Vortex Field Approach Modeling

```
% Potential and Vortex Field Approach to Collision Avoidance
% Problem in 3-D for 3 aircraft with Spherical Protection
% and Alert Zones

% Created 5/17/97 by Alexander Suchkov

% Aircraft origin, destination and definition of protection
% and alert zones

% Aircraft #1

x_1=-3000; y_1=5000;z_1=1000;  % Initial Configuration
xd1=7000; yd1=-2000;zd1=7000;  % Desired Configuration
XD1=[xd1 yd1 zd1]';
r1=500;                        % Radius of Protection Zone
dr1=3000;                      % Radius of Influence (Alert) Zone

% Aircarft #2

x_2=7000; y_2=-2000;z_2=7000;  % Initial Configuration
xd2=-3000; yd2=5000;zd2=1000;  % Desired Configuration
XD2=[xd2 yd2 zd2]';
r2=500;                        % Radius of Protection Zone
dr2=3000;                      % Radius of Influence (Alert) Zone

% Aircraft #3

x_3=4000; y_3=3500;z_3=4000;   % Initial Configuration
xd3=4000; yd3=3500;zd3=4000;   % Desired Configuration
XD3=[xd3 yd3 zd3]';
r3=0;                          % Radius of Protection Zone
dr3=7000;                      % Radius of Influence (Alert) Zone


% Trajectories Initialization

t(1,1)=0;       % Initial Time
dt=5;           % Time Step

x1(1,1)=x_1; y1(1,1)=y_1;z1(1,1)=z_1;
x2(1,1)=x_2; y2(1,1)=y_2;z2(1,1)=z_2;
x3(1,1)=x_3; y3(1,1)=y_3;z3(1,1)=z_3;

for k=1:2000;     % Beginning of Simulation
```

```
% Current Position of Aircarft

        X1=[x1(1,k) y1(1,k) z1(1,k) ]';
        X2=[x2(1,k) y2(1,k) z2(1,k) ]';
        X3=[x3(1,k) y3(1,k) z3(1,k) ]';

% Attractive Forces

        Fa1=-(X1-XD1);
        Fa2=-(X2-XD2);
        Fa3=-(X3-XD3);

% Distance between Aircraft

r12(1,k)=sqrt((x1(1,k)-x2(1,k))^2+(y1(1,k)-y2(1,k))^2+(z1(1,k)-z2(1,k))^2);
r13(1,k)=sqrt((x1(1,k)-x3(1,k))^2+(y1(1,k)-y3(1,k))^2+(z1(1,k)-z3(1,k))^2);
r23(1,k)=sqrt((x2(1,k)-x3(1,k))^2+(y2(1,k)-y3(1,k))^2+(z2(1,k)-z3(1,k))^2);

% Beginning of Logical Statements

        if r12(1,k)>r2+dr2    % No Conflict between Aircraft 1 & 2

        % Repulsive Forces

                Fr12=[0 0 0]';
                Fr21=[0 0 0]';

        % Vortex Forces

                Fv12=[0 0 0]';
                Fv21=[0 0 0]';

        else                  % Conflict Occurs

        % Repulsive Forces

                Fr12=1/dr2*((r2+dr2)/r12(1,k)-1).*(X1-X2);
                Fr21=1/dr1*((r1+dr1)/r12(1,k)-1).*(X2-X1);

        % Vortex Forces

                Fv1= [1/dr2*((r2+dr2)/r12(1,k)-1)*(z1(1,k)-z2(1,k))...
                    -1/dr2*((r2+dr2)/r12(1,k)-1)*(x1(1,k)-x2(1,k))...
                     1/dr2*((r2+dr2)/r12(1,k)-1)*(y1(1,k)-y2(1,k))]';
                Fv2=-[1/dr1*((r1+dr1)/r12(1,k)-1)*(z1(1,k)-z2(1,k))...
```

```
          -1/dr1*((r1+dr1)/r12(1,k)-1)*(x1(1,k)-x2(1,k))...
           1/dr1*((r1+dr1)/r12(1,k)-1)*(y1(1,k)-y2(1,k))]';

end

if r13(1,k)>r3+dr3    % No Conflict between Aircraft 1 & 3

% Repulsive Forces

     Fr13=[0 0 0]';
     Fr31=[0 0 0]';

% Vortex Forces

     Fv13=[0 0 0]';
     Fv31=[0 0 0]';

else                  % Conflict Occurs

% Repulsive Forces

     Fr13=1/dr3*((r3+dr3)/r13(1,k)-1).*(X1-X3);
     Fr31=1/dr1*((r1+dr1)/r13(1,k)-1).*(X3-X1);

% Vortex Forces

     Fv13= [1/dr3*((r3+dr3)/r13(1,k)-1)*(z1(1,k)-z3(1,k))...
          -1/dr3*((r3+dr3)/r13(1,k)-1)*(x1(1,k)-x3(1,k))...
           1/dr3*((r3+dr3)/r13(1,k)-1)*(y1(1,k)-y3(1,k))]';
     Fv31=-[1/dr1*((r1+dr1)/r13(1,k)-1)*(z1(1,k)-z3(1,k))...
          -1/dr1*((r1+dr1)/r13(1,k)-1)*(x1(1,k)-x3(1,k))...
           1/dr1*((r1+dr1)/r13(1,k)-1)*(y1(1,k)-y3(1,k))]';

end

if r23(1,k)>r3+dr3    % No Conflict between Aircraft 2 & 3

% Repulsive Forces

     Fr23=[0 0 0]';
     Fr32=[0 0 0]';

% Vortex Forces

     Fv23=[0 0 0]';
     Fv32=[0 0 0]';
```

```
        else                    % Conflict Occurs

        % Repulsive Forces

                Fr23=1/dr3*((r3+dr3)/r23(1,k)-1).*(X2-X3);
                Fr32=1/dr2*((r2+dr2)/r23(1,k)-1).*(X3-X2);

        % Vortex Forces

                Fv23= [1/dr3*((r3+dr3)/r23(1,k)-1)*(z2(1,k)-z3(1,k))...
                     -1/dr3*((r3+dr3)/r23(1,k)-1)*(x2(1,k)-x3(1,k))...
                      1/dr3*((r3+dr3)/r23(1,k)-1)*(y2(1,k)-y3(1,k))]';
                Fv32=-[1/dr2*((r2+dr2)/r13(1,k)-1)*(z2(1,k)-z3(1,k))...
                     -1/dr2*((r2+dr2)/r13(1,k)-1)*(x2(1,k)-x3(1,k))...
                      1/dr2*((r2+dr2)/r13(1,k)-1)*(y2(1,k)-y3(1,k))]';
                end

% Normalizing Attraction Forces

if norm(Fa3,3)<=0.0001
Fa3_norm=1;
end

        Fa1_norm=norm(Fa1,3);
        Fa2_norm=norm(Fa2,3);
 %      Fa3_norm=norm(Fa3,3);

% Gains:
%       kr - repulsive force gain
%       kv - vortex force gain
%       kd - speed gain


kr1=1;
kv1=1;
kd1=1.3;

kr2=1;
kv2=1;
kd2=1.3;

kr3=0.000001;
kv3=0.000001;
kd3=0.000001;
```

```
% Right Hand Sides of Differential Equations

        RHS1=Fa1/Fa1_norm+kr1*(Fr12+Fr13)+kv1*(Fv12+Fv13);
        RHS2=Fa2/Fa2_norm+kr2*(Fr21+Fr23)+kv2*(Fv21+Fv23);
        RHS3=Fa3/Fa3_norm+kr3*(Fr31+Fr32)+kv3*(Fv31+Fv32);

% Aircraft Speeds

        V1=kd1*RHS1/norm(RHS1,3);
        V2=kd2*RHS2/norm(RHS2,3);
%       V3=kd3*RHS3/norm(RHS3,3);

V3=[0 0 0]';

% Aircraft Trajectory Calculation

        x1(1,k+1)=x1(1,k)+dt*V1(1,1);
        y1(1,k+1)=y1(1,k)+dt*V1(2,1);
        z1(1,k+1)=z1(1,k)+dt*V1(3,1);

        x2(1,k+1)=x2(1,k)+dt*V2(1,1);
        y2(1,k+1)=y2(1,k)+dt*V2(2,1);
        z2(1,k+1)=z2(1,k)+dt*V2(3,1);

        x3(1,k+1)=x3(1,k)+dt*V3(1,1);
        y3(1,k+1)=y3(1,k)+dt*V3(2,1);
        z3(1,k+1)=z3(1,k)+dt*V3(3,1);

        t(1,k+1)=t(1,k)+dt;

end     % End of Simulation

for k=1:2000

% Preparing Information for Animation

        x(1,k)=x1(1,k);
        x(2,k)=x2(1,k);
        x(3,k)=x3(1,k);

        y(1,k)=y1(1,k);
        y(2,k)=y2(1,k);
        y(3,k)=y3(1,k);

        z(1,k)=z1(1,k);
        z(2,k)=z2(1,k);
```

```
        z(3,k)=z3(1,k);


% Travel Time Calculation

if abs(x1(1,k)-xd1)<=10 & abs(y1(1,k)-yd1)<=10 & abs(z1(1,k)-zd1)<=10
t1(1,k)=t(1,k);
else
t1(1,k)=inf;
end

if abs(x2(1,k)-xd2)<=10 & abs(y2(1,k)-yd2)<=10 & abs(z2(1,k)-zd2)<=10
t2(1,k)=t(1,k);
else
t2(1,k)=inf;
end

if abs(x3(1,k)-xd3)<=10 & abs(y3(1,k)-yd3)<=10 & abs(z3(1,k)-zd3)<=10
t3(1,k)=t(1,k);
else
t3(1,k)=inf;
end

end

% Travel Times

        T1=min(t1);
        T2=min(t2);
        T3=min(t3);

% Animation Graphics

axislimits = [min(min(x(:,:))) max(max(x(:,:))) min(min(y(:,:))) max(max(y(:,:))) ...
min(min(z(:,:))) max(max(z(:,:)))];

figure
line_handle = plot3(x(:,1),y(:,1),z(:,1 ),'c.');
grid
set(line_handle,'erasemode','none');
axis(axislimits);
for indexnumber = 2:length(x)
set(line_handle ,'xdata',x(:,indexnumber ),...
        'ydata',y(:,indexnumber ),...
        'zdata',z(:,indexnumber ));
drawnow;
```

```
 pause(1)
end
```

D.2 Optimal (Least Squares) Approach Modeling

```
function
[xs,ys,vs,ps,xc,yc,vc,pc,tt]=simulation(to,tf,dt,n,xo,yo,vo,po,vmin,pmin,vmax,pmax
,Ra,m)');

%Main file for simulation
global ind


%Define original (unconstraint) trajectories

[xs,ys,vs,ps,tt]=unconstrained(to,dt,tf,n,xo,yo,vo,po);


%Define effective constraints based on priority of an aircraft

ind=resolve(n,m);

%Define constrained trajectories

[xc,yc,vc,pc,tt]=constrained(to,dt,tf,n,xo,yo,vo,po,xs,ys,vs,ps);
```

```
%This function contains data for initializing simulation

global vmin pmin vmax pmax Ra
to=0;                       %initial simulation time      (sec)
dt=10;                      %simulation time step         (sec)
tf=500;                     %final simulation time        (sec)
n=2;                        %number of an aircraft in the system      (units)
xo=[0 5280*10];             %initial x-coordinates        (ft)
yo=[0 5280*20];             %initial y-coordinates        (ft)
vo=[500*1.47 600*1.47];     %initial velocities           (ft/sec)
po=[10/57.3 -15/57.3];      %initial heading angles       (rad)
vmin=[450*1.47 550*1.47];        %minimum velocities              (ft/sec)
pmin=[-180/57.3 -180/57.3];      %minimum heading angles          (rad)
vmax=[550*1.47 650*1.47];        %maximum velocities              (ft/sec)
pmax=[180/57.3 180/57.3];        %maximum heading angles          (rad)
Ra=[5280*10 5280*10];            %separation radii                (ft)
m=[2 1];                         %priority coefficients.          (units)
```

```
function [xs,ys,vs,ps,tt]=unconstrained(to,dt,tf,n,xo,yo,vo,po)
```

```
k=1;
u=fix((tf-to)/dt)+1;

tt=zeros(1,u);
xs=zeros(n,u);
ys=zeros(n,u);
vs=zeros(n,u);
ps=zeros(n,u);

tt(1,1)=to;
t=to;

for i=1:n
xs(i,k)=xo(1,i);
ys(i,k)=yo(1,i);
vs(i,k)=vo(1,i);
ps(i,k)=po(1,i);
end

while t<tf
for i=1:n;

xs(i,k+1)=xs(i,k)+vs(i,k)*cos(ps(i,k))*dt;
ys(i,k+1)=ys(i,k)+vs(i,k)*sin(ps(i,k))*dt;
ps(i,k+1)=ps(i,k);
vs(i,k+1)=vs(i,k);

end
k=k+1;
t=t+dt;
tt(1,k)=tt(1,k-1)+dt;

end
```

```
function ind=resolve(n,m);

%This function defines which constraints are going to be effective, i.e.
%priority of an aircraft with respect to the others
%Input parameters:
%n-number of aircraft in the system
%m-raw vector of the size (1xn), containing priority coefficients
%of an aircraft
%Output parameters:
%ind-matrix of the size(nxn), containing 1 if constraint should be considered
%and 0 if not. Row index corresponds to aircraft under consideration.
```

```
%Column index corresponds to the rest of the aircraft including the current
%one.

ind=zeros(n,n);
h=1;
q=1;

for i=1:n
for j=1:n
if i<j | i>j & m(1,i)<m(1,j)
ind(h,q)=1;
else
ind(h,q)=0;
end
q=q+1;
end
q=1;
h=h+1;
end
```

```
function [xc,yc,vc,pc,tt]=constrained(to,dt,tf,n,xo,yo,vo,po,xs,ys,vs,ps)
global xs ys ind i k dt n
global xc yc
global vmin pmin vmax pmax
k=1;
u=fix((tf-to)/dt)+1;

tt=zeros(1,u);
xc=zeros(n,u);
yc=zeros(n,u);
vc=zeros(n,u);
pc=zeros(n,u);

tt(1,1)=to;
t=to;

for ii=1:n
xc(ii,k)=xo(1,ii);
yc(ii,k)=yo(1,ii);
vc(ii,k)=vo(1,ii);
pc(ii,k)=po(1,ii);
end
xc(:,1);
yc(:,1);
vc(:,1);
```

```
pc(:,1);

while t<tf

for i=1:n;

X0=[vc(i,k) pc(i,k)];

[X]=CONSTR('FUNC1',X0,[],[vmin(1,i) pmin(1,i)],...
        [vmax(1,i) pmax(1,i)]);
xc(i,k+1)=xc(i,k)+vc(i,k)*cos(pc(i,k))*dt;
yc(i,k+1)=yc(i,k)+vc(i,k)*sin(pc(i,k))*dt;
vc(i,k+1)=X(1,1);
pc(i,k+1)=X(1,2);

end

k=k+1;
t=t+dt;
tt(1,k)=tt(1,k-1)+dt;

end
```

```
function [F,G]=FUNC1(X);
global xs ys ind i k dt n
global xc yc
global vmin pmin vmax pmax Ra

xc(i,k+1)=xc(i,k)+X(1,1)*cos(X(1,2))*dt;
yc(i,k+1)=yc(i,k)+X(1,1)*sin(X(1,2))*dt;

F=(xc(i,k+1)-xs(i,k+1))^2+(yc(i,k+1)-ys(i,k+1))^2;

for j=1:n

G(i,j)=(-(xc(i,k+1)-xc(j,k+1))^2-(yc(i,k+1)-yc(j,k+1))^2+4*Ra(1,1)^2)*ind(i,j);

end
end
end
```

```
function graphics(xs,ys,vs,ps,xc,yc,vc,pc,tt)

fignumber=(figure(...
```

```
'Color',[0 0 0],...
'Name','TIME HISTORY',...
'NumberTitle','off',...
'Units','inches',...
'Position',[6.6 1 4.5 8],...
'Resize','off'));

subplot(4,1,1), plot(tt,xs,tt,xc,'o')
title ('x-coordinate vs time (ft-sec)')
subplot(4,1,2), plot(tt,ys,tt,yc,'o')
title ('y-coordinate vs time (ft-sec)')
subplot(4,1,3), plot(tt,vs,tt,vc,'o')
title ('velocity vs time (ft/sec-sec)')
subplot(4,1,4), plot(tt,ps*57.3,tt,pc*57.3,'o')
title ('heading angle vs time (deg)')
end
```

Vita

Alexander Borisovich Suchkov was born in Moscow, Russia, on June 8, 1972. In June 1993 he graduated from Moscow Aviation Institute with an Engineer Diploma in Aerospace Engineering. After his graduation he then attended Virginia Polytechnic Institute and State University, under an exchange program. After two semesters he was accepted into their graduate school and received a degree of Master of Science in Aerospace Engineering in April 1995. Soon after, he decided to continue his education and joined the Masters of Science in Civil Engineering program in August 1996 at the same school. In the spring of 1998 he completed his degree of Master of Science in Civil Engineering, specializing in Transportation Engineering.

Mr. Suchkov accepted the position of Operations Research Analyst in CSSI, Inc. in Washington, D.C. He started his engineering career with this company in June 1997.

Alexander Suchkov

April, 1998